12-2020

Fractional Order Identification Method and Control: Development of Control for Non-Minimum Phase Fractional Order System

Majid Abdullah Alhomim
University of Arkansas, Fayetteville

Fractional Order Identification Method and Control: Development of Control for Non-Minimum Phase Fractional Order System

A dissertation submitted in partial fulfillment
of the requirements for the degree of
Doctor of Philosophy in Engineering with a concentration in Electrical Engineering

by

Majid Abdullah Alhomim
University of Hartford
Bachelor of Science in Electrical Engineering, 2011
University of New Haven
Master of Science in Electrical Engineering, 2013

December 2020
University of Arkansas

This dissertation is approved for recommendation to the Graduate Council

Roy A. McCann, Ph.D.
Dissertation Director:

Jingxian Wu, Ph.D.
Committee Member

Yue Zhao, Ph.D.
Committee Member

Mark E. Arnold, Ph.D.
Committee Member

ABSTRACT

The increasing use of renewable energy has resulted in the need for improved a dc-dc converters. This type of electronic-based equipment is needed to interface the dc voltages normally encountered with solar arrays and battery systems to voltage levels suitable for connecting three phase inverters to distribution level networks. As grid-connected solar power levels continue to increase, there is a corresponding need for improved modeling and control of power electronic converters. In particular, higher levels of boost ratios are needed to connect low voltage circuits (less than 1000 V) to medium voltage levels in the range of 13 kV to 34 kV. With boost ratios now exceeding a factor of 10, the inherent nonlinearities of boost converter circuits become more prominent and thereby lead to stability concerns under variable load conditions. This dissertation presents a new method for analyzing dc-dc converters using fractional order calculus. This provides control systems designers the ability to analyze converter frequency response with Bode plots that have pole-zero contributions other than +/- 20 dB/decade. This dissertation details a systematic method of deriving the optimal frequency-domain fit of nonlinear dc-dc converter operation by use of a modified describing function technique. Results are presented by comparing a conventional linearization technique (i.e., integer-order transfer functions) to the describing-function derived equivalent fractional-order model. The benefits of this approach in achieving improved stability margins with high-ratio dc-dc converters are presented.

ACKNOWLEDGEMENTS

Beginning this Ph.D. has a been a positive change in my life experience also I would not have possibly to proceed it without the supporting and direction that I obtained from my family, research adviser, advisory committee members, and mentors. I am grateful to my parents, my wife and my children Abdullah and Hessah. They have always put trust in me and encouraged me towards achieving my dreams. I am thankful for them all to being patient of the five years until to get this moment of writing this dissertation. I would like to send my unique appreciation, and thankful to my academic adviser Prof. Roy McCann, he is been a great instructor. I would like to thank him a lot for supporting my Ph.D. study and described research, for his patience, immense knowledge, and motivation. I could not have believed had a better administrator and instructor for my Ph.D. study. I would also like to thank the members of the esteemed dissertation committee, Prof. Mark E. Arnold, His door was always open for all students at any time with no doubt to get help from him and ran out of any kind of difficulties. Thanks to Prof. Jingxian Wu and Prof. Yue Zhao for their useful comments and time reading this dissertation. I would not forget Saudi Arabia of higher education ministry for administering my scholarship to the University of Arkansas.

DEDICATION

To my parents, my wife and my children Abdullah, Hessah and my big family.

TABLE OF CONTENTS

LIST OF FIGURE

LIST OF TABLES

1 Introduction

1.1 Overview

Methods for identifying the dynamic behavior of systems have long been a topic of research. Traditional methods are based on sets of differential equations the model the behavior of engineered systems. This involves the use of relationships derived from well-established analysis techniques such as Kirchhoff's current and voltage laws for electrical circuits and Newton's laws for mechanical elements. These are typically applied using conventional integer-order calculus. However, these are based on idealized mechanical and electrical components, whereas actual physical devices have been observer to behave in a manner that is more accurately described by fractional-order derivatives [1]. A number of researchers have documented the fractional order behavior of many physical systems [2] and has led to ongoing efforts to establish the theoretical foundations for fractional-order modeling techniques [3]. These methods are often extensions from standard integer-order calculus, such as state-space representations, Laplace transforms of linear differential equations and discrete-time equivalents. However, there is a tradeoff between the accuracy versus complexity in the mathematical modeling of a physical system. Most physical system exhibit varying degrees of nonlinear behavior. Given the rich theoretical and design capabilities associated with linear systems, then there is a preference for performing a linearization of the system dynamics to provide a model that is reasonably accurate for a least a limited range near its nominal operating condition. Switched-mode power electronics that are employed in dc-dc boost converters exhibit nonlinear behavior that becomes more acute as the boost ratios are increased. Consequently, conventional linearization methods result in progressively degraded accuracy under conditions where an accurate dynamic model is most needed. . In particular, dc-dc boost converters exhibit non-minimum phase effects in the linearized equivalent models associated

with emergent right-half plane (RHP) zeros. This research proposes a novel method the modeling dc-dc converters based on a fractional-order representation of the system dynamics.

1.2 Motivation and Contribution of the Dissertation

The principal aim of the dissertation is the development of a new modeling method that more accurately represents the actual behavior of dc-dc converter systems. The identification of dc-dc converters from data that includes nonlinear behavior is analyzed in the context of fractional-order system theory. The modeling method begins with discrete-time (sampled) input-output data. By utilizing fractional-order calculus, the input-out data is processed to derive a Laplace-domain non-integer order transfer function. This provides systems designers the ability to analyze converter frequency response with Bode plots that have asymptotic pole-zero contributions other than +/- 20 dB/decade. The details of the proposed method derives an optimal fit of the actual dc-dc converter data through a novel describing function technique. The benefits of this approach in achieving improved stability margins with high ratio dc-dc boost converters are presented: First, the proposed methods are applied to data from a detailed circuit simulation of a switched-mode dc-dc boost converter. Secondly, the system modeling method is applied to a laboratory prototype dc-dc boost converter to further verify the effectiveness of the proposed methods.

1.3 Dissertation Outline

This dissertation has seven chapters: Chapter 2 discusses the mathematical tools that will be needed for understanding fractional-order calculus. Chapter 3 explains the identification of fractional-order systems based on input-output data collected from open-loop measurements and the derivation of a fractional order transfer function for a dc-dc converter.

Chapter 4 describes a novel describing function method that can be used to quantify the nonlinear effects of dc-dc converter operation. Chapter 5 discusses system stability and robustness when a fractional-order controller is used.

Chapter 6 provides step-by-step procedures on how to identify the nonlinear behavior of a dc-dc converter using detailed simulations and experimental results from a laboratory prototype. A conclusion is provided in Chapter 7 for the results of the proposed new method and potential future research directions.

2 Preliminary Mathematical Knowledge

This chapter reviews the necessary background knowledge needed for developing fractional-order methods of system modeling and identification. Details in applying identification methods to dc-dc converters from input-output operational data is provided as a foundation for subsequent chapters.

2.1 Introduction for Fractional Calculus

The source of fractional-order behavior in electrical components is associated with the distributed internal losses present in all physical devices [4] [5]. The history of fractional calculus is well known and dates back to the original work by Newton and Leibniz [6]. Leibniz postulated derivatives and integrals of fractional order and the potential implications [7]. In recent times, there has been renewed interest in fractional-order calculus in order to meet challenges in systems analysis and engineering [8] [9]. Formal methods have been developed which encompasses and extends the concepts normally taken in conventional integer-order systems analysis [10].

2.1.1 Gamma Function

The gamma function is widely used in defining fractional-order integration. The gamma function integral is expressed as

$$\Gamma(x) = \int_0^\infty e^{-n} u^{x-1} du, Re(x) > 0 \tag{2.1}$$

which has properties

$$\Gamma(x) = 1, \tag{2.2}$$

$$\Gamma(m+1) = m!\,, where\ is\ (m = 0,1,2\ldots), \tag{2.3}$$

$$\Gamma\left(\frac{1}{2}\right) = \sqrt{\pi}, \tag{2.4}$$

$$\Gamma(x+1) = x\Gamma(x). \tag{2.5}$$

Integer-order and the fractional-order derivatives of a single variable defined as

$$\frac{d^{\alpha}}{dx^{\alpha}} x^{\alpha} = \frac{\Gamma(\alpha+1)}{\Gamma(\alpha-\alpha+1)} x^{\alpha-\alpha} = \Gamma(\alpha+1). \tag{2.6}$$

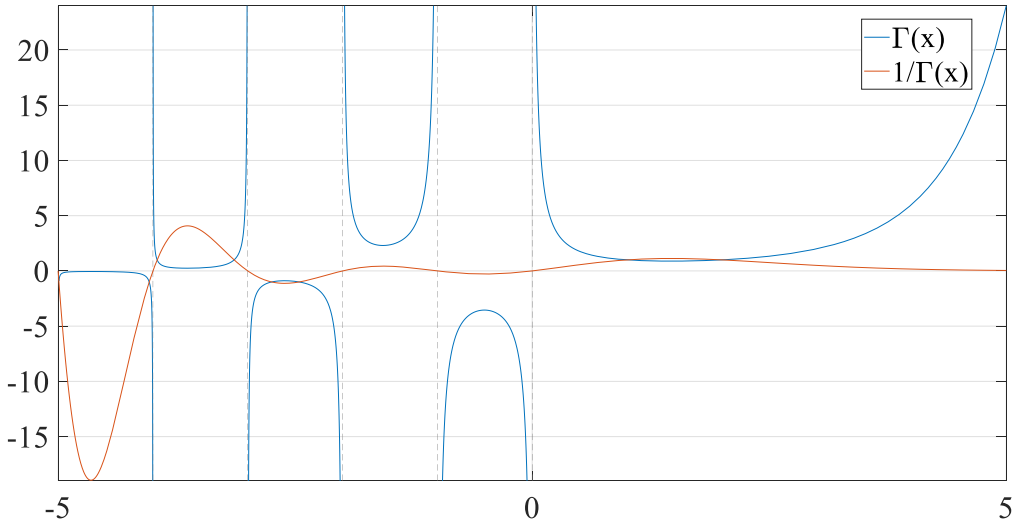

Figure 2.1: Graph of Gamma function.

Γ(x) and 1/Γ(x) is defined over the complex plane for positive and negative values of *x* is shown in Figure 2.1.

2.1.2 Mittag-Leffler Function

The Mittag-Leffler function is a generalization of the exponential function. That is needed in the resolution of fractional-order differential equations. There are several commonly used forms [11] [12], however this research relies upon the following version [13] for one parameter as

$$E_{\alpha}(t) = \sum_{k=0}^{\infty} \frac{t^{n}}{\Gamma(\alpha k+1)}, \tag{2.7}$$

and for two parameters as represented by

$$E_{\alpha,\beta}(t) = \sum_{k=0}^{\infty} \frac{t^n}{\Gamma(\alpha k + \beta)}, \tag{2.8}$$

where is $\Re(\alpha) > 0, \Re(\beta) > 0$. The Mittag-Leffler function $\mathrm{E}(.)$ is defined as

$$E_{1,1}(t) = e^k, \tag{2.9}$$

$$E_{1,2}(t) = \frac{e^k - 1}{t}. \tag{2.10}$$

For example,

$$\alpha = 1 \tag{2.11}$$

$$E_{\alpha}(t) = \sum_{k=0}^{\infty} \frac{t^n}{\Gamma(\alpha k + 1)} = e^k. \tag{2.12}$$

With $\alpha = 1$ and $\beta = 2$, (2.13)

$$E_{\alpha,\beta}(t) = \sum_{k=0}^{\infty} \frac{t^n}{\Gamma(\alpha k + \beta)} = \frac{e^k - 1}{t} \tag{2.14}$$

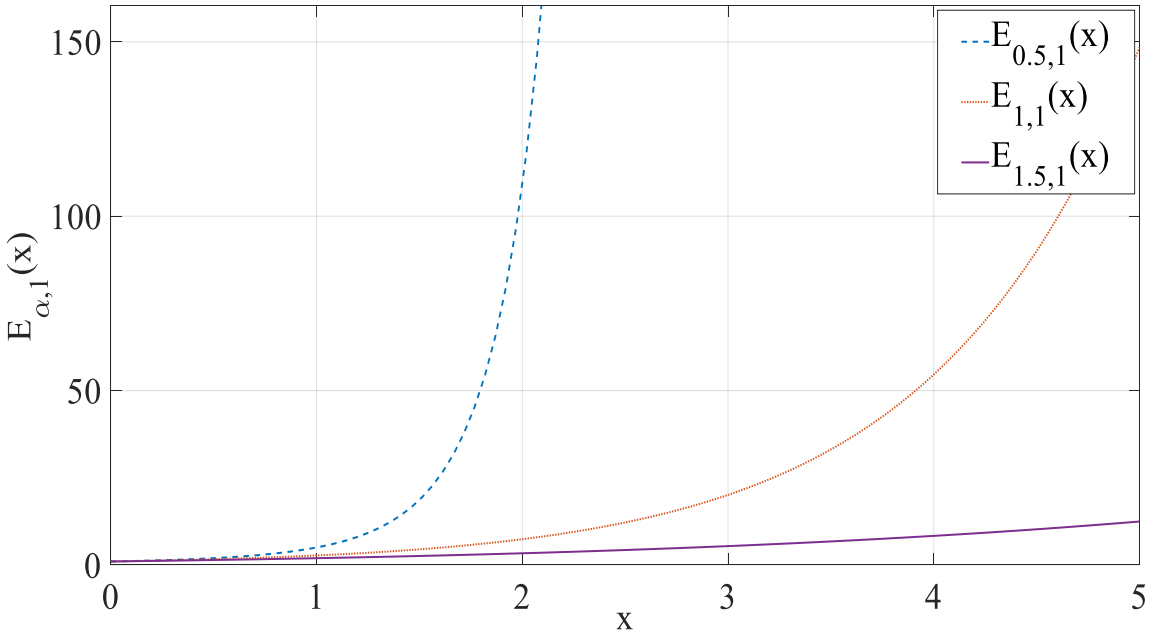

Figure 2.2: Mittag-Leffler function for Eα, 1(x) for α= 0.5, 1, 1.5.

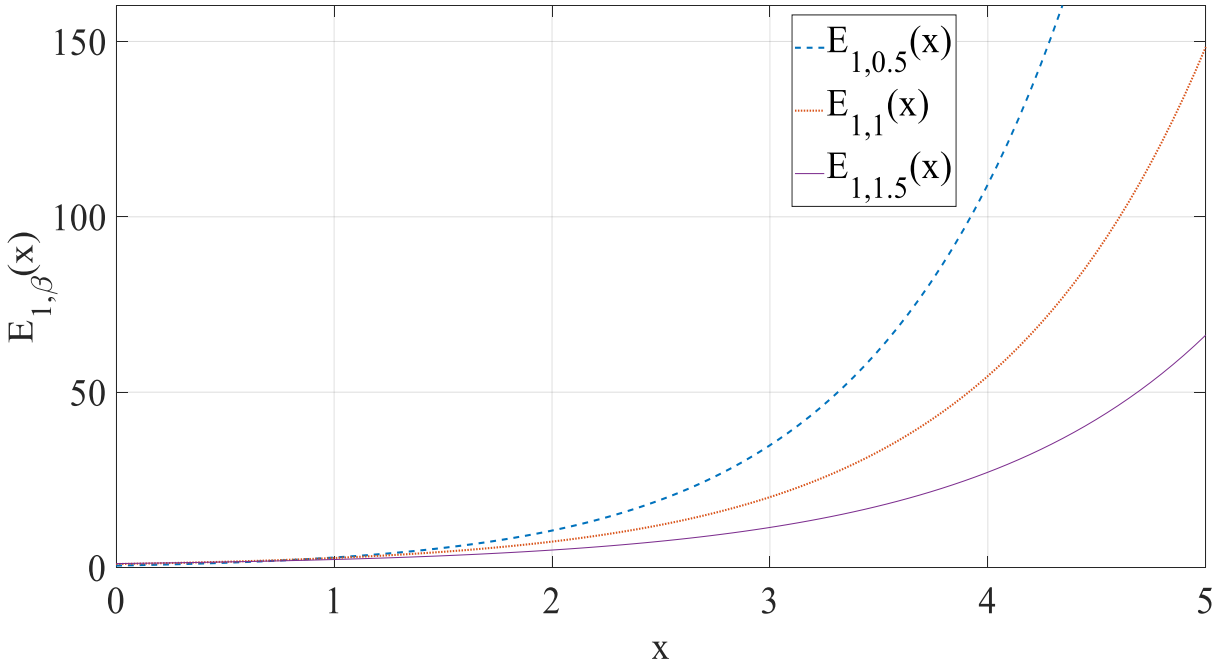

Figure 2.3: Mittag-Leffler function for E1, β(x) for β= 0.5, 1, 1.5.

2.2 Fractional Order Calculus

Fractional calculus is a general form of integral and derivative terms for non-integer order operators. It is an improvement for dynamic systems that are described by integration and differentiation operators D_t and ${}_a\mathcal{D}_t^{\alpha}$:

$$ {}_a\mathcal{D}_t^{\alpha} = \begin{cases} \dfrac{d^{\alpha}}{dt^{\alpha}} & \Re(\alpha) > 0, \\ 1 & \Re(\alpha) = 0, \\ \displaystyle\int_a^t (dt)^{-\alpha} & \Re(\alpha) < 0, \end{cases} \tag{2.15} $$

where the operator D and the parameter α and variable t express the limits of the operations and signifies the fractional-order operator, where $\alpha \in \mathbb{R}$ [14].

2.2.1 System Definitions

There are several definitions commonly applied for a fractional-order derivative of a function: Riemann Liouville's definition; Caputo's definition; and Grunwald-Letnikov's definition. The Riemann Liouville's definition is often chosen be to be applied for Laplace transform analysis. It is a method that begins with a generalization of Cauchy's theorems for integration with extension to non-integer order conditions. The fractional-order integral becomes

$$ I_c^{\alpha} f(t) = \mathcal{D}_t^{-\alpha}(t) = \frac{1}{\Gamma(\alpha)} \int_c^t (t-\tau)^{\alpha-1} \int (\tau)\, d\tau, \qquad t > c, \qquad \alpha \in R^{+} \tag{2.16} $$

where $\Gamma(\alpha)$, is the gamma function represented with the following definition

$$ \Gamma(\alpha) = \int_0^{\infty} e^{-n}\, u^{\alpha-1} du. \tag{2.17} $$

If α is a natural numbers then Eq. (2.17) then

$$\Gamma(n) = (n-1)!, \quad n \in N. \tag{2.18}$$

The fractional derivative as derived by the Rieman-Liouville definition for a fractional order derivative $\alpha \in R^+$, $\alpha > 0$ is

$$\begin{aligned} {}_c^R D_t^\alpha f(t) &\triangleq D^k I^{k-\alpha} f(t), \\ &= \frac{d^k}{dt^k}\left[\frac{1}{\Gamma(k-\alpha)}\int_0^t \frac{f(\tau)}{(t-\tau)^{\alpha-k-1}}\,d\tau\right], \end{aligned} \tag{2.19}$$

where $k-1 < \alpha \leq k, k = 0, and\ k \in N$. The representation of the Rieman-Liouville definition is R [15]. Caputo's definition with fractional derivative is shown as

$${}_cD^\alpha f(t) \triangleq I^{k-\alpha} D^k f(t) = \frac{1}{\Gamma(k-\alpha)}\int_0^t \frac{f^k(\tau)}{(t-\tau)^{\alpha-k+1}}\,d\tau. \tag{2.20}$$

This form applies to integer-order conditions if using a Laplace transform to solve fractional order differential equations, where $k-1 < \alpha < k,\ k \in N$ and C represents the Caputo definition. Grünwald determines a discrete time definition of fractional-order differentiation as [16]

$${}_c\mathcal{D}_t^\alpha f(t) = \lim_{m\to 0}\frac{1}{h^\alpha}\sum_{\tau=0}^{\left[\frac{t-c}{m}\right]}(-1)^\tau \binom{\alpha}{\tau} f(t-\tau m), \tag{2.21}$$

where m is a sampling period and $\binom{\alpha}{\tau}$ is Newton's binomial function.

2.3 Laplace Transform of Fractional Operator

The Laplace transform is one of the fundamental tools in dynamical systems and controls engineering. It is not only applied for functions of integer order operators; it can be applied for non-integer order functions as [17]

$$F(K) = \mathcal{L}\big(f(t)\big) = \int_0^{\infty} e^{-Nt} f(t)dt, \tag{2.22}$$

where the function $f(s)$ is obtained as the Laplace transform $F(K)$ by using the inverse Laplace transform represented as

$$f(s) = \mathcal{L}^{-1}[F(N)] = \frac{1}{j2\pi}\int_{c-j\infty}^{c+j\infty} e^{st}\, F(N)ds \tag{2.23}$$

where c is large and all the poles of function $F(z)$ are real valued [18]. The Laplace transform for fractional order versions of the Grünwald-Letnikov definition is

$$\mathcal{L}[\, D^{\alpha} f(s)] = s^{\alpha} F(z). \tag{2.24}$$

Laplace transform is defined of the Riemann-Liouville fractional operator definition for $f - 1 \leq \alpha < f$ as:

$$\mathcal{L}[{}_c D^{\alpha} f(t)] = s^{\alpha} F(s) - \sum_{k=0}^{f-1} s^{k} \times [D^{\alpha-k-1} f(u)]_{u=0}, \tag{2.25}$$

and it is defined with the Caputo fractional operator definition as

$$\mathcal{L}[{}_c D^{\alpha} f(u)] = s^{\alpha} F(s) - \sum_{k=0}^{n-1} s^{\alpha-k-1} f^{(k)}(0). \tag{2.26}$$

Example 2.1

Calculating the inverse Laplace transform for the following example [18]:

$$F(s) = \left\{\frac{1}{s\sqrt{s+nm}}\right\} \text{ where } c \text{ is a real-valued constant} \tag{2.27}$$

$$\mathcal{L}^{-1}[F(s)] \tag{2.28}$$

By applying the shift $\mathcal{L}\,[e^{a\tau} f(\tau)] = F(s - nm)$

$$\mathcal{L}^{-1}\left[\frac{1}{s\sqrt{s+nm}}\right]=\frac{e^{-a\tau}}{\sqrt{\pi t}} \tag{2.29}$$

Laplace transform integral

$$\mathcal{L}^{-1}\left[\frac{1}{s\sqrt{s+nm}}\right]=\int_0^{\tau}\frac{e^{-a\tau}}{\sqrt{\pi\tau}}d\tau \tag{2.30}$$

That is represented as for $u^2=nm\tau$

$$\mathcal{L}^{-1}\left[\frac{1}{s\sqrt{s+c}}\right]=\frac{1}{\sqrt{c}}\mathrm{erf}\left(\sqrt{nm\tau}\right). \tag{2.31}$$

2.4 The Fractional Fourier Transform

The fractional-order integral and derivative is applied to the as well to the Fourier transform. The fractional Fourier transform is [19]:

$$X_\alpha(u)=\mathcal{F}_\alpha\big(x(\tau)\big)=\int_{-\infty}^{\infty}x(\tau)K_\alpha(\tau,u)d\tau, \tag{2.32}$$

where $K_\alpha(\tau,u)$ is the kernel function determinate:

$$K_\alpha(\tau,u)=\begin{cases}\sqrt{\dfrac{1-j\cot\alpha}{2}}\times e^{j\left(\frac{u^2}{2}\right)\cot\alpha}e^{j\left(\frac{\tau^2}{2}\right)\cot\alpha-ju\tau\cos(ec\alpha)} & For\ \alpha\neq 2\pi\\ \delta(\tau-u) & For\ \alpha=2\pi\\ \delta(\tau+ut) & For\ \alpha=(2n-)\pi\end{cases} \tag{2.33}$$

This becomes the conventional Fourier transform when $\alpha=2\pi$, and $\frac{\pi}{2}$ multiples of α. Properties of the fractional Fourier transform are detailed in [20].

2.5 Fractional-Order Differential Equation

The Fractional-order differential equation is fundamental for expressing the fractional-order dynamical behavior of electrical systems. This section describes the needed background for applying and solving fractional-order differential equations.

2.5.1 Linear Fractional Order Differential Equation

Fractional-order differential equations in this research will typically be in the form:

$$a_c \mathcal{D}^{\alpha_c} y(t) + a_{c-1} \mathcal{D}^{\alpha_{c-1}} y(t) + \cdots + a_0 \mathcal{D}^{\alpha_0} y(t)$$

$$= b_n \mathcal{D}^{\beta_n} u(t) + b_{n-1} \mathcal{D}^{\beta_{n-1}} u(t) + \cdots + b_0 \mathcal{D}^{\beta_0} u(t) \quad (2.34)$$

where is , $a_i, b_j \in \mathbb{R}$, and $y(t)$ and $u(t)$ represent the input and output of the system. The form given by (2.34) is defined as commensurate-order when the orders of the system derivatives are integer multiples of a common factor, q such as $\alpha_k, \beta_k = kq, q \in \mathbb{R}^+$. The system is represented as follows [21]:

$$\sum_{c=0}^{n} a_c \, \mathcal{D}^{cq} y(t) = \sum_{c=0}^{m} b_c \mathcal{D}^{cq} \gamma(t), \quad (2.35)$$

where is $q = \frac{1}{l}, and \; l \in \mathbb{Z}_+$.

The relationships among the various forms for linear time-invariant (LTI) systems analysis are summarized in Figure 2.4.

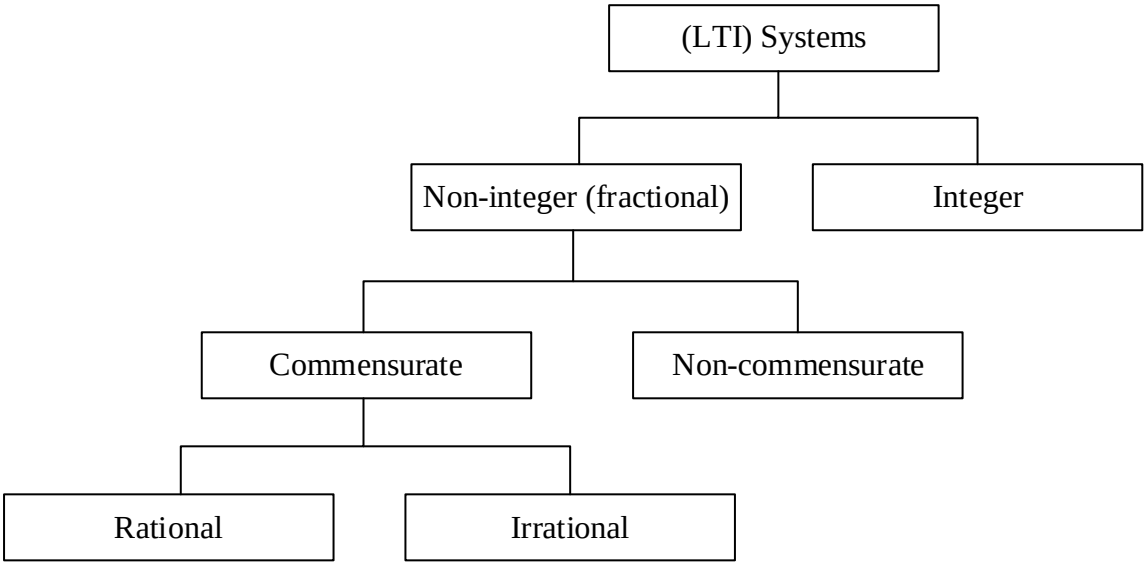

Figure 2.4: Classification of LTI system.

2.5.2 Nonlinear Fractional-Order Differential Equations

Pereira et al. [22] examined the fractional derivative for the Van der Pol equations by considering capacitance with a fractional order in a nonlinear electrical circuit design,

$$D^{\alpha}x + \gamma(x^2 - 1)\dot{x} + x = 0, \qquad 1 < \alpha < 2. \tag{2.36}$$

Barbosa et al. [23] presented fractional order Van der Pol equations by two part derivatives in fractional form as,

$$D^{1+\alpha}x + \gamma(x^2 - 1)D^{\alpha}x + x = 0, \qquad 0 < \alpha < 1. \tag{2.37}$$

2.6 State-Space Representation

The state-space description is often the most useful form for designing feedback control systems. When the Fractional-order differential equations have commensurate order then the state-space equations can be represented as:

$$ {}_0D_t^{\alpha}x(\tau) = f(x, u, \tau), \tag{2.38}$$

$$y(\tau) = g(\tau), \tag{2.39}$$

where is $0 < \alpha < 2$, and $x \in R^n$state vector of *n* dimension. For linear fractional-order differential equations as in (2.34) can then be expressed in matrix form as

$$_0D_t^{\alpha} x(\tau) = Ax(\tau) + Bu(\tau), \tag{2.40}$$

$$y(\tau) = Cx(\tau), \tag{2.41}$$

where are *A*, *B* and *C* real-values system matrices of appropriate dimensions.

2.7 Stability of Fractional Differential Equations

Understanding and ensuring the stability of feedback control systems is essential for developing power electronic dc-dc converters. Stability analysis is carried out using a modified Mittag-Letter form [24]. Analyzing the stability of nonlinear fractional differential equations is considerably more complicated than the linear case. Stability in general is determined from a fractional-order description for a state vector *x*,

$$D^{\alpha} x = f(x), \tag{2.42}$$

where is $x \in \mathbb{R}^n$ and $0 < \alpha < 1$. For the $f(x) = 0$ defines an equilibrium point of the system. It is asymptotically stable when the eigenvalues of a Jacobian matrix meets the condition [25]

$|\angle(eig(\mathbf{J}))| = |\angle(\lambda_j)| > \alpha \frac{\pi}{2}$,

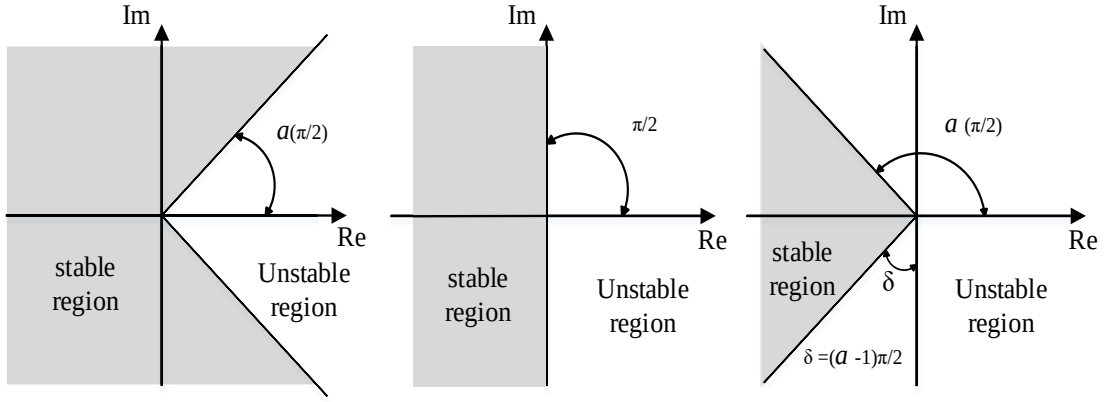

(a) $0 < a < 2$ (b) $a = 1$ (c) $1 < a < 2$

Figure 2.5: Stability region for all position.

where is λ_j the eigenvalues and $\mathbf{J}|_{x=x_0} = \partial f/\partial x$, and $J = 1,2,\dots,n$.

2.8 Fractional Order Transfer Functions

A fractional order transfer function represents the input-output relationship for a linear time-invariant continuous time dynamical system. Using the Laplace transform based on zero initial conditions, the input-output description of a fractional-order system is expressed as:

$$G(s) = \frac{Y(s)}{U(s)} = \frac{b_m s^{\beta_m} + b_{m-1} s^{\beta_{m-1}} + \cdots + b_0 s^{\beta_0}}{a_n s^{\alpha_n} + a_{n-1} s^{\alpha_{n-1}} + \cdots + a_0 s^{\alpha_0}} \tag{2.43}$$

where the Laplace transform is given for the input-output signals $Y(s), U(s), for\ m, n \in \mathbb{N}_+$. It is considered the zero initial condition of $y(s) = 0$ and $u(s) = 0$. The continuous-time transfer function for the case of a commensurate-order system is :

$$G(s) = \frac{Y(s)}{U(s)} = \frac{\sum_{k=0}^{m} b_k (s^{\alpha})^k}{\sum_{k=0}^{n} a_k (s^{\alpha})^k}. \tag{2.44}$$

Example 2.2

For the fractional-order system [25]:

$$G(s) = \frac{1}{(Ts)^{\alpha}} \tag{2.45}$$

The associated transfer function with $s = j\omega$ is the following:

$$G(s) = \frac{1}{(Tj\omega)^{\alpha}} = \frac{1}{T\omega^{\alpha}(\cos\frac{\pi}{2}\alpha + j\sin\frac{\pi}{2}\alpha)} \tag{2.46}$$

The magnitude is:

$$A(\omega) = \sqrt{\frac{(\cos^2\frac{\pi}{2}\alpha + j\sin^2\frac{\pi}{2}\alpha)}{(T\omega)^{2\alpha}}} = \frac{1}{(T\omega)^{\alpha}}, \tag{2.47}$$

$$M(\omega) = 20\log A(\omega) = -\alpha 20\log(T) - \alpha 20\log(\omega) \tag{2.48}$$

The phase of the transfer function is defined as:

$$\emptyset(\omega) = \arg\left[\frac{1}{(T\omega)^{\alpha}} j^{-\alpha}\right] = -\alpha\frac{\pi}{2}, \tag{2.49}$$

The information is provided from the amplitude and phase can be used to create a Bode diagram of the fractional-order frequency response for various values $\alpha = 0.5, .08, 1, 1.2, 1.5$ as shown in Figure. 2.6.

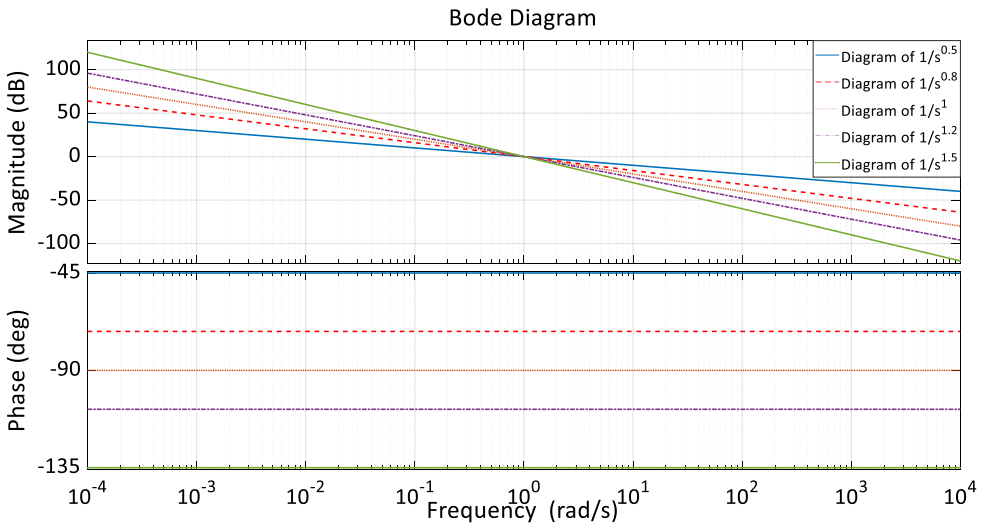

Figure 2.6: Bode diagrams of (s) =1/ (Tsα) systems for α= 0.5, 0.8, 1, 1.2, 1.5.

The fractional order state-space representation by a fractional-order transfer function expression as [26]

$$s^{\alpha}X(s) = AX(s) + BU(s), \tag{2.50}$$

$$Y(s) = CX(s), \tag{2.51}$$

with assumed zero initial conditions. The system transfer function is determined by

$$G(s) = \frac{Y(s)}{U(s)} = N(s^{\alpha}I - A)^{-1}B. \tag{2.52}$$

The obtained $G(s)$ of fractional order transfer function is a matrix when B is multi-input (multiple columns) and output C matrix has multiple rows (multi-output). The numerator and denominator of fractional order polynomials are of the general form

$$N(s) = a_n s^{\alpha_n} + a_{n-1}s^{\alpha_{n-1}} + \cdots + a_0 s^{\alpha_0}, \tag{2.53}$$

where is $\alpha_i \in \mathbb{N}_0^+$ and $\alpha_i \in \mathbb{R}$. The corresponding commensurate fractional degree polynomial is

$$N(s) = a_n s^{\frac{\lambda_n}{\lambda}} + a_{n-1}s^{\frac{\lambda_{n-1}}{\lambda}} + \cdots + a_0 s^{\frac{\lambda_0}{\lambda}} \quad \lambda_i \in \mathbb{R}. \tag{2.54}$$

2.8.1 Fractional-Order Transfer Function Stability

The stability of a fractional-order system can be determined by extending root locus methods or the Nyquist theorem [27] concepts. The root locus method approach analyzes the pole locations of a linear input-output feedback system with respect a variation of a parameter in terms of the corresponding loop gain. Stability in the time-domain for an LTI system is ensured when it satisfies the condition of its impulse response of $h(t)$ [28] as

$$\int_0^\infty \|h(\tau)\| d\tau < \infty . \tag{2.55}$$

The *s*-domain fractional-order transfer function is stable when there are no poles located in the right-half complex plane [29]. A simplified Nyquist principle for fractional-order transfer function that is presented by Trigeassou et. When *G(s)* operated in a unity-gain closed-loop, the input-output transfer function bacomes

$$\widetilde{G_{nm}}(s) = \frac{G_{nm}(s)}{G_{nm}(s)+1}, \tag{2.56}$$

$$G_{nm}(s) = \frac{1}{a_{nm}s^{\alpha_{nm}} + a_{nm-1}s^{\alpha_{nm-1}} + \cdots + a_0 s^{\alpha_0}} . \tag{2.57}$$

By factoring,

$$G_{nm}(s) = \frac{1}{a_1 s^{\alpha_1}} \frac{1}{\frac{a_{nm}}{a_1} s^{\alpha_{nm}-a_1} + \frac{a_{nm-1}}{a_1} s^{\alpha_{nm-1}-a_1} + \cdots + 1} \tag{2.58}$$

$$= \frac{1}{a_1 s^{\alpha_1}} \widetilde{G_{nm-1}}(s). \tag{2.59}$$

$\widetilde{G_{nm-1}}(s)$ is then written as a closed-loop system:

$$\widetilde{G_{nm-1}}(s) = \frac{G_{nm-1}(s)}{G_{nm-1}(s)+1}\,, \tag{2.60}$$

with the following

$$G_{nm-1}(s) = \frac{1}{\frac{a_2}{a_1}s^{a_2-\alpha_1}} \frac{1}{\frac{a_{nm}}{a_2}s^{\alpha_{nm}-a_2} + \frac{a_{nm-1}}{a_2}s^{\alpha_{nm-1}-a_2} + \cdots + 1}, \tag{2.61}$$

$$= \frac{1}{\frac{a_2}{a_1}s^{a_2-\alpha_1}} \widetilde{G_{nm-2}}(s)\,, \tag{2.62}$$

where the stability is determined by utilizing the Nyquist principle for the system loop gain.

2.8.2 Discrete Fractional-Order Systems

A brief summary of discrete-time fractional-order systems is given in the following. This definition is the generalization of the conventional definition for the fractional-order systems. Grünwald-Letnikov extended the definition for the fixed time-step of h for the first and second order increments as

$$\Delta x_k = x_k - x_{k-1}\,, \tag{2.63}$$

$$\Delta^2 x_k = x_k - 2x_{k-1} + x_{k-2}. \tag{2.64}$$

For generalization form of order n this becomes:

$$\Delta^n x_k = \sum_{a=0}^{n} (-1)^a \binom{n}{r} x_{k-a.} \tag{2.65}$$

The fractional-order difference equation can be determined for the α fractional order as

$$\Delta^\alpha x_k = \sum_{l=0}^{k} (-1)^l \binom{\alpha}{l} x_{k-l}, \tag{2.67}$$

where is $\alpha \in \mathbb{R}$ and $k \in \mathbb{N}$ number of sampling.

2.8.3 Discrete-Time Fractional-Order State-Space Models

Dzieliński and Sierociuk have introduced fractional-order state-space models [30] [31]. The state-space description of the fractional-order system in discrete-time is represented as

$$\Delta^{\alpha} x_{k+1} = A_a x_k + B u_k, \tag{2.68}$$

$$x_{k+1} = \Delta^{\alpha} x_{k+1} - \sum_{l=1}^{k+1} (-1)^l \binom{\alpha}{l} x_{k-l+1}, \tag{2.69}$$

$$y_k = C x_k + D u_k, \tag{2.70}$$

where $x_k \in \mathbb{R}^N, A_a \in \mathbb{R}^{N \times N}, B \in \mathbb{R}^{N \times m}, C \in \mathbb{R}^{p \times N}, D \in \mathbb{R}^{p \times m}, m = input$ and $p = output$. The nonlinear discrete-time model of a fractional-order system for the state-space description is represented as

$$\Delta^{\alpha} x_{k+1} = f(x_k, u_k), \tag{2.71}$$

$$x_{k+1} = \Delta^{\alpha} x_{k+1} - \sum_{l=1}^{k+1} (-1)^l \binom{\alpha}{l} x_{k-l+1}, \tag{2.72}$$

$$y_k = h(x_k), \tag{2.73}$$

where $\alpha \in \mathbb{R}$ and $f(x), h(x)$ are nonlinear functions.

3 Identification of Fractional-Order Models

The research now proceeds with developing methods for identification of transfer functions for unknown systems. This is needed in order to develop dynamic models for dc-dc boost converters that encompasses their complex behavior in manner such that closed-loop feedback controllers can be developed.

3.1 System Identification

The objective of system identification is to find a suitable dynamical system model by using either experimental or simulation-based data to determine input-output behavior. This is accomplished by injecting a known set of input signals with corresponding observations of the system output response. These observations are repeated over a range of possible input frequencies in order to map the system behavior over a complete operational range. Most typically, sinusoidal input signals are applied with a set of specified magnitudes u_0 and frequencies ω [rad/s] [11].

$$u(\mathrm{t}) = u_0 \sin(\omega \mathrm{t} + \alpha), \tag{3.1}$$

Fourier analysis of the output is performed and the component that corresponds to the same fundamental frequency of the input is identified [12]:

$$\mathrm{y}(\mathrm{t}) = \mathrm{y}_0 \sin(\omega \mathrm{t} + \beta) \tag{3.2}$$

where u_0 and y_0 denote magnitudes and are phase angle both are non-negative. It is noted that the output sinusoid has different amplitude y_0 and is shifted in phase from the input:

$$\emptyset = \triangleq \beta - \alpha. \tag{3.2}$$

In general, the output will contain harmonic components that are created due to nonlinearities and fractional order effects:

$$y(t) = \alpha \sum_{z=-\infty}^{\infty} g(z)\ \mathrm{Im}\left(e^{j\omega(t-z)}\right) = \alpha\ \mathrm{Im} \sum_{z=-\infty}^{\infty} g(z)e^{-j\omega(t-z)}. \tag{3.3}$$

$$y(t) = \alpha\ \mathrm{Im}\left\{e^{j\omega t} \sum_{z=-\infty}^{\infty} g(z)e^{-j\omega z}\right\} = \alpha\ Im\{e^{j\omega t}G(e^{j\omega})\} \tag{3.4}$$

$$= \alpha\left|G(e^{j\omega})\right| \sin(\omega t + \emptyset) \tag{3.5}$$

3.2 Identification Concepts

The identification of a linear dynamical system has been established in manner that provides this capability in various software and laboratory instruments ([32] - [38]). Nonlinear system identification is applied when linear system identification is unsuccessful in proving a suitable model ([39] - [42]). In this research, an approach is developed based on extracting a fractional order derived from either detailed simulation results or experimentally collected data. In either case, this approach uses a sinusoidal varying signal applied to the input [43]:

$$u(\mathrm{t}) = u_0 \sin(\omega \mathrm{t} + \alpha). \tag{3.6}$$

A frequency dependent function $G(e^{\omega k})$ is defined from the discrete Fourier transform of $u(k)$:

$$G(e^{\omega k}) = \sum_{k=-\infty}^{\infty} g(k)e^{-j\omega k} \tag{3.7}$$

For this research, the input signal is the duty-cycle applied to a dc-dc converter and the output is a voltage with a conceptual relationship provided in Figure 3.1.

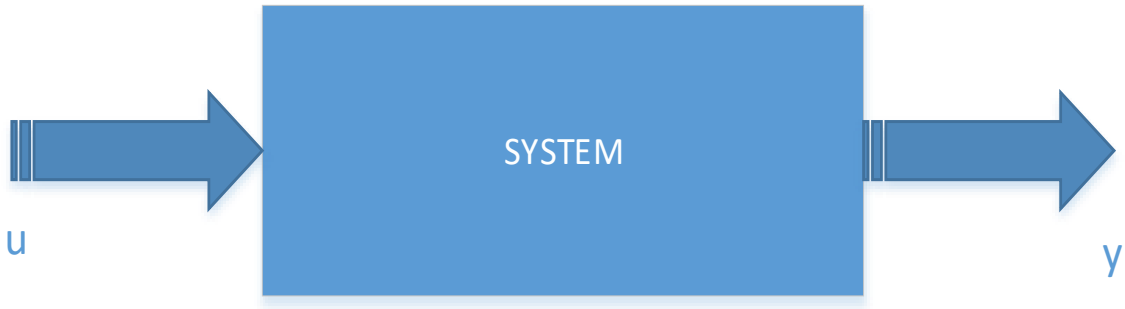

Figure 3.1: A system with input and output signal.

3.2.1 Open Loop Identification

The open loop Identification method is extracted from experimental or simulation data obtained from what is generally a nonlinear system. The frequency range of the input is smaller than the cut-off frequency of the system state variables [44][45]. The output is analyzed using a fast Fourier transform (FFT) method to obtain the magnitude and phase angles of all of the output signal components. The FFT component for the fundamental frequency associated with the sinusoidal input is retained. The method repeats for series of input frequencies. The result of this method is identify the general response for a particular dc-dc converter configuration. This method is automated using MATLAB [46] [47].

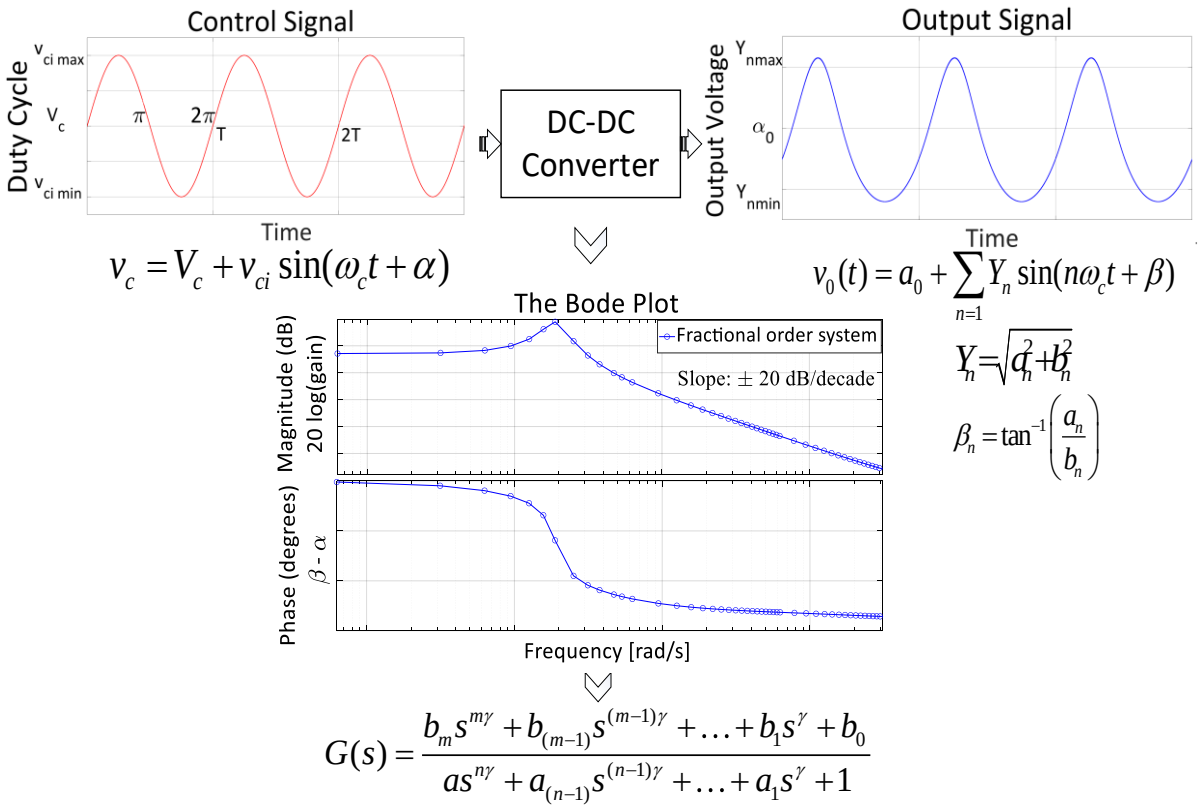

Figure 3.2: The system identification procedure.

Algorithm for the proposed method:

Step 1: Choose the frequency limit of concern where *f* is an array of frequencies.

Step 2: Assign a variable PWM corresponding to a desired nominal offset (boost gain) for the injected sinusoidal modulation such that the converter operates in continues conduction mode.

Step 3: Implement a simulation or experiment (time-domain) and record the V_{in}, and V_{out} signals.

Resample *y* on a uniform grid tt = min(t) : dt : max(t). The y may have *n* columns but should have length (t) rows. This calls Matlab interp1 (with 'linear' as METHOD), and preprocess *t* (and *y*) so that tt is monotonically increasing. The *dtol* is a threshold such that *t*(j+1)-t(j) < *dtol*, then *t*(j+1) and *y*(j+1,:) is removed. *NN* is the number of new sample

points (defaults to length(*t*)), given *dt* above as *dt* =(max(*t*)-min(*t*))/(*NN*-1), (refer to MATLAB code in the Appendix A).

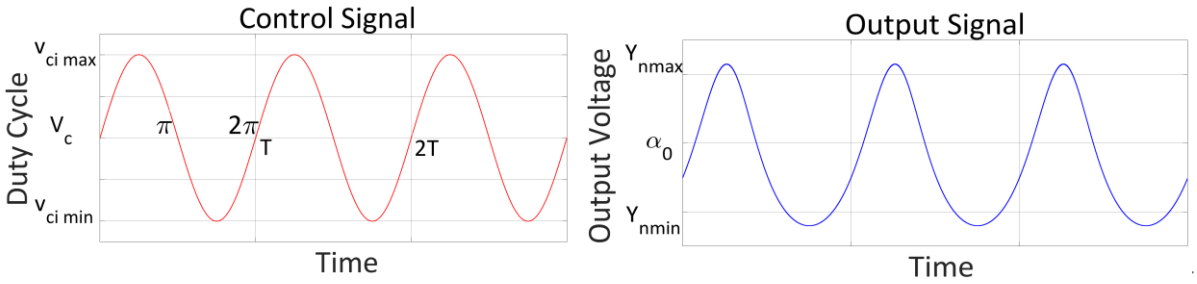

Figure 3.3: Example of signal input-output signals.

Step 4: Select the injected sinusoidal signal cycle (*t* are sampled points of each signal) of *input signal* and *out signal* in sampled points (*t*). Sort *y* and *t* for increasing *t* and remove duplicate entries in *t* (assuming *y* = *y* (*t*)). Duplicates are defined by *t* (*j*+1)-*t* (*j*) < *dtol*. The *p* is a permutation into *1: length (t)*, so that *yy* = *y* (*p*,:) and *tt* = *t*(*p*). If *y* is a (2*d*) matrix, then one of its dimensions must be *length (t)*. If number of rows*(y) is ~= length (t)*, then it is transposed. The output number of rows *(yy)* = *length (tt)*, and *tt* is a column vector (refer to MATLAB code in Appendix B).

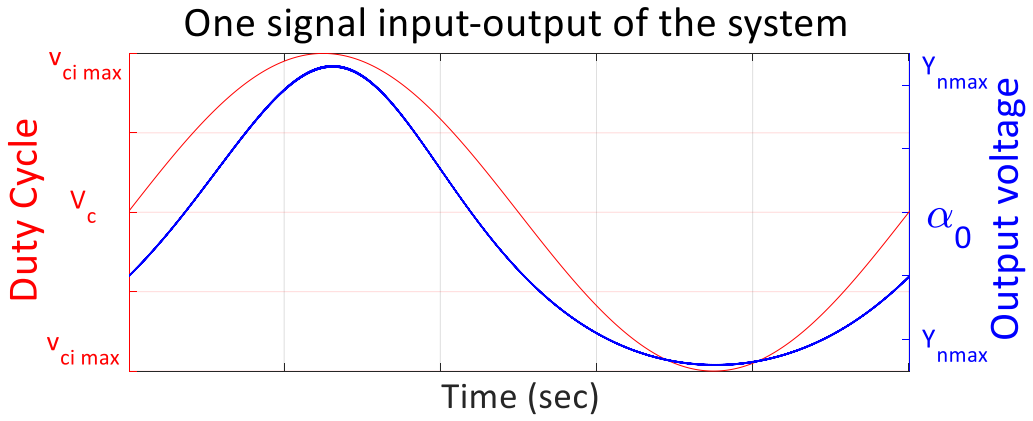

Figure 3.4: Example of sinusoidal wave input and output.

Step 5: Compute the respective FFT for (*Vin and Vout*), ft_i=fft(*y_i* or *y_o*) where *y_i or y_o* are one of the time-domain samples, in evaluating the series of input amplitudes and the series of output amplitudes with the phase angle for input and output suitably correlated. The fi_i(2) or if_o are the complex value of the fundamental frequency in V_{in} *and* V_{out}, where the gain and phase angles form the FFT are coded that in Matlab as:

Gain = abs(value of ft_i or ft_o)

Phase = tan (imaginary of of ft_i or ft_o, real value of ft_i or ft_o))

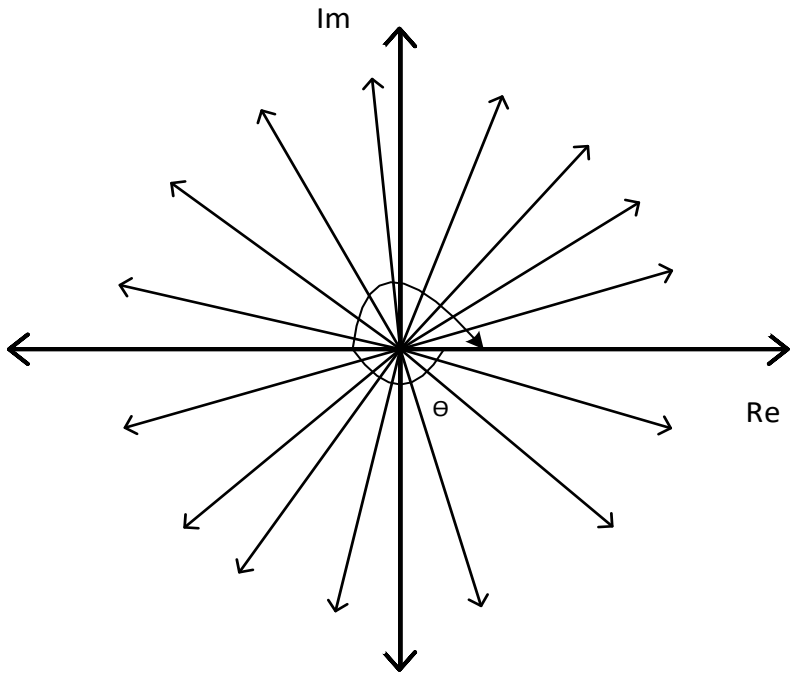

Figure 3.5: Example of signal input-output phase angle shift.

Step 6: Record the gain and phase angle of *input signal* and *output signal.* Generate a Bode plot by graphing the gain and phase shift of the open-loop transfer function using Matlab as:

$$Magnitude \ = \ 20 * Log \left[\frac{Gain\left(ft_{i(2)}\right)}{Gain\left(ft_{o(2)}\right)}\right] dB,$$

$$\theta = (Phase(ft\_i(2)) - Phase(ft\_o(2))) * 180/\pi degrees.$$

Step 7: Plot the collected data as a Bode plot.

Step 8: From the Bode plot defined the fractional order system by using an approximation of the fractional order representation.

3.3 System Identification Procedure

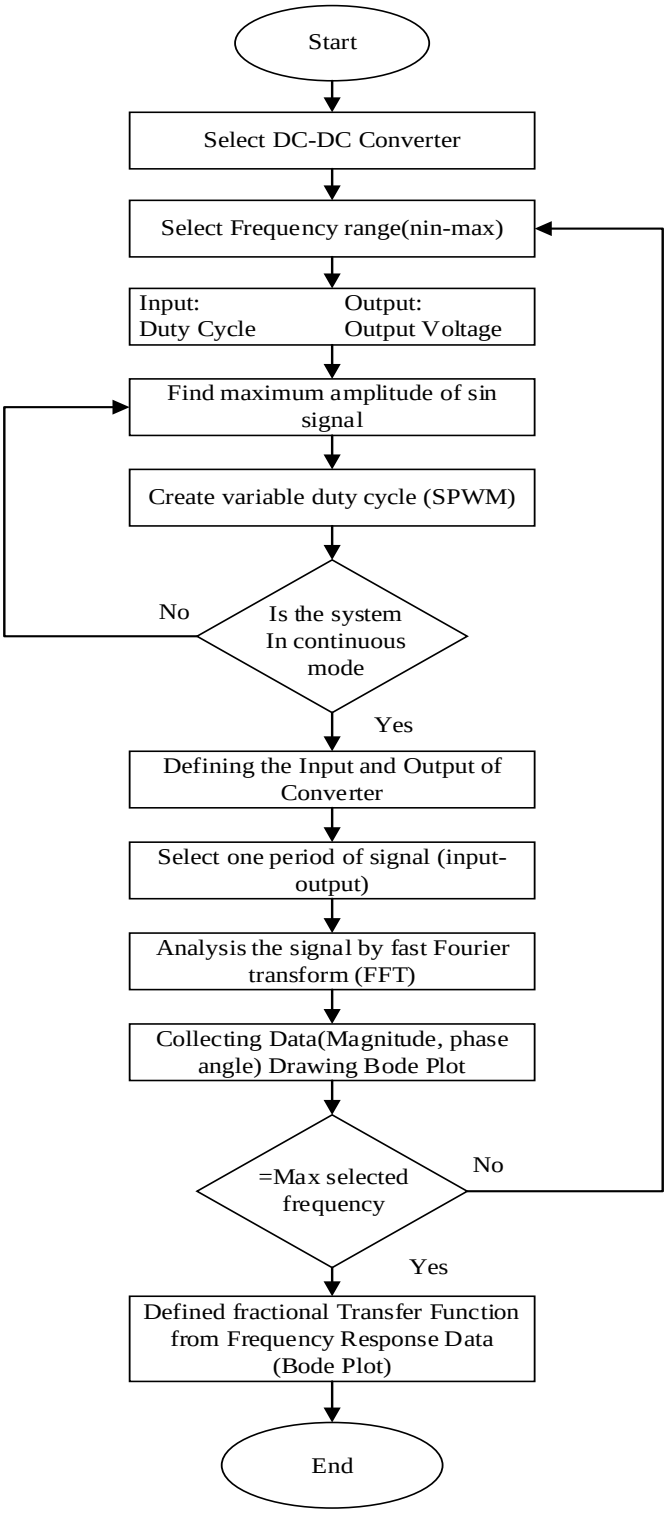

Figure 3.6: The system identification flowchart.

The general method of system identification is shown in Figure 3. 6. The analytical process is described in the following:

Step 1: Design the simulation or hardware prototype with methods for collecting the output FFT (magnitude and phase angle).

Step 2: Select a range of frequencies based on the type of power electronic converter.

Step 3: Determine the largest allowable amplitude for the injected control signal (duty cycle) to operate the system in continues conduction mode.

Step 4: Select a one period input switching sinusoidal signal function and determine the number of sample per period the will be used for the FFT.

Step 5: Determine and record the amplitude and phase shift using Fast Fourier Transform (FFT).

Step 6: Record the data of the amplitude and phase shift. The data is collected is used as one point of a Bode plot.

Step 7: Repeat this process for a frequencies defined from Step 2.

Step 7: Compile the tabulate date to determine the corresponding fractional-order transferfunction.

3.4 Sine-Wave Response

The fractional order system identification begins with the Bode plot derived from the fundamental component of the FFT that was obtained in Section 3.3. The Bode plot representation analogous to a describing function method that would produce a discrete set of points. Each particular input frequency has a corresponding fundamental component that is observed at the output. The relationship is shown at one particular case in Fig. 3.7. This process is repeated for all frequencies within the range of interest determined in Section 3.3. The resulting response $H(j\omega)$ has a magnitude and its phase angle:

$$H(s)|_{s=j\omega} = H(j\omega) = |H(j\omega)|e^{j\angle H(j\omega)} \tag{3.8}$$

where is $|H(j\omega)|$ the amplitude and $\angle H(j\omega)$ is the phase angle.

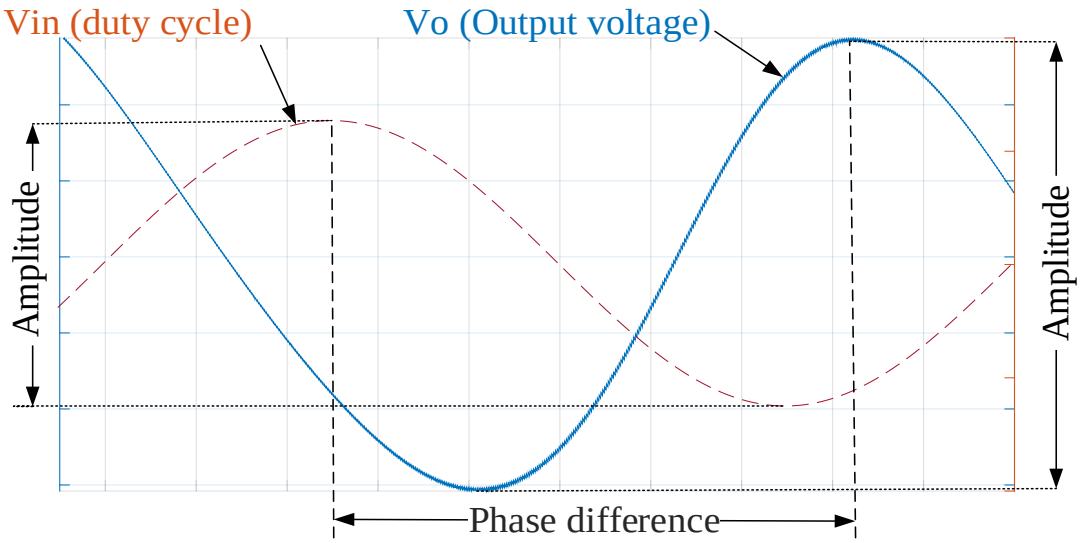

Figure 3.7: One signal responses the gain and phase angle of input-output.

3.5 Time-Domain Identification

The identification of fractional-order models in the time-domain is now described. Analyzing input-output frequency response achieves the fractional-order transfer function for a set of collected data. The general form of the transfer function [48]:

$$G(s) = \frac{b_m s^{\beta_m} + b_{m-1} s^{\beta_{m-1}} + \cdots + b_0 s^{\beta_0}}{a_n s^{\alpha_n} + a_{n-1} s^{\alpha_{n-1}} + \cdots + a_0 s^{\alpha_0}} \tag{3.9}$$

where is ak and bk indicate to poles and zeros of polynomial differential operator coefficients. By optimizing:

$$b_z = [b_m \quad b_{m-1} \quad \cdots \quad b_0], \tag{3.10}$$

$$\beta_z = [\beta_n \quad \beta_{n-1} \quad \cdots \quad \beta_0], \tag{3.11}$$

$$a_p = [a_n \quad a_{n-1} \quad \cdots \quad a_0], \tag{3.12}$$

$$\alpha_p = [\alpha_n \quad \alpha_{n-1} \quad \cdots \quad \alpha_0], \tag{3.13}$$

where a_p and b_z are pole and zero polynomial and α_p, β_z the orders of differentiation.

3.6 Frequency-domain Identification

Hartley and Lorenzo provide an approach to achieve a fractional-order model by substitution of $s = j\omega$ as all zeros [49]:

$$G(s) = c_n s^{n\gamma} + c_{n-1} s^{(n-1)\gamma} + \cdots + c_1 s^{\gamma} + c_0. \tag{3.14}$$

The all-pole form is given by:

$$G(s) = \frac{1}{c_n s^{n\gamma} + c_{n-1} s^{(n-1)\gamma} + \cdots + c_1 s^{\gamma} + c_0}. \tag{3.15}$$

where n is the integer order of the system and γ is the commensurate operator. Duarte Valério and Levy propose the frequency-domain identification approach. The complex term of a frequency $\omega \in (0{:}\,\infty)$ and j is the imaginary part as the following:

$$G(j\omega) = \frac{1}{c_n(j\omega)^{n\gamma} + c_{n-1}(j\omega)^{(n-1)\gamma} + \cdots + c_1(j\omega)^{\gamma} + c_0}, \tag{3.16}$$

Or more generally as

$$G(j\omega) = \frac{P(j\omega)}{Q(j\omega)} = \frac{b_m(j\omega)^{m\gamma} + b_{m-1}(j\omega)^{(m-1)\gamma} + \cdots + b_1(j\omega)^{\gamma} + b_0}{a(j\omega)^{n\gamma} + a_{n-1}(j\omega)^{(n-1)\gamma} + \cdots + a_1(j\omega)^{\gamma} + 1}, \tag{3.17}$$

minimizing the square norm as:

$$\begin{aligned} \varepsilon = G(j\omega)\left[a_n(j\omega)^{n\gamma} + a_{n-1}(j\omega)^{(n-1)\gamma} + \cdots + a_1(j\omega)^{\gamma} + 1\right] \\ - \left[b_m(j\omega)^{m\gamma} + b_{m-1}(j\omega)^{(m-1)\gamma} + \cdots + b_1(j\omega)^{\gamma} + b_0\right] \end{aligned} \tag{3.18}$$

with a resulting matrix form expressed as:

$$\begin{bmatrix} \frac{1}{G(j\omega_1)} \\ \frac{1}{G(j\omega_2)} \\ \vdots \\ \frac{1}{G(j\omega_m)} \end{bmatrix} = \begin{bmatrix} 1 & (j\omega_1)^{\gamma} & (j\omega_1)^{2\gamma} & \cdots & (j\omega_1)^{n\gamma} \\ 1 & (j\omega_2)^{\gamma} & (j\omega_2)^{2\gamma} & \cdots & (j\omega_2)^{n\gamma} \\ \vdots & \vdots & \vdots & \ddots & \vdots \\ 1 & (j\omega_m)^{\gamma} & (j\omega_m)^{2\gamma} & \cdots & (j\omega_m)^{n\gamma} \end{bmatrix} \begin{bmatrix} c_0 \\ c_1 \\ c_2 \\ \vdots \\ c_n \end{bmatrix}, \tag{3.19}$$

where $\omega_1, \omega_2, \ldots, \omega_n$ indicates the frequencies that have been selected. When using this form the operator must satisfy the order n and commensurate order γ. This method determines parameters from an experiment or simulated response of $G(j\omega) = \Re(\omega) + j\Im(\omega)$ [49]:

$$\begin{bmatrix} A & B \\ C & D \end{bmatrix} \begin{bmatrix} b_0 \\ \vdots \\ b_m \\ a_1 \\ \vdots \\ a_n \end{bmatrix} = \begin{bmatrix} e \\ g \end{bmatrix}, \tag{3.20}$$

where are *A, B, C, D* are the following:

$$A_{k,l} = \sum_{c=1}^{f} (-\Re[(j\omega_c)^{k\gamma}]\Re[(j\omega_c)^{l\gamma}] - \Im[(j\omega_c)^{k\gamma}]\Im[(j\omega_c)^{l\gamma}]),$$

$$k = 0, \ldots, m\,, l = 1, \ldots, m. \tag{3.21}$$

$$B_{k,l} = \sum_{c=1}^{f} \Big(\Re[(j\omega_c)^{k\gamma}]\Re\left[\left(j\omega_p\right)^{l\gamma}\right] R_p + \Im[(j\omega_c)^{k\gamma}]\Re[(j\omega_c)^{l\gamma}] I_c - \Re[(j\omega_c)^{k\gamma}]\Im[(j\omega_c)^{l\gamma}] I_c$$

$$+ \Im[(j\omega_c)^{k\gamma}]\Im[(j\omega_c)^{l\gamma}] R_c\Big), k = 0, \ldots, m \text{ and } l = 1, \ldots, n. \tag{3.22}$$

$$C_{k,l} = \sum_{c=1}^{f} (\{\Im[(j\omega_c)^{k\gamma}] I_c - \Re[(j\omega_c)^{k\gamma}] R_c\}\Re[(j\omega_c)^{l\gamma}]$$

$$+ \{-\Re[(j\omega_c)^{k\gamma}] I_c - \Im[(j\omega_c)^{k\gamma}] R_c\}\Im[(j\omega_c)^{l\gamma}]), k = 1, \ldots, n.\, l = 0, \ldots, m. \tag{3.23}$$

$$D_{k,l} = \sum_{c=1}^{f} [(R_c^2 + I_c^2)\{\Re[(j\omega_c)^{k\gamma}]\Re[(j\omega_c)^{l\gamma}] + \Im[(j\omega_c)^{k\gamma}]\Im[(j\omega_c)^{l\gamma}]\}], k = 1, \dots, n\,, l$$

$$= 1, \dots, m. \tag{3.24}$$

$$e_{k,l} = \sum_{c=1}^{f} \{-\Re[(j\omega_c)^{k\gamma}]R_c - \Im[(j\omega_c)^{k\gamma}]I_c\}, k = 0, \dots, m\,, \tag{3.25}$$

$$g_{k,l} = \sum_{c=1}^{f} \{-\Re[(j\omega_c)^{k\gamma}](R_c^2 + I_c^2)\}, k = 1, \dots, n. \tag{3.26}$$

3.7 Nonlinear Fractional-Order System Identification

Nonlinear effects are accounted for with a new method of extending the describing function approach. This goes beyond the existing methods as in [50] to utilize fractional-order dynamical characteristics

$$\hat{y}(t) = \mathcal{L}^{-}\left[\frac{b_m s^{\beta_m} + b_{m-1} s^{\beta_{m-1}} + \cdots + b_0 s^{\beta_0}}{a_n s^{\alpha_n} + a_{n-1} s^{\alpha_{n-1}} + \cdots + a_0 s^{\alpha_0}}\right] * \sum_{k=1}^{M} \alpha_k u^k(t) \tag{3.27}$$

considering that the nonlinearity produces a polynomial model $\varphi(u) = \sum_{i=0}^{n} \beta_i u^i$, and the linear term from the commensurate fractional-order described as:

$$G(p) = \frac{B(p)}{A(p)} = \frac{\sum_{i=0}^{m} b_i p^{i\alpha}}{1 + \sum_{j=0}^{n} a_j p^{j\alpha}} \tag{3.28}$$

The proposed approach of system identification is to identify parameters associated with the nonlinear parts for a best fit equivalent fractional-order transfer functions.

3.7.1 Linearization of nonlinear fractional order systems

Conventional linearization techniques are commonly applied to achieve a linear approximation of a nonlinear system. This is ordinarily valid for a small region near the nominal

operating point. The proposed new nonlinear fractional-order approach provides a wider region of valid operating conditions from the nominal operating point. This is a new extension to fractional-order models. In the following, recall that the fractional differential equation in the Caputo function are given by

$$ {}_0^C D_t^\alpha x(t) = f\big(x(t)\big), \tag{3.29} $$

$$ Df(x)|_{x=x_\omega} . \tag{3.30} $$

Linearization is with respect to the point x_ω. The following are defined:

Definition 1:

$$ E \in \mathbb{R}^{n_a \times n_p}, F \in \mathbb{R}^{1 \times n_p} $$

$$ n_{p=\binom{n_a+1+d}{d}-n_a-2} \tag{3.31} $$

$$ n_\theta = (n_a + 1)n_p \tag{3.32} $$

$$ r(\theta) \triangleq \tilde{y}(\theta) - y \in \mathbb{R}^m \tag{3.33} $$

where is $m > n_\theta$.

$$ f(\theta) \triangleq \frac{1}{2}\|r(\theta)\|^2 , \in \mathbb{R} \tag{3.34} $$

Definition 2:

Jacobian of residual vector r:

$$ J(\theta) \triangleq \frac{\partial r}{\partial \theta} \in \mathbb{R}^{n_\theta \times m} \tag{3.35} $$

Definition 3:

Gradient of function (f):

$$\nabla f(\theta) \triangleq \frac{\partial r}{\partial \theta} = \left(\frac{\partial r^T}{\partial \theta}\right) r = J^T r \in \mathbb{R}^{n_\theta \times m} \tag{3.36}$$

Definition 4:

Hessian of function (*f*):

$$H(\theta) \triangleq \frac{\partial^2 f}{\partial \theta^2} \approx J^T J \in \mathbb{R}^{n_\theta \times m}. \tag{3.37}$$

3.8 Discrete-Time Delta Operator

Discretization is needed for the implementation of feedback controllers. The discrete-time techniques is extended to fractional-order systems. The discrete-time approximation for the continuous-time of transfer functions can be based on an Oustaloup filter [50]:

$$\begin{aligned} \frac{dy}{dz} &\approx \frac{y(z+1) - y(z)}{T} \\ &= \frac{(q-1)}{T} y(z) \\ &= \delta y(t) \end{aligned} \tag{3.38}$$

where δ is an operator that provides an equivalence of continuous and discrete-time systems [49].

4 Sinusoidal Pulse Width Modulation

This research is based on pulse width modulation (PWM) for switched-mode dc-dc converters . The switching state is obtained by comparing the desired reference wave with a carrier triangular waveform. When the reference signal is higher or lower than the carrier waveform, the active power transistor goes to the corresponding high (on) or low (off) state. Hard-switching (power transistors that change from on-state to off-state during a period of electrical conduction) tend to further increase the harmonic content of the associated state variables (inductor currents and capacitor voltages). Harmonic elements that are artifacts of PWM operation are filtered based on the inductance and capacitance of the overall systems [51].

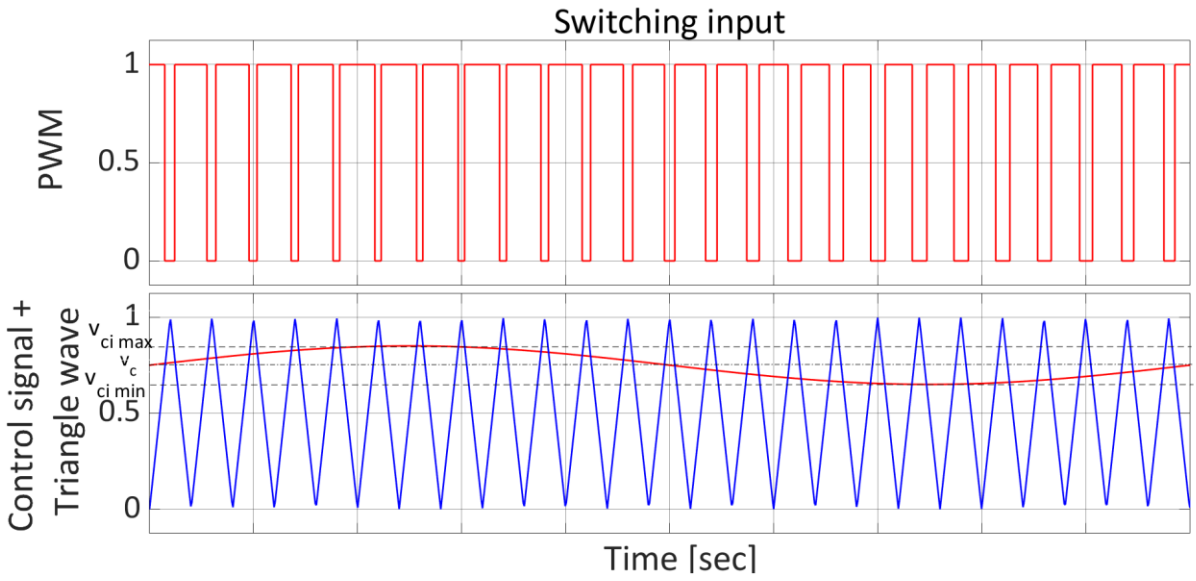

Figure 4.1: Principal of Sinusoidal Pulse Width Modulation.

As an example, the reference modulation signal is $V(t)$ and V_m is an amplitude of the carrier triangular function as is shown in Fig. 4.1.

4.1 Sinusoids

For this research, the following notation is used for a reference sinusoidal modulating function:

$$x(t) = A\sin(\omega_0 t + \emptyset) \tag{4.1}$$

where A represents the amplitude, $\omega_0 = 2\pi f_0$ denotes the frequency(radian frequency), and $\emptyset$ represents the phase angle [52].

$$x(t) = A\sin(\omega_0 t + \emptyset) = A\cos(\omega_0 t + \emptyset' - \pi/2) \tag{4.2}$$

where is $\emptyset = \emptyset' - \pi/2$. Trigonometric relationships to describe sin and cos functions are represented as follows:

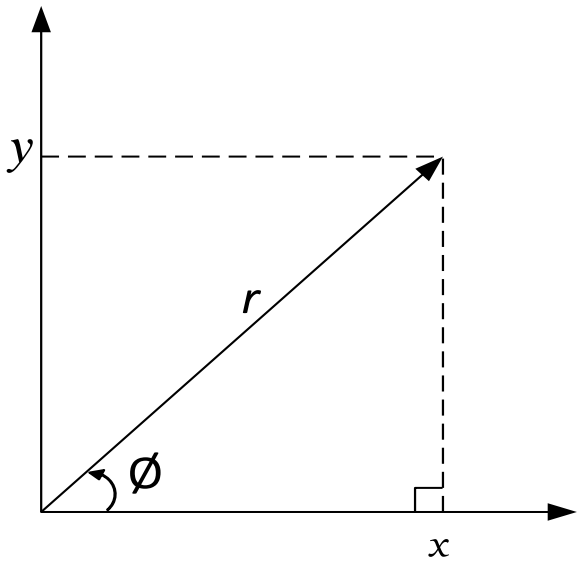

Figure 4.2: Sine and cosine functions.

$$\sin\emptyset = \frac{y}{r} \tag{4.3}$$

$$y = r\sin\emptyset. \tag{4.4}$$

For cosine

$$\cos \emptyset = \frac{x}{r} \tag{4.5}$$

$$x = r \cos \emptyset. \tag{4.6}$$

The triangle appeared of the first quadrant of length x and y, and hypotenuse of length r. The angle of sine described as y/r and cosine described as x/r. A complex number is an obtained couple from real numbers expressed as:

$$D = (x, y) \tag{4.7}$$

where is *D* the real part and y the imaginary part. Algebraically the following is noted:

$$(D, y) = D + iy = D + iy, \quad \text{which is } i = j = \sqrt{-1}. \tag{4.8}$$

Recall that $j^2 = (\sqrt{-1})^2 = -1$. The rectangular model of a complex number is determined [53]:

$$x = (D, y) = D + jy = D + iy \tag{4.9}$$

The polar form is given as:

$$x = re^{j\emptyset} = r\angle\emptyset = |x|e^{j \arg D} \tag{4.10}$$

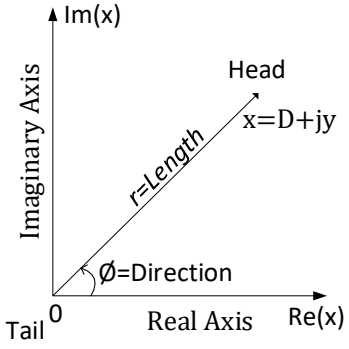

Figure 4.3: complex number as a vector.

Example 4.1

For complex numbers as, 1- $D = 2 + j5$. 2- $D = 4 - j3$. 3- $D = -5 + j0$. 4- $D = -3 - j3$.

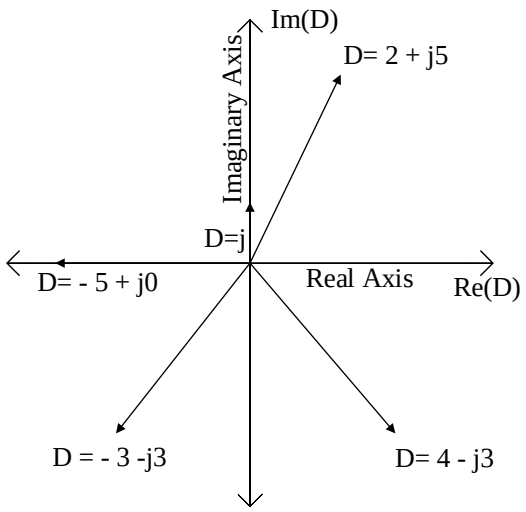

Figure 4.4: complex number of z=2+j5, =4-j3, z=-5+j0, and z=-3-j3.

Example 4.2

For complex numbers as 1- $x = 2\angle 45^{\circ}$, 2 - $x = 3\angle 150^{\circ}$, 3 - $x = 3\angle -80^{\circ}$.

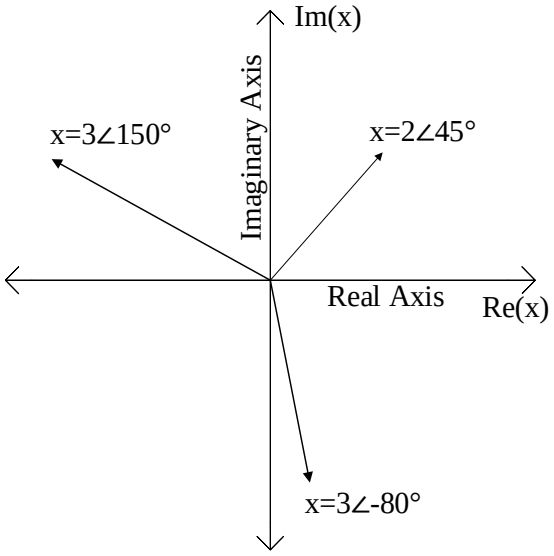

Figure 4.5: Complex number of x=2∠45°, x=3∠150°, and x=3∠-80°.

4.2 Describing Function (DF)

Nikolay Bogoliubov developed the describing function approach in 1930s [54] - [56]. It is a standard method for investigating limit cycle instabilities in a nonlinear system. The DF of a nonlinear component is comparable to the transfer function of a linear component. However, the DF leads to simplistic analyses and synthesis methods for nonlinear systems. Therefore this research developed an improved method of the input-output characteristics that encompass nonlinear dc-dc converters. The PWM duty-cycle command is considered as the input:

$$x(t) = A\sin(\omega t) \tag{4.11}$$

and the output signal (converter output voltage under load) is given by its Fourier decomposition:

$$y(t) = \frac{a_0}{2} + \sum_{n=1}^{\infty}(a_n\cos(n\omega_t t) + b_n\sin(n\omega_t t)) \tag{4.12}$$

The Fourier description includes the dc offset $a_0 = 0$ which corresponds to a nominal dc boost gain for a dc-dc converters considered in this research. Using the first harmonic $n = 1$ of the Fourier series of the signal is:

$$\frac{y(t)}{x(t)} = \frac{a_1\cos(\omega_t t) + b_n\sin(\omega_t t)}{A\sin(\omega t)}\,. \tag{4.13}$$

Applying the trigonometric identity:

$$a_1\cos(\omega_t t) + b_n\sin(\omega_t t) = \sqrt{a_1^2 + b_1^2}\sin(\omega_t t + \emptyset) \tag{4.14}$$

where is $\emptyset = \tan^{-1}\frac{a_1}{b_1}$

$$\frac{y(t)}{x(t)} = \frac{\sqrt{a_1^2 + b_1^2}\sin(\omega_t t + \emptyset)}{A\sin(\omega t)}\,. \tag{4.15}$$

The conventional describing function $N(A,\omega)$ is determined the ratio of the phasor description of input element and output element by frequency ω [57].

$$N(A,\omega)=\frac{\left(\sqrt{a_1^2+b_1^2}\right)e^{j(\omega t+\emptyset)}}{Ae^{j\omega t}}=\frac{1}{A}(b_1+ja_1) \tag{4.16}$$

where a_1 and b_1 are coefficients from the first harmonic of Fourier description provided as [58]:

$$a_1=\frac{\omega}{\pi}\int_0^{2\pi/\omega} y(\tau)\cos(\omega\,\tau)\,d\tau, \tag{4.17}$$

$$b_1=\frac{\omega}{\pi}\int_0^{2\pi/\omega} y(\tau)\sin(\omega\,\tau)\,d\tau \tag{4.18}$$

By substitution for a_1 and b_1

$$N(A,\omega)=\frac{\omega}{\pi A}\int_0^{2\pi/\omega} y(\tau)\sin(\omega\,\tau)\,d\tau+\frac{j\omega}{\pi A}\int_0^{2\pi/\omega} y(\tau)\cos(\omega\,\tau)\,d\tau. \tag{4.19}$$

4.2.1 PWM Effects

The effects of PWM harmonics challenging in order to achieve a good overall accounting for the nonlinear behavior of the overall system.

Example: PWM harmonic elements with fundamental of peak magnitude as:

$$h_1=\left(4\frac{E}{\pi}\right)[1-2\cos\alpha_1+2\cos\alpha_2-2\cos\alpha_3\cdots 2\cos\alpha_n] \tag{4.20}$$

$$h_2=\left(4\frac{E}{2\pi}\right)[1-2\cos 2\alpha_1+2\cos 2\alpha_2-2\cos 2\alpha_3\cdots 2\cos 2\alpha_n] \tag{4.21}$$

$$\vdots$$

$$h_m=\left(4\frac{E}{m\pi}\right)[1-2\cos m\alpha_1+2\cos m\alpha_2-2\cos m\alpha_3\cdots 2\cos m\alpha_n] \tag{4.22}$$

where E is the dc bus voltage, h_m represents the magnitude of m , and α_n switching angles. The period of 2π Fourier coefficients are represented as:

$$a_0 = \frac{1}{2\pi}\int_0^{2\pi} f(\theta)d\theta, \tag{4.23}$$

$$a_k = \frac{1}{\pi}\int_0^{2\pi} f(k\theta)\cos(k\theta)\,d\theta, \tag{4.24}$$

$$b_k = \frac{1}{\pi}\int_0^{2\pi} f(k\theta)\sin(k\theta)\,d\theta. \tag{4.25}$$

Based on symmetry, a quarter-cycle is determined by the Fourier coefficients as fowling [59]:

$$b_k = \frac{4}{\pi}\int_0^{2\pi} f(k\theta)\sin(k\theta)\,d\theta, \tag{4.26}$$

$$b_n = \left(4\frac{E}{\pi}\right)\left[\int_0^{\alpha_1}\sin(k\theta)\,d\theta - \int_{\alpha_1}^{\alpha_2}\sin(k\theta)\,d\theta + \int_{\alpha_2}^{\alpha_3}\sin(nk)\,d\theta \cdots \int_{\alpha_n}^{\frac{\pi}{2}}\sin(k\theta)\,d\theta\right]$$

$$= \left(4\frac{E}{\pi}\right)\left[-\cos k\theta|_0^{\alpha_1} + \cos k\theta|_{\alpha_1}^{\alpha_2} - \cos k\theta|_{\alpha_2}^{\alpha_3}\ldots\right]$$

$$= \left(4\frac{E}{m\pi}\right)[1 - 2\cos m\alpha_1 + 2\cos n\alpha_2 - 2\cos n\alpha_3 \cdots 2\cos n\alpha_m]. \tag{4.127}$$

4.2.2 DC-DC Converter Nonlinear Modeling with New Describing Function

The following is a new type of describing function technique compared to traditional methods as in [60]. Considering the input of the nonlinear behavior is x_{in} and the output is y_{out}. The input-output behavior of a nonlinear model for the converter is assumed by replacing the describing function definition for the nonlinearty of the converter as shown in Figurer 4.6.

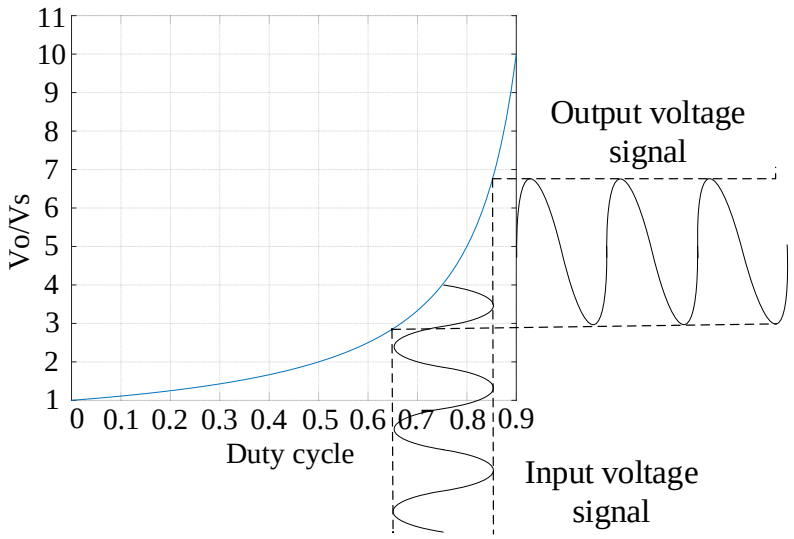

Figure 4.6: Boost curve and sine input-output.

The modified describing function method defines the model based on the input of the switching of the dc-dc converter output voltage. The input contains a low frequency sinusoidal signal (PWM duty cycle) as $v_c = V_{c+} v_{ci} \sin(\omega_c t)$ is compared with a high frequency carrier (saw tooth or triangular waveform). This produces a switching a waveform of $v_c(t)$ with the amplitude of V_c. The output voltage signal of the converter is $v_o(t) = v_m \sin(\omega_c t + \theta)$. The modified describing function is defined as $(j\omega) = \frac{v_m e^{j\theta}}{v_{ci}}$, which is defined as a Fourier series:

$$v_o(t) = a_0 + \sum_{n=1}^{\infty} (a_n \cos \omega_t t + b_n \sin \omega_t t), \tag{4.28}$$

$$a_n = \frac{2}{T_x} \int_0^{T_x} v_o(\tau) \cos \omega \tau \, d\tau, \tag{4.29}$$

$$b_n = \frac{2}{T_x} \int_0^{T_x} v_o(\tau) \sin \omega \tau \, d\tau, \tag{4.30}$$

It is found that

$$v_m e^{-i\theta} = \frac{2}{T_x}\int_0^{T_x} v_o(\tau) e^{-i\omega\tau} d\tau, \tag{4.31}$$

where T_x is the one period.

4.2.3 Property of Modified Describe Function

The modified DF (MDF) in this research accounts for the nonlinear boost characteristics of the converter. It is defined as linearization and minimization of the mean-squared approximation error, which results from the analysis.

$$\overline{e^2} = \frac{\omega}{2\pi}\int_0^{2\pi/\omega} e^2(t) dt \tag{4.32}$$

where

$$e = y\,(x, \dot{x}) - y_{approx}(A, \omega) \tag{4.33}$$

$$= y\,(A\sin\emptyset, A\omega\cos\emptyset) - A_{pN}\sin(\omega t + \vartheta_N), \tag{4.34}$$

where PN is gain and ϑ_N, for stationary point as:

$$\frac{\partial\overline{e^2}}{\partial_{PN}} = \frac{\partial\overline{e^2}}{\partial\vartheta_N} = 0. \tag{4.35}$$

By differentiation respect to *PN*:

$$PN = \frac{\omega}{A\pi}\int_0^{2\pi/\omega} y(A\sin\emptyset, A\omega\cos\emptyset)\sin(\omega t + \vartheta_N)\, dt\,, \tag{4.36}$$

and by differentiation respect to ϑ_N:

$$\frac{\omega}{A\pi}\int_0^{2\pi/\omega} y(A\sin\emptyset, A\omega\cos\emptyset)\cos(\omega t + \vartheta_N)\, dt = 0 \tag{4.37}$$

and combining results in

$$PN = \frac{\omega}{A\pi}\int_0^{2\pi/\omega} y(A\sin\emptyset, A\omega\cos\emptyset)\,[\sin(\omega t + \vartheta_N) + j\cos(\omega t + \vartheta_N)]\,dt \tag{4.38}$$

$$j\frac{\omega}{A\pi}e^{-j\vartheta_N}\int_0^{2\pi/\omega} y(A\sin\emptyset, A\omega\cos\emptyset)e^{-i\omega t}dt. \tag{4.39}$$

4.2.4 Harmonic of Nonlinearity

The MDF represents the fundamental harmonic gain with inclusion on nonlinearities. The input-output gain due to nonlinearities from a sinusoid input with dc offset has been analyzed as an average of the effects of Fourier components. Therefore, when the input sinusoid represents the fundamental harmonic gain of the real nonlinearities as $v_c = V_{c+}v_{ci}\sin(\omega_c t)$. The MDF for harmonic nonlinearities is represented by [62]:

$$\begin{aligned} N(A) &= \frac{4}{A\pi}\int_0^{\pi/2} y(A\sin\emptyset)\sin\emptyset\, d\emptyset \\ &= \frac{4(V_{c+}v_{ci})}{A\pi}\int_0^{\pi/2} \sin(\omega_c\sin\emptyset)\sin\emptyset\, d\emptyset \\ &= \frac{2(V_{c+}v_{ci})j(\omega_c)}{A} \end{aligned} \tag{4.40}$$

where $(V_{c+}v_{ci})j$ is the Bessel functions.

4.2.5 Accuracy

Accuracy in the modeling of dynamical systems is an essential part in designing control systems. However, system analysis and identification utilizing conventional integer order differential equations has limitations ([63] - [68]) in systems that exhibit fractional order behavior [65].

4.3 Harmonic-Based Fractional Oder Modelling

The previous analysis assumed the availability of the fast Fourier transform (FFT) as a method to quickly analyze large amounts of input-output data. Another use of the FFT is to improve the accuracy of multiplication of high-degree order polynomials. This can be leverage to improve the ability to derive an equivalent fractional order transfer function realization that can be used in control system design. Transfer function polynomials coefficients, p and q are [69]:

$$\begin{aligned} r(x) = p(x)q(x) &= \left(\sum_{m=0}^{N-1} f_m x^m\right)\left(\sum_{n=0}^{N-1} g_n x^n\right) \\ &= (f_o + f_1 x + f_2 x^2 + \cdots)(g_o + g_1 x + g_2 x^2 + \cdots) \\ &= f_o g_o + (f_o g_o + f_1 g_o)x + (f_o g_2 + f_1 g_1 + f_2 g_o)x^2 + \cdots \\ &= \sum_{m=0}^{2N-2} h_m x^m \end{aligned} \tag{4.41}$$

Whereas, $\sum_{i=0}^{N-1} f_i g_{n-i}$ and $h = f \circledast g$. Therefore, calculating the production of polynomials includes the convolution of the coefficient sequence.

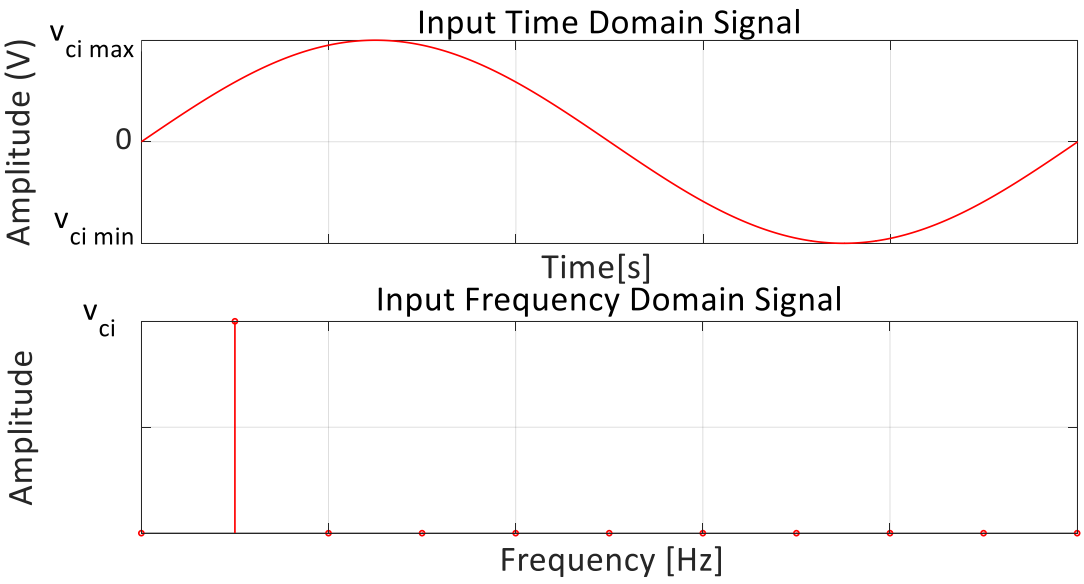

Figure 4.7: Fast Fourier Transform for input.

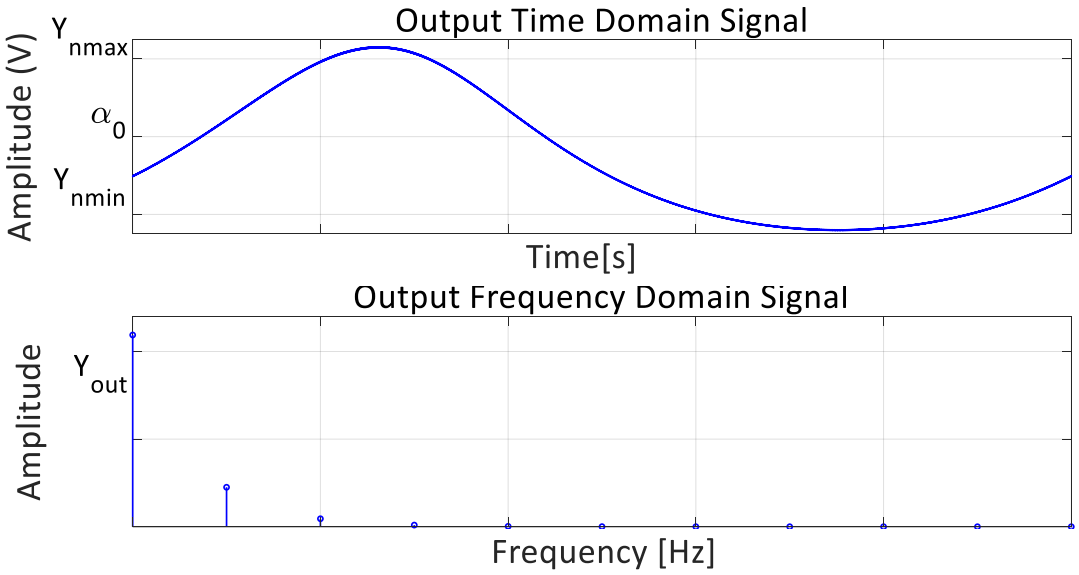

Figure 4.8: Fast Fourier Transform for output.

The amplitude for the input switching sinusoidal signal and output voltage across the load is utilizing by an FFT as shown in the Figs. 4.7 - 4. 8.

4.4 The Bode Plot

The Bode plot is description of the frequency response behavior of the system. A general example of the magnitude and phase plots are shown as in Fig. 4.9:

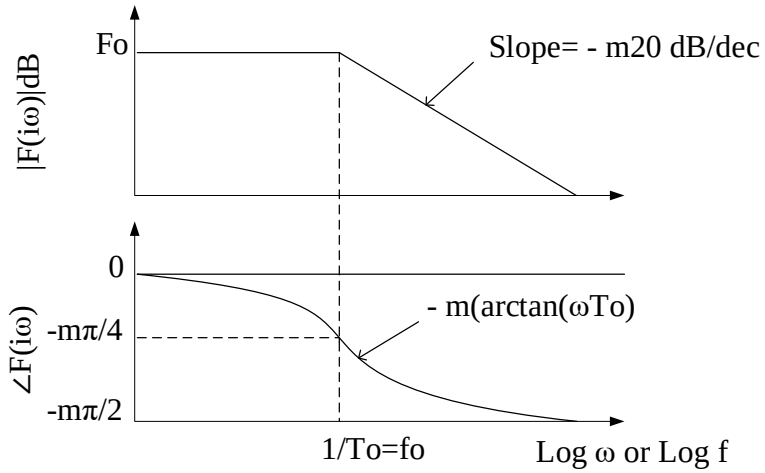

Figure 4.9: The magnitude in dB and phase angle in degree.

The first plot shows the magnitude in decibels (dB) [70] and the second plot is r the phase shift in radians. The construction of Bode plots for integer order transfer functions is explained in [71], with dB log scale

$$Lm(K) = 20\log|K| \tag{4.42}$$

where Lm is magnitude, and K is constant. For log of the magnitude and the phase shift.

$$Lm(j\omega)^{\mp k} = \mp 20k\log\omega, \tag{4.43}$$

$$\angle(j\omega)^{\mp} = \mp\frac{k\pi}{2}, \tag{4.44}$$

where the slope is $\mp 20k$ dB/decade and the phase shift $\mp\frac{k\pi}{2}$ is constant. For complex numbers $z = a + bj \in \mathbb{C}$ and $a, b \in \mathbb{R}$, $|z| = \sqrt{a^2 + b^2}$ and $\angle z = \tan^{-1}\frac{\mathrm{Im}\, z}{\mathrm{Re}\, z} = \tan^{-1}\frac{b}{a}$.

$$Lm(1+j\omega T)^{-1} = [20] * \log\left|\frac{1}{1+j\omega T}\right|, \tag{4.45}$$

$$= [20] * \log\left|\frac{1-j\omega T}{1+j\omega T}\right|, \tag{4.46}$$

$$= [20] * \log\sqrt{\frac{1}{(1+\omega^2T^2)^2} + \frac{\omega^2T^2}{(1+\omega^2T^2)^2}}, \tag{4.47}$$

$$= [20] * \log\sqrt{\frac{1}{(1+\omega^2T^2)}}, \tag{4.48}$$

$$= [-20] * \log\sqrt{1+\omega^2T^2} \tag{4.49}$$

$$\angle(1+i\omega T)^{-1} = \tan^{-1}\frac{-\omega T}{1} = -\tan^{-1}\omega T. \tag{4.50}$$

For log magnitude and phase shift by $e^{\mp j\omega t}$

$$Lme^{\mp i\omega t} = [20] * \log\left|e^{\mp j\omega t}\right|$$

$$= [20] * \log|\cos(\mp\omega t) + j\sin(\mp\omega t)|$$

$$= [20] * \log 1 = 0 \tag{4.51}$$

$$\angle e^{\mp i\omega t} = \tan^{-1}\frac{\sin\mp\omega t}{\cos\mp\omega t} = \mp\omega t. \tag{4.52}$$

At 0 dB the magnitude is equal to one, which is the magnitude plotted of a horizontal line and the phase shift is corresponded to the frequency ω.

4.5 Approximation of Fractional Order Systems

The rational approximation of the higher order transfer functions is employed in order to increase the modeling accuracy. The approximation of fractional order transfer functions can be

applied on continuous-time and discrete-time systems. The fractional-order approximation method is detailed in [72], [73].

4.5.1 Oustaloup's Method

Oustaloup's recursive filter is provides a band-limited version of fractional-order (FO) elements. The frequency range is (ω_b, ω_h), with operation as $s^\gamma, 0 < \gamma < 1$ and order N as:

$$G_f(s) = K \prod_{m=-N}^{N} \frac{s + \omega'_m}{s + \omega_m}, \tag{4.53}$$

where

$$\omega'_m = \omega_b \left(\frac{\omega_h}{\omega_b}\right)^{\frac{m+N+\frac{1}{2}(1-\gamma)}{2N+1}}, \tag{4.54}$$

and

$$\omega_m = \omega_b \left(\frac{\omega_h}{\omega_b}\right)^{\frac{m+N+\frac{1}{2}(1+\gamma)}{2N+1}}, \quad K = \omega_h^\gamma. \tag{4.55}$$

When the output is considered as an approximation of the fractional differentiated or integrated signal, the Oustaloup filter is purposed as [74] [75]:

$$s^\alpha \approx \left(\frac{d\omega_h}{b}\right)^\alpha \left(\frac{ds^2 + b\omega_h s}{d(1-\alpha)s^2 + b\omega_s s + d\alpha}\right) \prod_{m=-N}^{N} \frac{s + \omega'_m}{s + \omega_m}, \tag{4.56}$$

where

$$\omega'_m = \left(\frac{d\omega_b}{b}\right)^{\frac{\alpha-2m}{2N+1}}, \omega_m = \left(\frac{b\omega_b}{d}\right)^{\frac{\alpha+2m}{2N+1}}. \tag{4.57}$$

Applying the Oustaloup filter is often recommended to obtain a good results with b = 10 and d = 9. For fractional orders $\alpha \geq 1$:

$$s^{\alpha} = s^{m} s^{\gamma}, \tag{4.58}$$

where $m = \alpha - \gamma$ indicates the integer term of α and the Oustaloup Approximation is represented by s^{γ}.

4.5.2 Levy's method

Levy's method of least-squares fitting of data can be extended to fractional-order functions. This includes transfer function approximations applying the input and output as in [76]:

$$\emptyset_j = \left|e_j\right| \sin\left(\omega t + \vartheta_j\right) \tag{4.59}$$

and

$$\emptyset_0 = |e_0| \sin(\omega t + \vartheta_0) \tag{4.60}$$

where $\frac{E_0(\omega)}{E_j(\omega)}$ amplitude ratio and $\theta_0(\omega) - \theta_j(\omega) = \Delta\theta\,(\omega)$ for frequencies within the range of modeling concerns.

4.6 Commensurate Fractional-Order Transfer Functions

The Levy identification approach is applied for identifying the fractional-order model represented in (4.60). It calculates the parameters of data frequency response by $G(j\omega) = \Re(\omega) + j\Im(\omega)$ as in [77]:

$$\begin{bmatrix} A & B \\ C & D \end{bmatrix} \begin{bmatrix} b_0 \\ \vdots \\ b_m \\ a_1 \\ \vdots \\ a_n \end{bmatrix} = \begin{bmatrix} e \\ g \end{bmatrix}, \tag{4.61}$$

where $b_0, \ldots b_m$ and $a_1, \ldots a_n$ represents the identified parameters defined as *A, B, C, D, e* and g to obtained from the collected data [78]. The identification of fractional-order versions of the transfer function by using Levy's technique results in

$$\epsilon = \mathrm{G(j\omega)[a_n(j\omega)^{n\gamma} + \cdots + a_1(j\omega)^{\gamma} + 1] - [b_m(j\omega)^{m\gamma} + \cdots + b_1(j\omega)^{\gamma} + b_0]}. \quad (4.62)$$

The Vinagre technique supplements weights for the norm of approximation at any frequency $\epsilon' = \mathit{w} \cdot \epsilon$, whereas weight w is based on a frequency, frequencies ω_i, $i = 1, \ldots, f$ are defined as [79].

$$\mathit{w} = \begin{cases} \dfrac{\omega_2 - \omega_1}{2\omega_1^2} & ,i = 1, \\ \dfrac{\omega_{i+1} - \omega_{i-1}}{2\omega_i^2} & ,1 < i < f\,, \\ \dfrac{\omega_f - \omega_{f-1}}{2\omega_f^2} & ,i = f. \end{cases} \quad (4.63)$$

The operator must provides the commensurate order and fractional polynomial orders of *n* with m for an additional optimization of parameters $\theta = [\gamma \;\; n \;\; m\,]$. The function for minimization is of the form:

$$J = \frac{1}{n_\omega} \sum_{i=1}^{n_\omega} \left| G(i\omega) - \hat{G}(i\omega) \right|^2, \quad (4.64)$$

whereas n_ω signify the number of frequencies in ω, $\hat{G}$ denotes the identified plant *G*. The error index is utilized to calculate the identification accuracy [78] [79]. The time-domain identification is labelled as a data structure using a MATLAB (ffidata) command as follows:

id1 = ffidata(*mag, ph, w*), the mag characterizes to determine magnitude in dB, ph represents the phase angle by degree and *w* in rad/s.

5 Fractional PI Controller

There is increasing attention in using fractional calculus to control dynamical systems. After applying identification techniques to achieve the plant transfer function, the feedback control system for a non-integer order can be designed ([80], [81]). The use of a feedback controller requires measuring a performance error. This is typically determined as difference between the various outputs of the system and the desired value. The controller parameters are adjusted based on the system performance objectives such as settling time, steady-state tracking and percent overshoot ([82], [83]). The fractional-order proportional-integral (PI^{λ}) and lead-lag compensators have potential advantages compared to classical integer-order controllers ([84], [85]). Podlubny ([86]) introduced a form of the PI controller using fractional order operator as PI^{λ} (FO-PI) controller, for which an integral term of order λ is provided by assuming real-values non-integer numbers. Consideration of the general dynamical system as in [86]:

$$\dot{x}(t) = f[x(t), u(t)], \tag{5.1}$$

$$y = h[x(t)]\,, \tag{5.2}$$

where $x(t) \in \mathbb{R}^m, u(t) \in \mathbb{R}, f(x,u) \in \mathbb{R}^m \times \mathbb{R} \to \mathbb{R}^m \; and \; h: \mathbb{R}^m \to \mathbb{R}$. The control operation of the PI^{λ} controller express as following:

$$u(t) = K_p e(t) + K_i \mathcal{D}^{-\lambda} e(t), \tag{5.3}$$

where $e(t) = -y(t) + s(t)$ is an error signal and $s(t)$ is the desired control reference value. The Laplace transform is applied with zero initial conditions. The fractional order (FO) order controller has shown advantages compared to conventional integer order controllers [87].

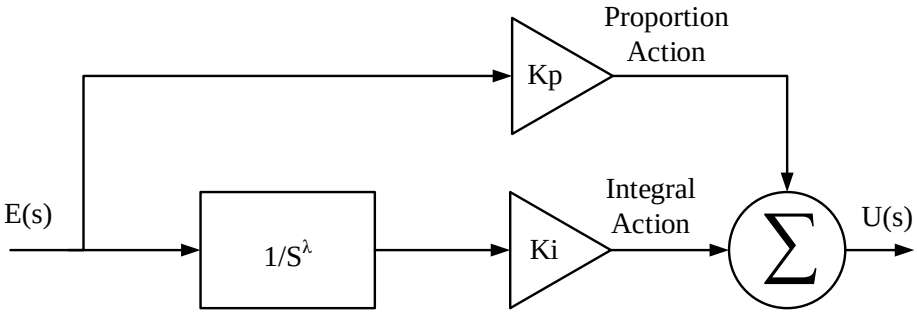

Figure 5.1: Fractional-order proportional and integrator controller model.

The transfer function of the FO PI$^{\lambda}$ controller general expression is

$$G_c(s) = K_p + \frac{K_i}{s^{\lambda}} \tag{5.4}$$

where K_p, and K_i are the proportional and integral gains, respectively, of the PI$^{\lambda}$controller. The PI$^{\lambda}$ controller retains the general properties of the integer order PI controller. The advantages of additional parameter λ is that it provides additional freedom in designing the controller. The fractional PI controller is particularly advantageous to for nonlinear systems. However, the tuning of the controller of the FO controller is more complicated compared to a conventional PI element. The representation of fractional-order proportional-integral-derivative (FO-PID) controller

$$G_c(s) = K_p + \frac{K_i}{s^{\lambda}} + K_d s^{\mu}, \tag{5.5}$$

can similarly be defined. For the PI$^{\lambda}$ controller, the effect of $\frac{1}{s^{\lambda}}$ is to produce an integral effect to guarantee there is no residual error in the closed-loop system [83].

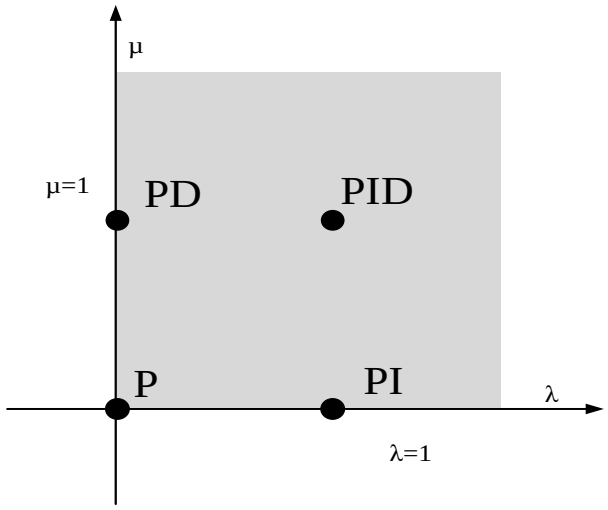

Figure 5.2: The $PI^{\lambda}D^{\mu}$ controller plane.

It is noted that selecting $\lambda = \mu = 1$ resulting that is classic integer-order PID controller. The FO-PI controller has more freedom of tuning the controller, duo to the additional parameter such λ and μ. The PID controller plane of the four-point PID diagram as showing in Figure 5.2. However, the derivative term μ will not be considered in this research due to noise present in switched-mode power converters that results in poor results for PID controllers.

5.1 Fractional Order Robust Control

The robustness of the fractional order controllers is particularly effective when there are uncertainties and the toleration of error. Research in the advances of fractional controllers is demonstrated in the robustness of tuning FO-PI controller and the H_{∞} controller in [88]. Tavazoei proposed designs for robust control with constant phase margin using FO models [89]:

$$G(s) = (hs^{\alpha} + L)\hat{G}^{-1}(s), \tag{5.6}$$

with feedback for the resulting FO system:

$$G(s) = \frac{1}{Ts^{\beta} + 1}\hat{G}(s), \tag{5.7}$$

where $\beta \in (0,2)$ and $T > 0$, is the relationship between the gain (0 dB) crossover frequencies and phase margins. Extending integration and derivative control operations is used in the fractional operation is given in [90] as

$$C(s) = Ks^{\gamma}, \tag{5.8}$$

where $\gamma \in [-1: 1]$ the fractional integrator.

Example 5.1

Consider an integer-order system with given transfer function as the following:

$$G(s) = \frac{1}{(s+1)^3}, \tag{5.9}$$

with a FO-PI controller as:

$$C(s) = K_p\left(1 + \frac{1}{T_j s^{\lambda}}\right) \tag{5.10}$$

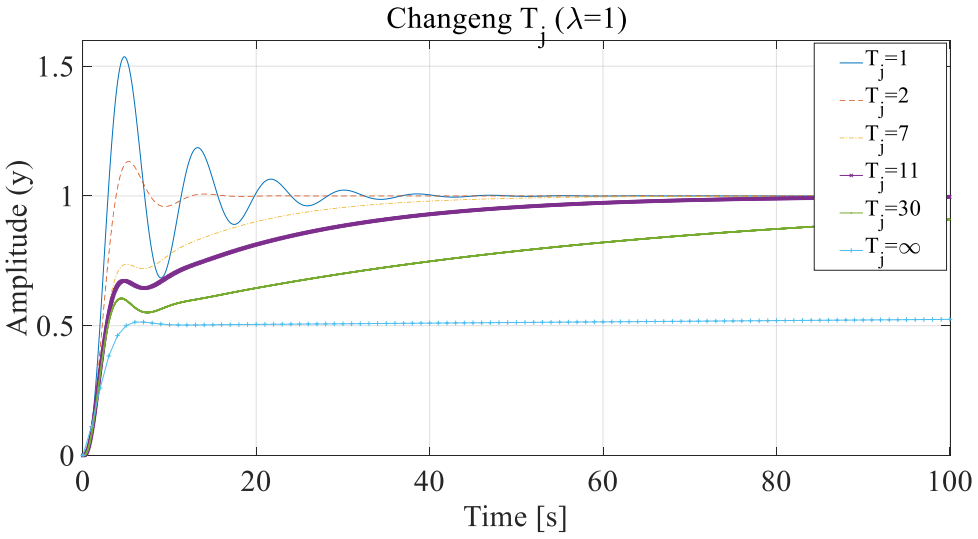

Figure 5.3: Step responses FOPI with variant integral of Tj.

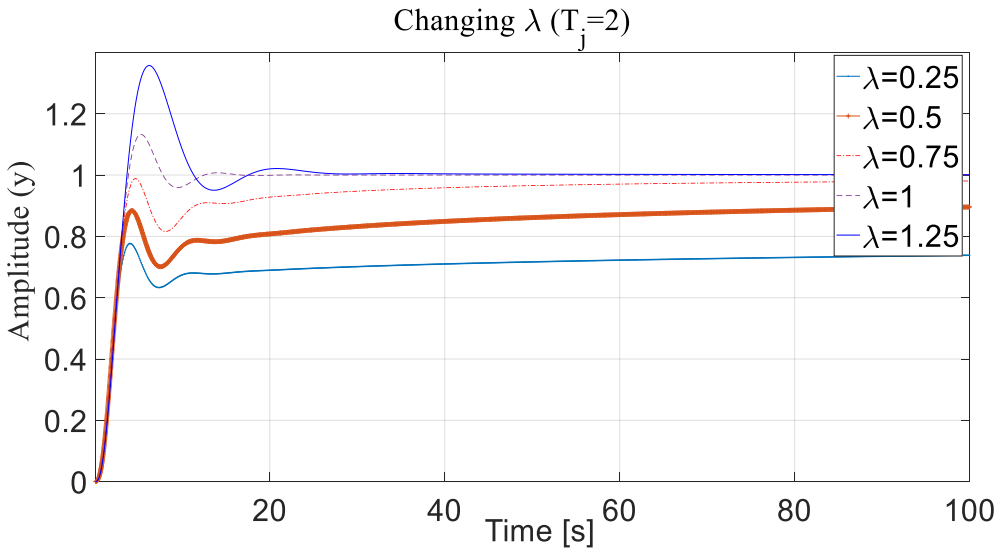

Figure 5.4: Step responses FO PI controller with variant integration order λ.

To demonstrate the characteristics of integration part with fractional order is shown in Figure 5.3 and Figure 5.4, which presents unit step response for the closed-loop of the system. Selecting proportional gain is $K_p = 1$ as a fixed value but the integral time of T_j are varied independently (Fig. 5.3 - 5.4). The integer case of $\lambda = 1$ are considered in Figure 5.3, with a steady-state error approaching zero. Furthermore, when T_j small there is a faster response with larger oscillatory overshoots. In Figure 5.4, T_j is constant with varied λ showing that the parameter does not affect oscillations. Overall, the FO-PI controller shows improved capability for tuning the systems response.

5.2 Optimization Controller Design

There are many perspectives that make designing a FO-PI controller difficult. Nevertheless, several approaches for tuning techniques have been developed ([91] – [92]). The most common optimization criteria is to minimize the integral squared error:

$$ISE = \int_0^t e^2(t)dt. \tag{5.13}$$

Also considered are the integral absolute error,

$$IAE = \int_0^t |e(t)|dt, \tag{5.14}$$

the integral time-square error as,

$$ITSE = \int_0^t te(t)^2 dt, \tag{5.15}$$

And the integral time-absolute error as:

$$ITAE = \int_0^t t|e(t)\,|dt. \tag{5.16}$$

The frequency domain specifications provide accuracy and stability for the control system. However, specifications can be commanded of open-loop frequency response $F(j\omega) = C(j\omega)G_p(j\omega)$, where is $C(j\omega)$ a FO-PI controller [93], with gain margin A_m:

$$A_m = 1 - \left|F\left(j\omega_g\right)\right|, \tag{5.17}$$

$$\arg\left(F\left(j\omega_g\right)\right) = -\pi. \tag{5.18}$$

Phase margin φ_m and critical frequency ω_c are given by

$$\arg\left(F(j\omega_c)\right) = -\pi + \varphi_m\,, \tag{5.19}$$

$$|F(j\omega_c)| = 1. \tag{5.20}$$

Gain variation for a plant robustness is defined by

$$\left.\frac{d\arg\left(F(j\omega)\right)}{d\omega}\right|_{\omega=\omega_c} = 0. \tag{5.21}$$

Noise rejection at high frequency is specified by

$$\left| T(j\omega) = \frac{F\ (j\omega)}{1 + F\ (j\omega)} \right|_{\text{dB}} \leq N \text{ dB}, \tag{5.22}$$

where frequencies $\omega \geq \omega_t$ rad/s, and N dB is noise attenuation.

Disturbance rejection is defined as

$$\left| C(j\omega) = \frac{F\ (j\omega)}{1 + F\ (j\omega)} \right|_{\text{dB}} \leq K \text{ dB}, \tag{5.23}$$

where K dB is a constraint on the sensitivity function.

Example 5.6

A dc-dc converter fractional order transfer function is modeled by a fractional-order differential equation. The fractional transfer function and controller is determined to be

$$G(s)_{FO} = \frac{-0.323s^{0.78} - 15.58s^{0.52} - 96.03s^{0.26} + 340.9}{0.00156s^{1.3} - 0.02s^{1.04} - 0.1002s^{0.78} + 0.295s^{0.52} - 0.67s^{0.26} + 1}, \tag{5.24}$$

$$C_{FO}(s) = K_p + \frac{K_i}{s^{\lambda}}. \tag{5.25}$$

Applying the Ziegler-Nichols PI tuning method, PI parameters are determined as K_p = 476.7 and K_i = 0.011 where λ is the parameter for optimizing the performance.

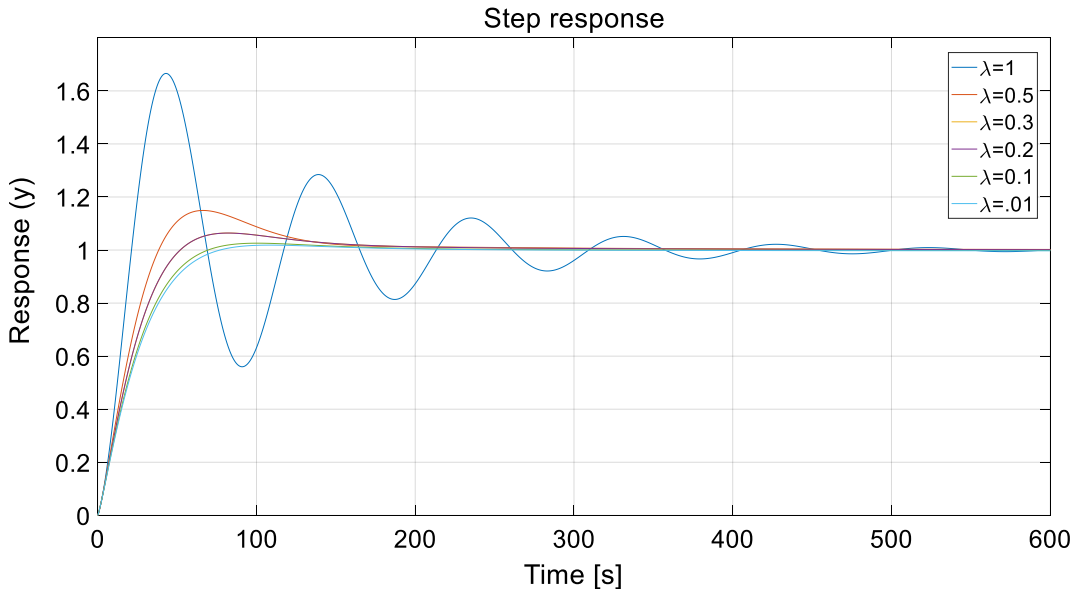

Figure 5.5: Closed loop step responses for $G_{FO}(s)$ under various λ.

5.3 FO-PI Tuning Formulation

The transfer function of the open-loop is represented by its Bode plot. Designing the feedback FO-PI controller as [80]:

$$G_{ref}(s) = \frac{K_r}{s^{\lambda}}, \qquad (1 < \lambda < 2) \tag{5.26}$$

Achieving the best performance of the feedback loop controller is investigated. With respect to the Bode plot:

Magnitude curve is constant slope of -20λ dB/dec, the critical pint of $\omega_c = (Kr)^{\frac{1}{\lambda}}$

Phase angle curve is horizontal at $-\frac{\lambda\pi}{2}$

Nyquist curve line at arg $-\frac{\lambda\pi}{2}$

These are shown in Figure 5.6 . Robustness of the closed-loop system is achieved when the loop gain achieves [80]

$$G_{refCL}(s) = \frac{1}{\left(\frac{1}{K_r}\right)s^{\lambda} + 1}. \tag{5.27}$$

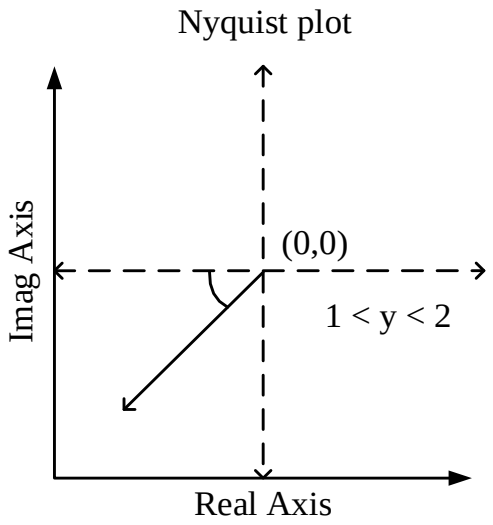

Figure 5.6: Nyquist Bode plot of ideal transfer function.

5.4 Gain Scheduling Methods

Gain scheduling methods assist in obtaining robust controller operation for a wider range of operating conditions. A fractional-order transfer equation can be achieved for a set of operating points $\{(u_k;\ y_k), k\ =\ 1, 2, \dots, n\}$ for the system [87] as the set

$$\Psi = \{G_1, G_2, \dots, G_n\}, \tag{5.28}$$

where $G_i \in \Psi$ narrowly meets a set of performance designations

$$\Omega = \{C_1, C_2, \dots, C_n\}. \tag{5.29}$$

Considering a controller defined as

$$\Upsilon(x,f) = \sum_{s=1}^{k} \beta_k(x) C_s(f), \tag{5.30}$$

where β_s is weighting function and $x(t)$ is scheduled state, $C_s(f) \in \Omega$. suppose that it is given that $k = 2$. Then the following controller is defined as

$$\Upsilon(x,f) = \beta_1(x) C_1(s) + \beta_2(x) C_2(f), \tag{5.31}$$

where $x(t) \in [0, x_{max}]$ and that

$$\beta_1(x) := \frac{[1 - \lambda(x)]}{2}, \tag{5.32}$$

$$\beta_2(x) := \frac{\lambda(x)}{2}, \tag{5.33}$$

$$\lambda(x) := \frac{x(t)}{x_{max}}. \tag{5.34}$$

5.5 Linear Quadratic Regulator (LQR) Design

The LQR design is a commonly used approach in an optimal control design. The LQR design method provides assurances for phase and gain margins, and some tolerance for nonlinearities [94]. Connections between robustness and LQR designs have been established ([95], [96]). The LQR design technique adds additional state variable as:

$$\dot{x}_1 = e(t) = V_{ref} - V_{out} \tag{5.35}$$

Consideration of the tracking error is given by an integral term,

$$x_1 = \int e(t). \tag{5.36}$$

Optimization with respect to the input is minimized by the cost function

$$J(t) = \int_0^{\infty} (z^T Q z + v^2) dt, \tag{5.37}$$

where Q represents a symmetric positive semidefinite matrix and is often selected as $Q = diag(q1, q2, q3)$. The q_i parameters are adjustable to meet a particular performance objective. The design of a closed-loop controller for a dc-dc converter is given in Figure 5.7.

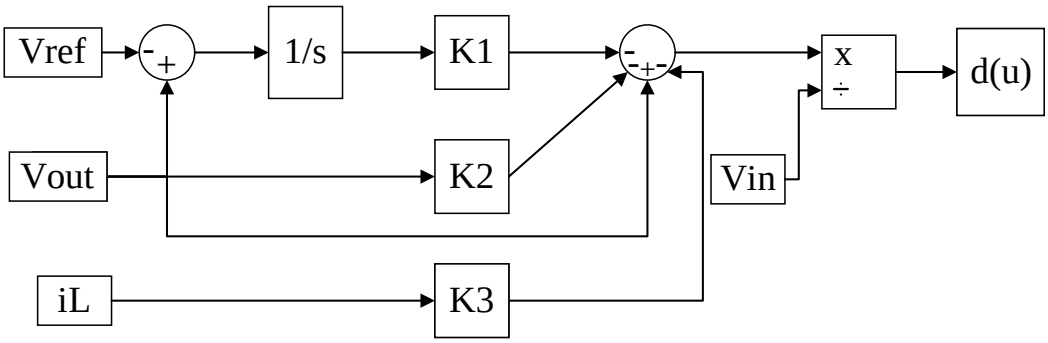

Figure 5.7: Control diagram of voltage to dc-dc converter.

The controller for a dc-dc converter is often configured with an inner and outer loop feedback path. The inner-loop is controlling the inductor current which is tracked as a reference value

$$\dot{x}_1 = e(t) = i_{lref} - i_l, \tag{5.38}$$

Where an augmented state variable is defined from the tracking error as:

$$x_1 = \int e(t), \tag{5.39}$$

The current controller is shown in Figure 5.8.

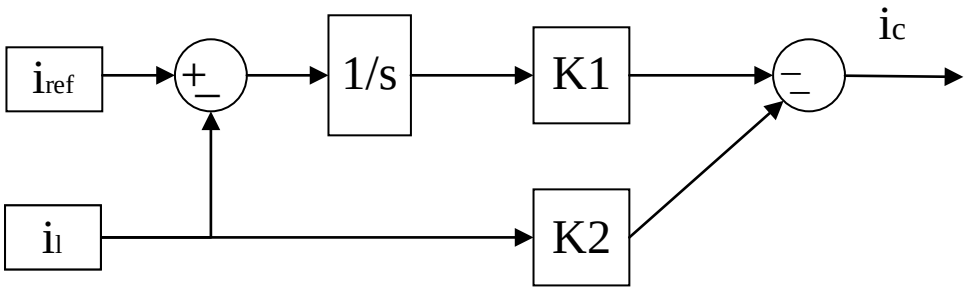

Figure 5.8: Inner current control for converter.

The outer-loop is controlling output voltage of the converter. The LQR design technique defines an error state as

$$\dot{x}_1 = e(t) = V_{ref} - V_{out}\,. \tag{5.40}$$

with an additional state variable of the tracking error as

$$x_1 = \int e(t). \tag{5.41}$$

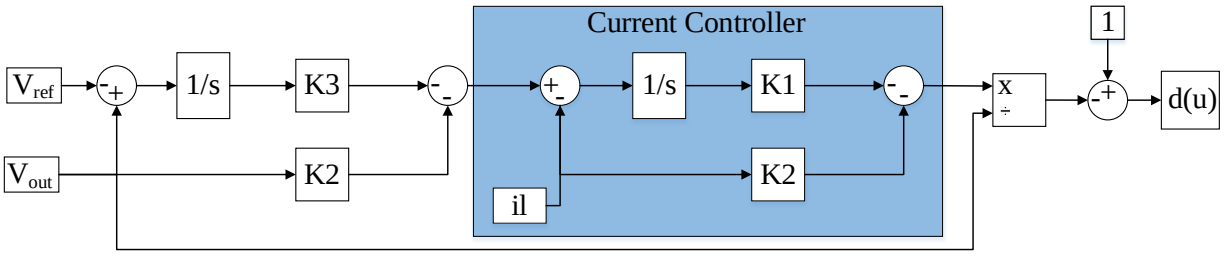

Figure 5.9: Control diagram of inner loop and outer loop controller.

5.5.1 First Order Plus Dead Time (FOPDT)

The (FOPDT) models are commonly applied in machine control design [94]. As an example,

$$G(j\omega) = \frac{Ke^{-Lj\omega}}{T(j\omega)+1}, \tag{5.35}$$

where K is the static gain of the model:

$$K = \frac{\Delta y}{\Delta u}, \tag{5.36}$$

where Δy is the incremental change of the output and Δu an incremental change of the input. Lag L is defined as

$$L = t_u - t_r, \tag{5.37}$$

where t_u the time instance of the control input, and t_r is the time instance of system output. Define the control dead-band as

$$\delta = \{(1-\gamma)u_s, (1+\gamma)u_s\}, \ \ \gamma \in (0,1) \tag{5.38}$$

where u_s represents the current steady-state control. A control input signal is defined as:

$$u(t) = \mp\delta \tag{5.39}$$

After many cycles, the ultimate gain A_u and final period T_u are determined as an ultimate frequency ω_u:

$$\omega_u = \frac{2\pi}{T_u}, A_u = \frac{4\delta}{\pi a}. \tag{5.40}$$

5.5.2 The Fractional First Order Plu Dead-Time (FFOPDT)

The FFOPDT model is similar to the FOPDT design methods ([95], [96]). Consider the FFOPDT by

$$G(j\omega) = \frac{Ke^{-Lj\omega}}{T(j\omega)^{\alpha}+1}, \tag{5.41}$$

where it is assumed that $K > 0, L > 0, T > 0$ and $\alpha \in (0,2)$, for obtaining the magnitude and phase angle of $G(j\omega)$ from the following:

$$|G(j\omega)| = \frac{|K|}{\sqrt{1 + T^2\omega^{2\alpha} + 2T\omega^{\alpha}\cos\left(\frac{\alpha\pi}{2}\right)}}, \tag{5.42}$$

and

$$\arg\big(G(j\omega)\big) = -L\omega - \tan^{-1}\left(\frac{T\sin\left(\frac{\alpha\pi}{2}\right)}{\omega^{-\alpha} + T\cos\left(\frac{\alpha\pi}{2}\right)}\right). \tag{5.43}$$

To obtain the gain crossover frequency $|G(j\omega_c)| = 1$,

$$\omega_c = \left(\frac{\sqrt{\theta(K,\alpha)} - \cos\left(\frac{\alpha\pi}{2}\right)}{T}\right)^{\frac{1}{\alpha}}, \tag{5.44}$$

where $\sqrt{\theta(K,\alpha)} = K^2 + \cos^2\left(\frac{\alpha\pi}{2}\right) - 1 \; and \; \omega_c \in \mathbb{R}_+$.

$$\theta(K,\alpha) \geq 0, \tag{5.45}$$

$$\sqrt{\theta(K,\alpha)} - \cos\left(\frac{\alpha\pi}{2}\right) \geq 0. \tag{5.46}$$

The phase margin of the system is defined by:

$$\varphi_m = \pi - \arg\big(G(j\omega_c)\big) + 2\pi n \quad , \quad n \geq 0. \tag{5.47}$$

The transcendental equation

$$-L\omega_u - \tan^{-1}\left(\frac{T\sin\left(\frac{\alpha\pi}{2}\right)}{\omega_u^{-\alpha} + T\cos\left(\frac{\alpha\pi}{2}\right)}\right) = -\pi - 2\pi n, \tag{5.48}$$

where *n* is defined by obtaining a minimum gain margin of $1/|G(\omega_c)|$ is achieved in practice by tuning the system response [92]. It is analogous to the case of a conventional PI controller [97]. A helpful summary of accurate approximations of fractional operatives is presented in [98]. The time

constant T_c can be calculated from the frequency ω_u. The final gain of the system can be observed as:

$$T_c = \frac{\tan(\pi - L_c\omega_u)}{\omega_u}. \tag{5.49}$$

FOPI controller design seeks a suitable integrator order of λ, which can be evauated through the closed-loop gain relationship:

$$\tau_c = \frac{L_g}{L_c + L_g}, \tag{5.50}$$

where τ_c is the dead-time parameter. The approximate guideline for λ is given by:

$$\lambda = \begin{cases} 1.1 & \tau_c \geq 0.6, \\ 1.0 & 0.4 \leq \tau_c < 0.6, \\ 0.9 & 0.1 \leq \tau_c < 0.4, \\ 0.7 & \tau_c < 0.1. \end{cases} \tag{5.51}$$

The gain robustness is given by:

$$\psi_g'(\omega_c) = 0, \tag{5.52}$$

$$\psi_g(\omega) = \arg\big(C(j\omega)\big) + \arg\big(G(j\omega)\big) + \pi + 2\pi n. \tag{5.53}$$

The minimal gain margin G_m of the resulting functions can be determined from

$$k1\big(K_p, K_i, K_d\big) = |C(j\omega)| \cdot |G(j\omega)| - 1, \tag{5.54}$$

$$k2\big(K_p, K_i, K_d\big) = \arg(C(j\omega)) + \arg\big(G(j\omega)\big) + \pi - \varphi_m - 2\pi n, \tag{5.55}$$

$$k3\big(K_p, K_i, K_d\big) = \psi_{gm}'(\omega), \tag{5.56}$$

where $\omega = \omega_c$. Finding gains of the FOPI controller is notated by:

$$g = \big[\, K_p, K_i \,\big]^T. \tag{5.57}$$

To determine the control coefficients a control vector is defined with a constraint:

$$F_s = [k1(\cdot)\ k2(\cdot)]^T = 0. \tag{5.58}$$

A solution can be found numerically to the relationship

$$J\Delta g = -F_s, \tag{5.59}$$

With the control gain vector of g^+ is calculated:

$$g^+ = g + \Delta g. \tag{5.60}$$

Elements of the Jacobian matrix J are defined by

$$J_{n,1} = \frac{\partial k_n}{\partial K_p}, \tag{5.61}$$

$$J_{n,2} = \frac{\partial k_n}{\partial K_i}, \quad \text{For } n = 1,2: \tag{5.62}$$

$$J_{1,1} = \frac{A_G A_{CR}}{A_C}, \tag{5.63}$$

$$J_{1,2} = \frac{A_G A_{12}}{A_C}, \tag{5.64}$$

where $A_G = |G(j\omega)|, A_C = |C(j\omega)|,$ and $A_{CR} = C_R(\omega),$

$$A_{12} = \omega^{-2\lambda}\left(K_i + \omega^{\lambda}\cos\left(\frac{\lambda\pi}{2}\right) K_p\right), \tag{5.65}$$

$$J_{2,1} = \frac{A_{21}}{A_2}, \tag{5.66}$$

$$J_{2,2} = \frac{A_{22}}{A_2}, \tag{5.67}$$

$$A_{21} = \omega^{\lambda}\left(\sin\left(\frac{\lambda\pi}{2}\right) K_i\right), \tag{5.68}$$

$$A_{22} = \omega^{\lambda}\left(\sin\left(\frac{\lambda\pi}{2}\right) K_p\right), \tag{5.69}$$

j is determined by a stopping criterion for the iteration method,

$$\|F_s(\cdot)\|_2 < \epsilon. \tag{5.70}$$

5.5.3 Review of Conventional PI Controller Design Methods

Prior to showing the experimental results of a prototype dc-dc converter, it is important to establish a baseline reference for which the resulting FO-PI controller can be compared. The section provides a brief review of root locus based design methods for integer order PI controllers. For obtaining values for K_p and K_i , the root locus method can be applied ([101], [102], [103]):

$$\Delta(s) = 1 + \mathrm{PI(s)}\, G(s) = 0 \tag{5.71}$$

$$C(s) = K_p + \frac{K_i}{s} \tag{5.72}$$

The root locus for the open loop system (K_pG) is obtained using commercially available software tools. Specifications are usually given in terms percentage overshoot, rise time, gain margin, phase margin, and settling of time to first determine the proportional gain:

$$K_p = \overline{K_P} \tag{5.73}$$

The integral term is found from and evaluation of the characteristic equation:

$$1 + (PI)(G(s)) = 0$$

No solving for the new root locus expression where $\overline{K_P}$ is held fixed and K_m is to be determined

$$1 + \left(\frac{s\overline{K_p} + K_m}{s}\right)[G(s)] = 0 \tag{5.74}$$

$$1 + \left(\frac{s\overline{K_p} + K_m}{s}\right)[G(s)] = 0 \tag{5.74}$$

$$\overline{K_p}(G) + \frac{K_m G}{s} + 1 = 0 \tag{5.75}$$

$$\overline{K_p}\frac{N(s)}{D(s)} + \left(\frac{K_m}{s}\right)\frac{N(s)}{D(s)} + 1 = 0 \tag{5.76}$$

$$s\overline{K_p}N(s) + K_m N(s) + sD(s) = 0 \tag{5.77}$$

$$sK_p N(s) + sD(s) + K_m N(s) = 0 \tag{5.78}$$

$$1 + K_m * \frac{N(s)}{sK_p N(s) + sD(s)} \tag{5.79}$$

A root locus plot is then used to determine the integral term K_m,

$$root\ locus\left(\frac{N(s)}{sK_p N(s) + sD(s)}\right). \tag{5.80}$$

6 Simulation and Experiment Identification of DC-DC Converter

6.1 Introduction

In this research, the previously defined method for fractional order identification and control is applied to switched-mode power electronic dc-dc converters. Results confirm the benefits of the new analysis method and it applicability to the improved operation of switched-mode power converters.

6.2 Identification of a DC-DC Buck Converter

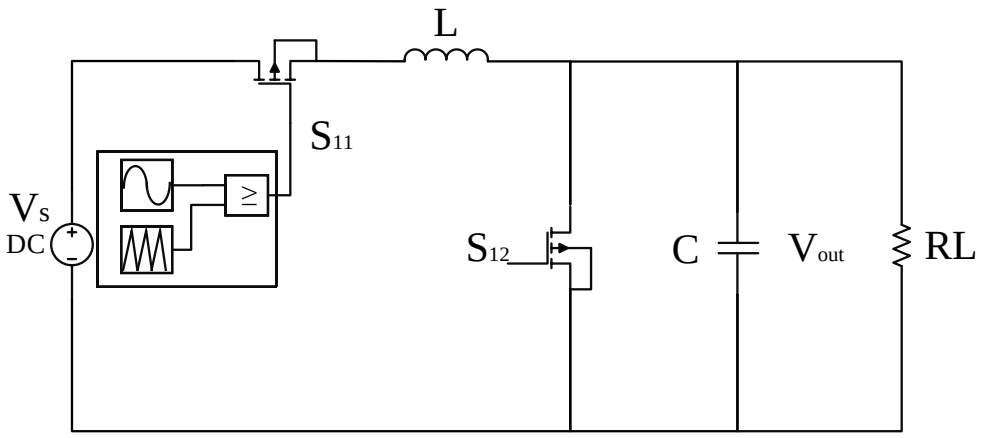

Figure 6.1: Identification of dc-dc buck converter.

The circuit configuration of the buck converter is presented in Figure. 6.1. The input voltage is a constant value of V_s=20 V. A time-varying reference signal is a combination of a dc voltage with an added sinusoidal component over a frequency range of $f = \{5 - 5\text{K}\}$ Hz. The average duty ratio is $d(t)$=0.6.

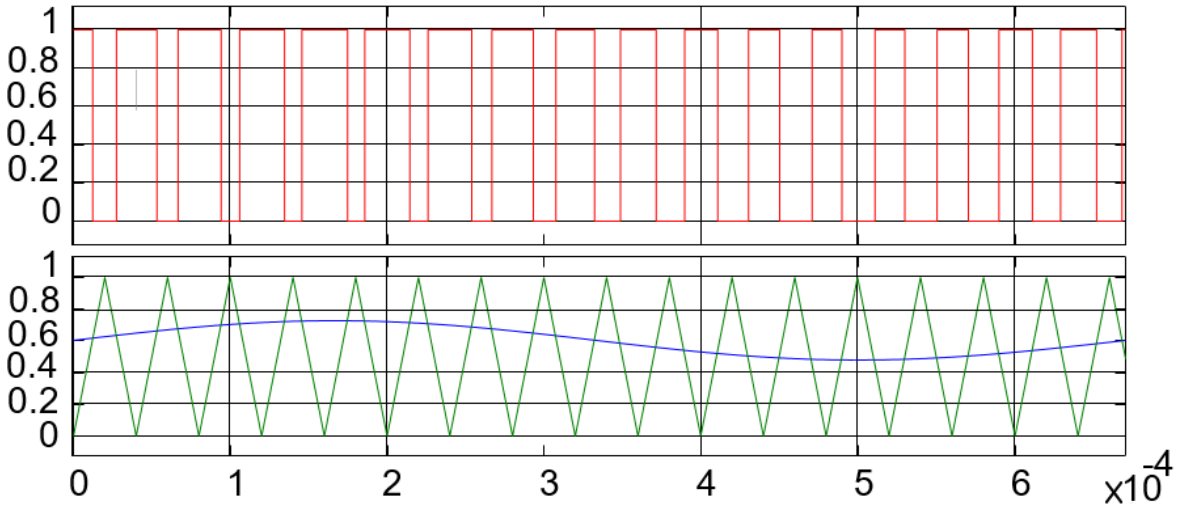

Figure 6.2: Example of control signal for buck converter of 1500Hz.

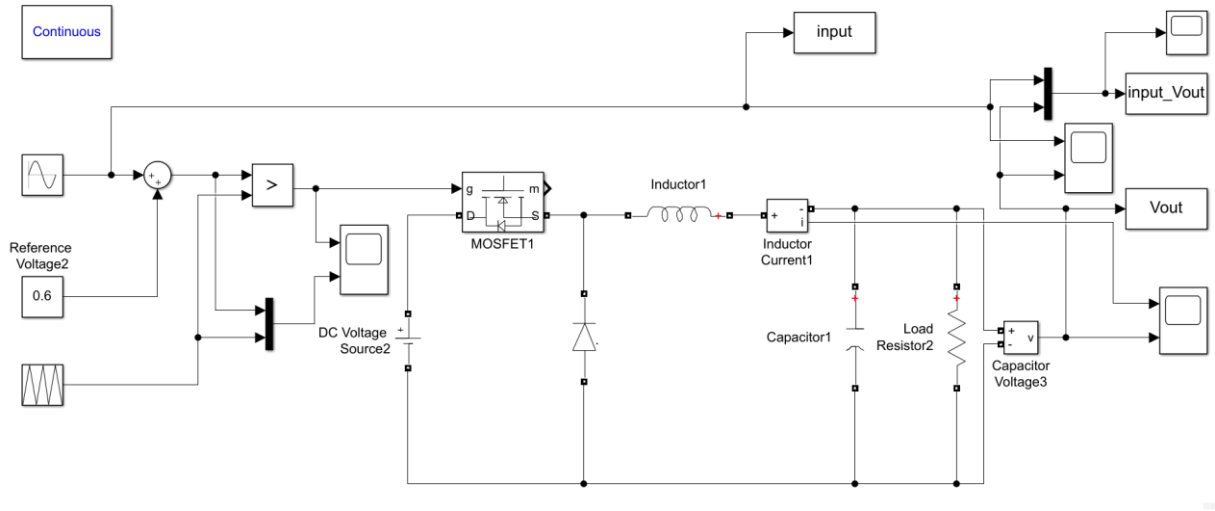

Figure 6.3: DC-DC Buck converter Matlab Simulink.

6.2.1 Fast Fourier Transform (FFT) Algorithm for the Buck Converter

The FFTs is applied to define the amplitude and phase angle from the output signal to determine the gain and the phase shift between the input and output signal as shown in Figure 6.4.

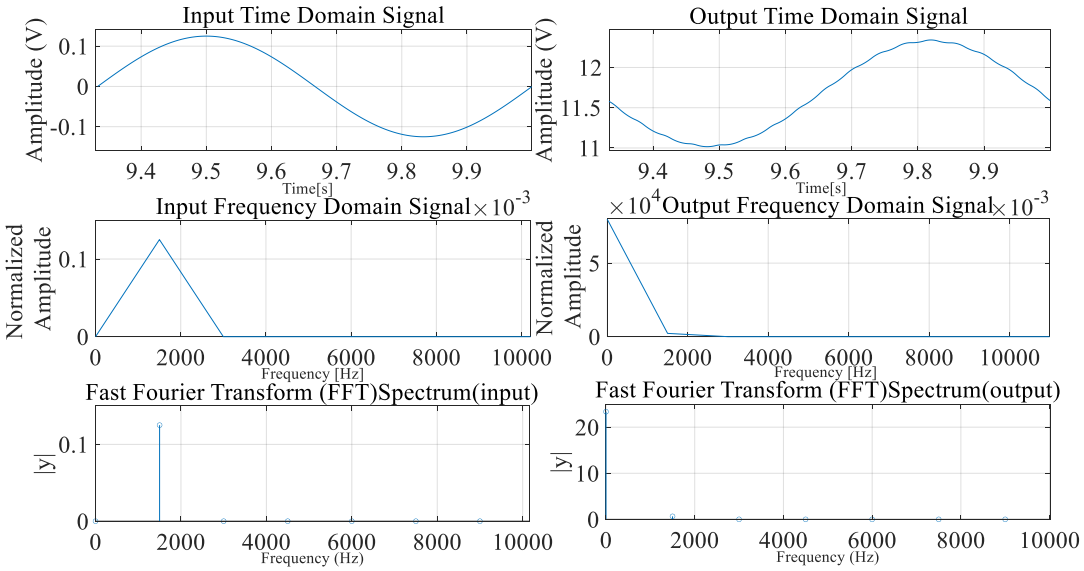

Figure 6.4: Example of FFT analysis for buck converter of 1500Hz.

Consequently, the magnitude and the phase shift for each frequency is tabulated for producing a Bode plot for the buck converter with values shown in Table 6.1.

Table 6.1: Collected data bode plot for buck converter.

Frequency (Hz)	Magnitude (dB)	Phase shift (degrees)
5	26.3518	-0.1019
10	26.3532	-0.2038
20	26.3588	-0.4079
100	26.5396	-2.0829
200	27.1286	-4.4615
300	28.2006	-7.5865
500	31.2667	-46.6346

Continued Table 6.1: Collected data bode plot for boost converter.

Frequency(Hz)	Magnitude (dB)=20*log(gine)	Phase shift Degree
600	30.2814	-83.0687
700	28.6248	-108.1775
800	26.8768	-126.7498
900	25.1362	-141.3072
1000	23.34	-153.3525
1500	14.4072	-172.1569
2000	8.6764	-174.1601
2500	4.6062	-175.2553
3000	1.1723	-175.8845
3500	-1.7045	-176.1434
4000	-3.9727	-176.2405
4500	-6.1259	-177.142
4700	-6.8691	-176.3831
4800	-6.8691	-176.3831
5000	-6.8691	-176.3831

6.2.2 Bode Plot Formulstion for the Buck Converter

From the frequency response derived from simulation data, the Bode plot is created for the system. Results ar shown in Fig. 6.5.

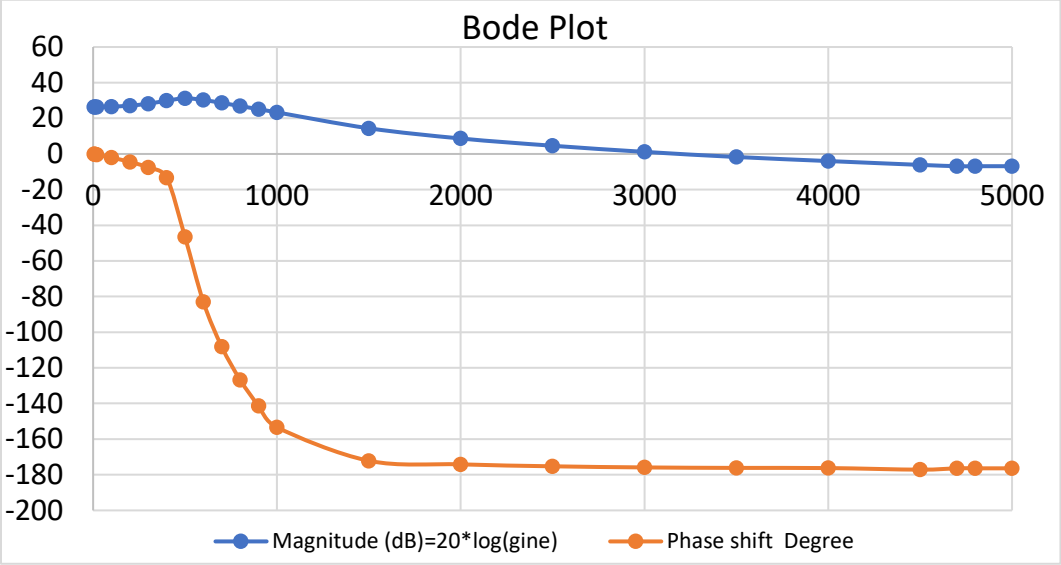

Figure 6.5: Bode Plot of buck converter form the Powersim simulation data.

The simulated buck converter is compared with a high-order integer transfer function by using the estimation Matlab command (TFEST). The system estimation fits 84.01% of the buck converter simulated results

$$G(s)_{sose} = \frac{3.226\times10^{8}}{s^2 + 2271\,s + 1.601\times10^{7}}.$$

A third-order integer transfer function is estimated for the buck converter. The results is fitted to estimation data of 85.98% of the simulated buck converter:

$$G(s)_{tose} = \frac{1.063 \times 10^{13}}{s^3 + 3.315 \times 10^{4}\, s^2 + 5.939 \times 10^{7}\, s + 5.27 \times 10^{11}}$$

A third-order system is estimated system with a zero included in the transfer function. The results fit the data by 84.95% of the simulated behaviour system as:

$$G(s)_{tosez} = \frac{2.545 \times 10^8\ s\ -\ 9.328 \times 10^{11}}{s^3\ +\ 925.8\ s^2 +\ 9.286 \times 10^6\ s\ +\ 4.4 \times 10^{10}}$$

A sixth-order integer estimation function is fitted to the data by 97.3% of the converter hehavior.

$$G(s)_{sxose}$$

$$= \frac{4.041 \times 10^8\ s^4\ -\ 9.786e10\ s^3\ +\ 7.506e15\ s^2\ +\ 1.116 \times 10^{18} s\ +\ 6.171 \times 10^{22}}{s^6 +\ 1338\ s^5\ +\ 3.382 \times 10^7\ s^4\ +\ 7.949 \times 10^9\ s^3\ +\ 4.971 \times 10^{14}\ s^2\ +\ 1.539 \times 10^{17}\ s\ +\ 2.951 \times 10^{21}}.$$

The comparison between all the estimated systems for simulation data is made to show the high order system is equivalent to the original system behavior as shown in the Figs. 6.6 and 6.7.

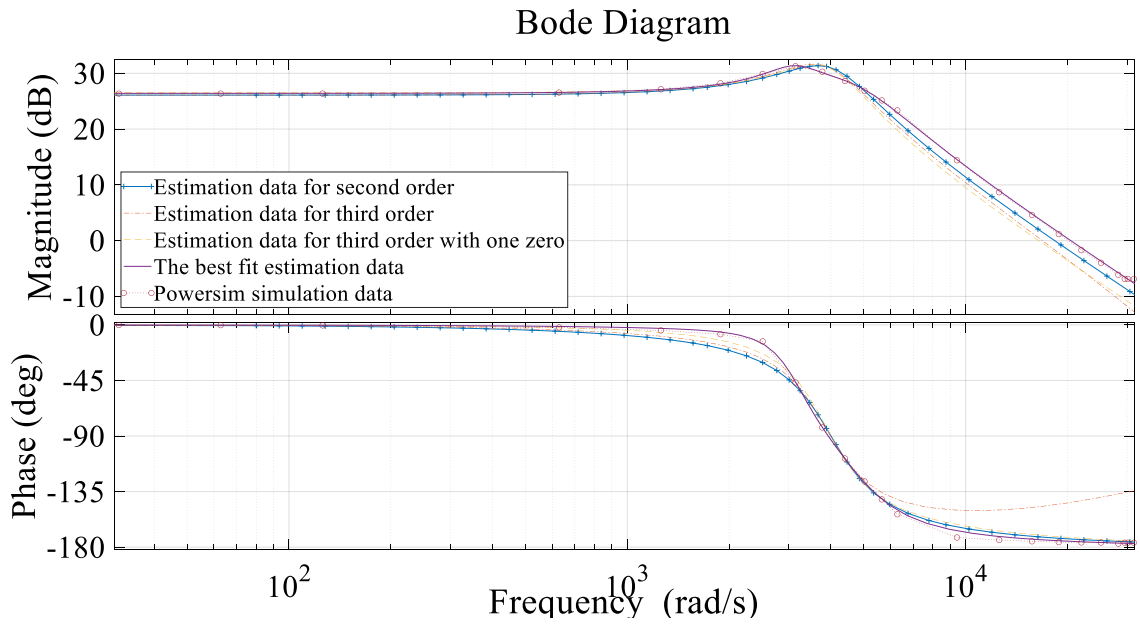

Figure 6.6: Bode Plot of buck converter simulated and estimated system.

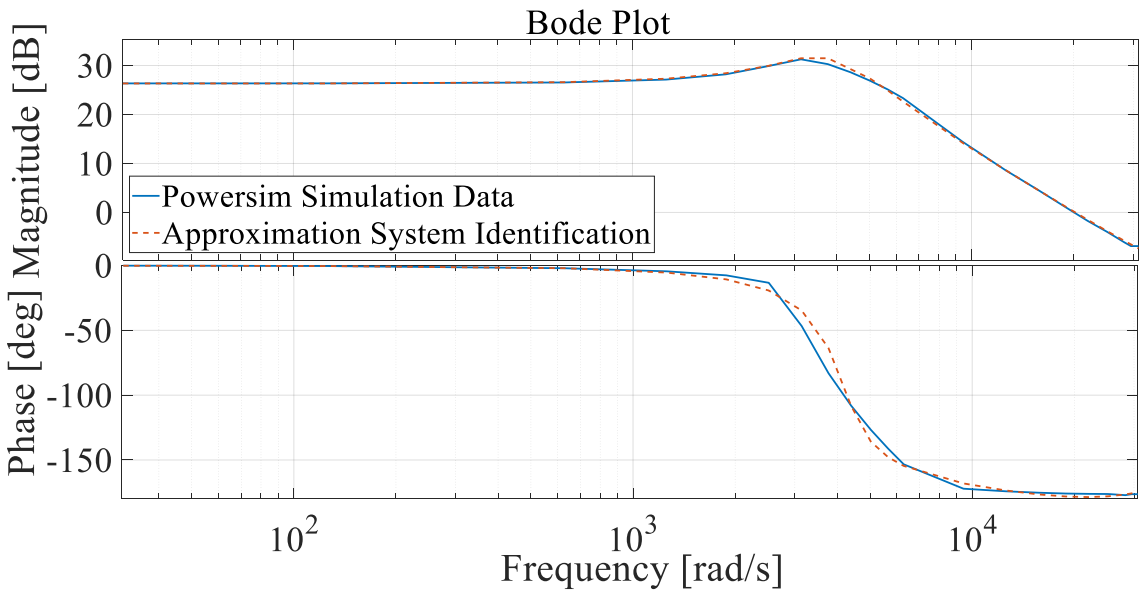

Figure 6.7: Bode Plot of buck converter simulated and approximation system.

The actual simulated response of the buck converter demonstrates a fractional order behavior since the asymptotic magnitude sloes at a rete different from -20 dB/decade. A fractional order transfer function is derived using Levy's method. The transfer function results the estimation error by 9% as showing:

$$G(s)_{FO} = \frac{-8.8396e{-}06s\text{^}1.5{+}0.00077031s\text{^}1.2{-}0.028416s\text{^}0.9{+}0.54375s\text{^}0.6{-}5.2383s\text{^}0.3{+}20.793}{1.6537e{-}07s^{1.8}{+}5.2915e{-}06s^{1.5}{+}9.2978e{-}05s^{1.2}{+}0.0016539s^{0.9}{+}0.026898s^{0.6}{+}0.2521s\text{^}0.3{+}1}.$$

6.2.3 Controller for the DC-DC Buck Converter

A controller for the output voltage of the dc-dc buck converter is designed. The LQR design technique is used with error function defined:

$$\dot{x}_1 = e(t) = V_{ref} - V_{out},$$

with the buck converter model with a tracking error state variable defined as

$$x_1 = \int e(t),$$

$$x_2 = i_l,$$

$$x_3 = V_{out},$$

$$\dot{x}_1 = V_{ref} - x_3$$

$$\dot{x}_2 = \frac{1}{C} x_2 - \frac{1}{C\,R_L} x_3$$

$$\dot{x}_3 = -\frac{rL}{L} x_2 - \frac{1}{L} x_3 + \frac{V_{in}}{L} u$$

For determine the tracking error behavior is the following:

$$\dot{z}_1 = -z_3$$

$$\dot{z}_2 = \frac{1}{C} z_2 - \frac{1}{C\,R_L} z_3$$

$$\dot{z}_3 = -\frac{rL}{L} z_2 - \frac{1}{L} z_3 + \frac{V_{in}}{L} u$$

For control input *u* is optimized by the cost quadratic cost function:

$$J(t) = \int_0^\infty (z^T Q z + v^2) dt,$$

where Q is a symmetric positive semi-definite matrix. The root-locus plot for the buck converter is shown in Fig. 6.8.

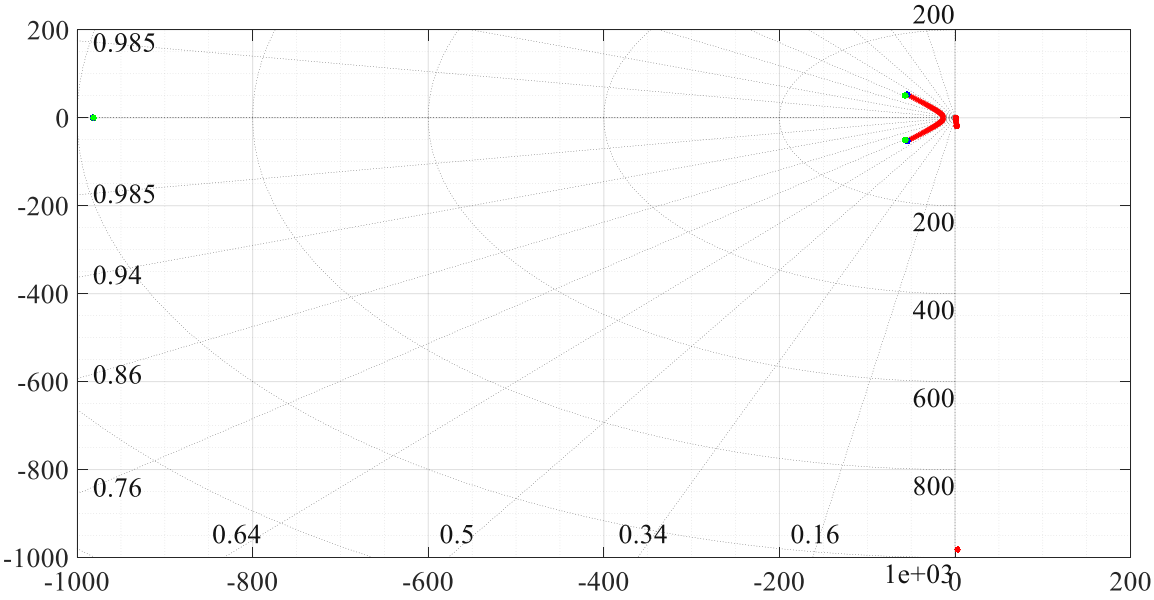

Figure 6.8: Movement of poles in LQR of buck converter.

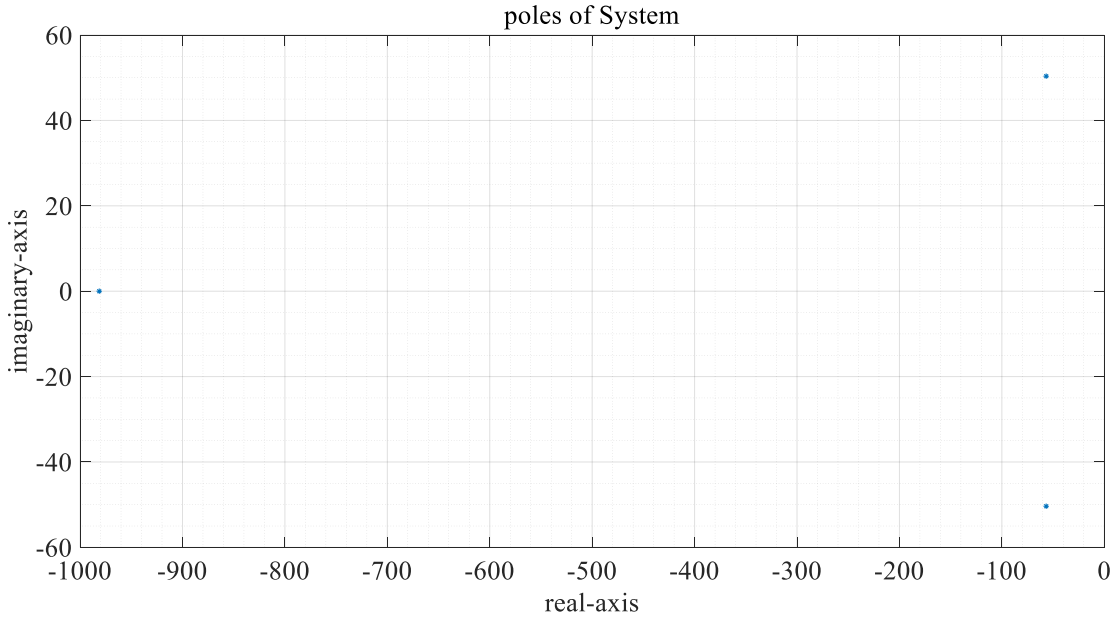

Figure 6.9: Poles location of system of buck converter.

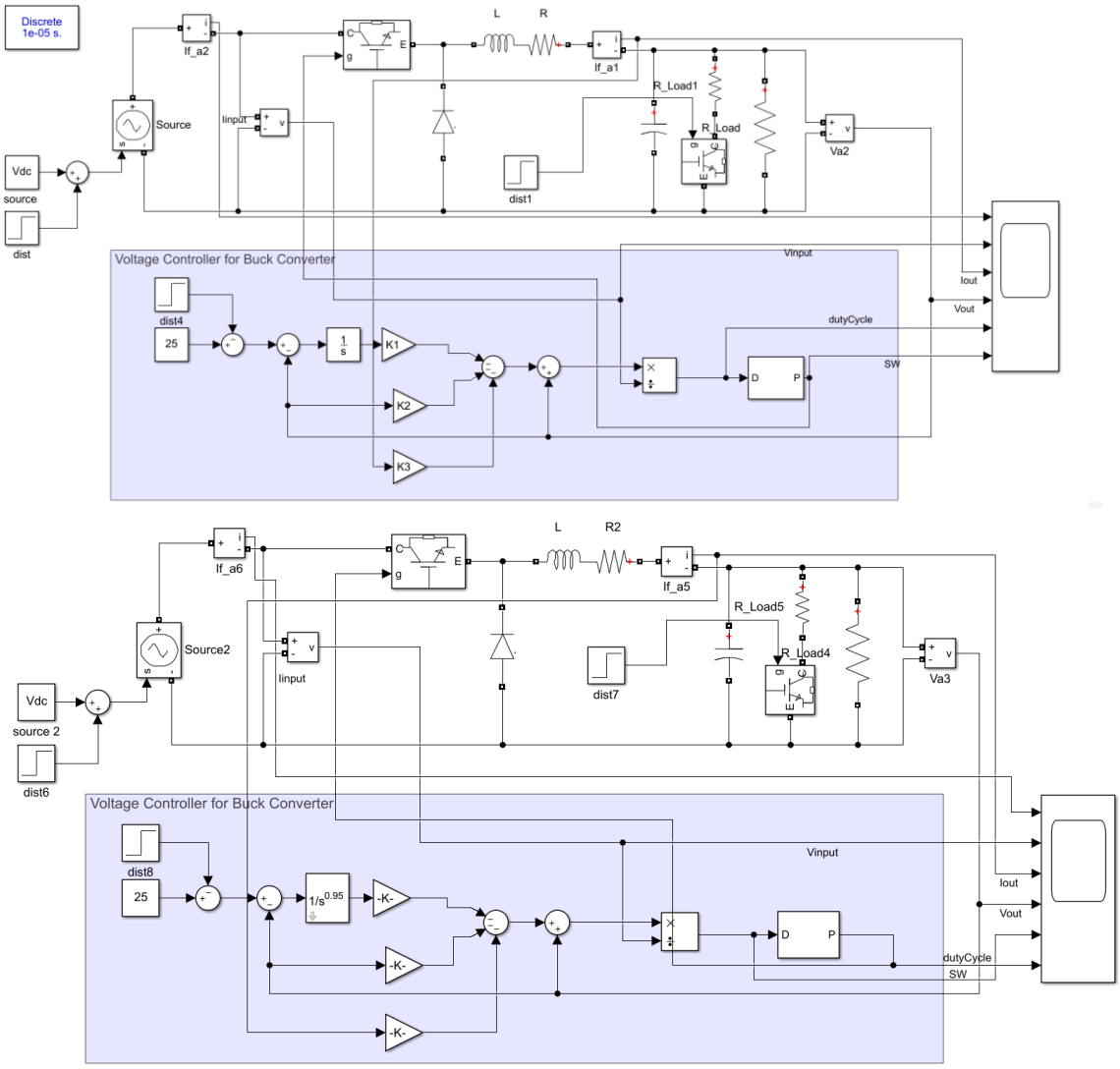

Figure 6.10: Simulation of fractional-order and integer-order controller of buck converter.

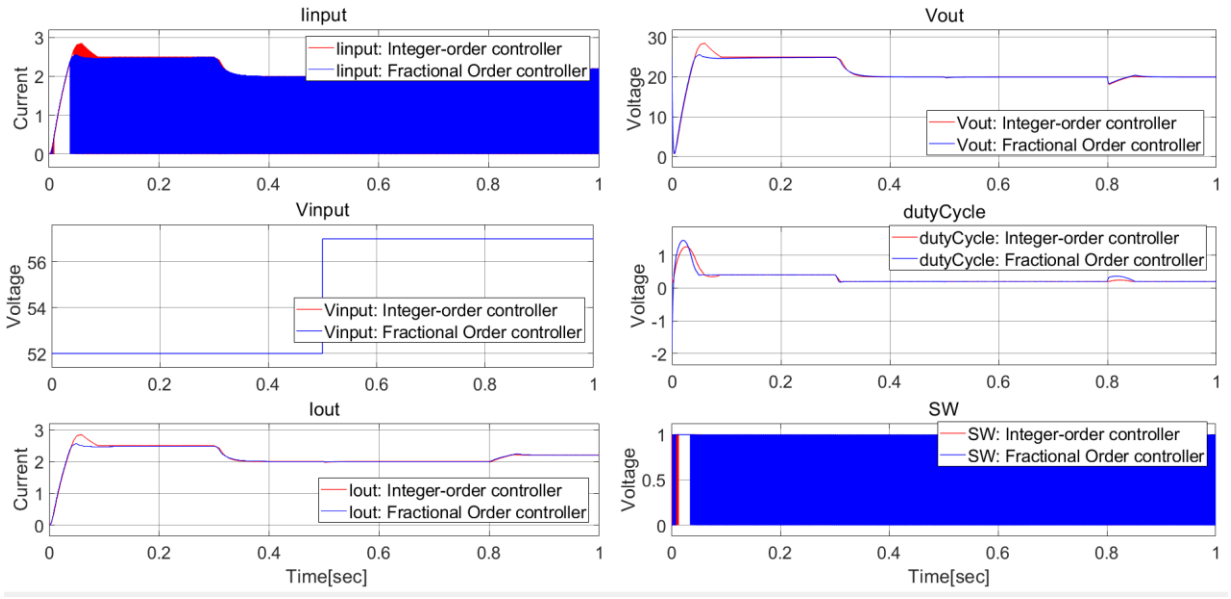

Figure 6.11: Result of fractional-order and integer-order controller of buck converter.

In Fig. 6.11 it is shown that the system behavior with a fractional-order controller has reduced overshoot. Disturbances are applied to the systems as a load change. At 0.3 s the output voltage is tracking the reference command value. At 0.5 s the input voltage is increased to evaluate tracking of the output value. At 0.8 s the resistive load is decreased to show the performance of the controller in regulating the output voltage.

6.2.4 Experimental Verification for the Buck Converter

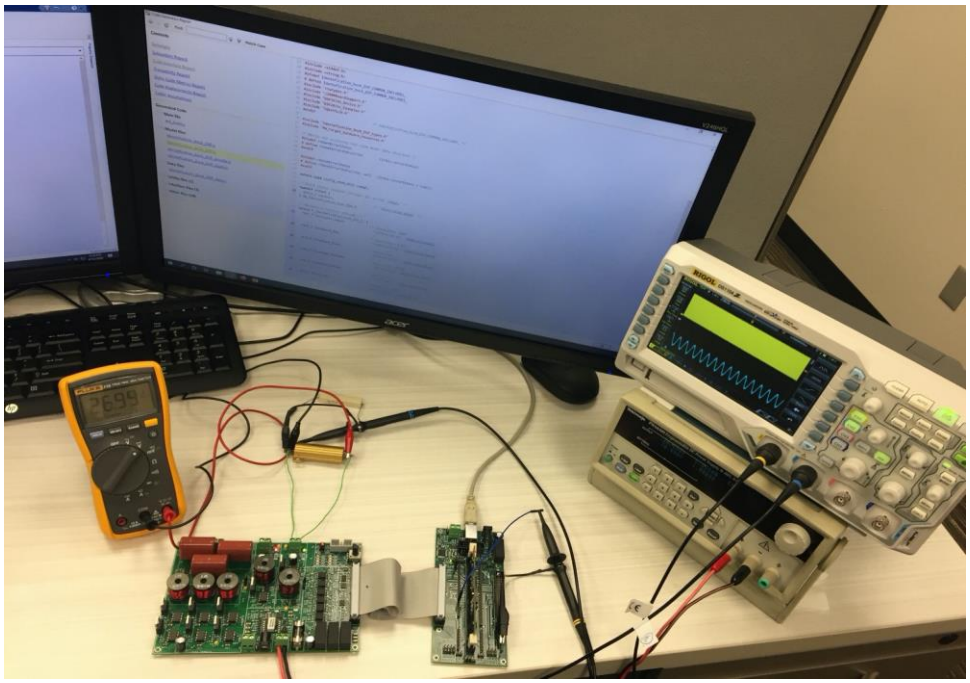

Figure 6.12: Experimental configuration for the buck converter controller.

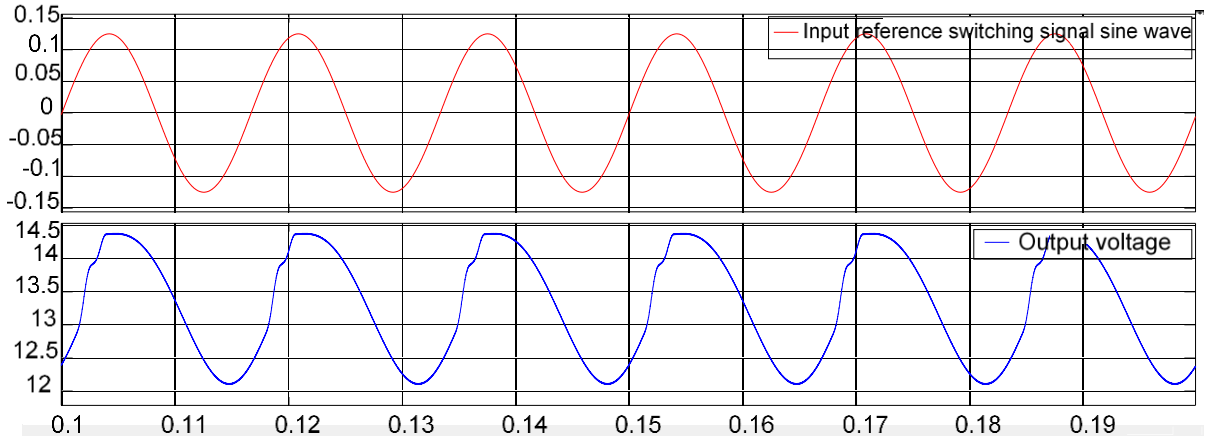

Figure 6.13: Simulation of control signal at 60Hz and output voltage of the buck converter.

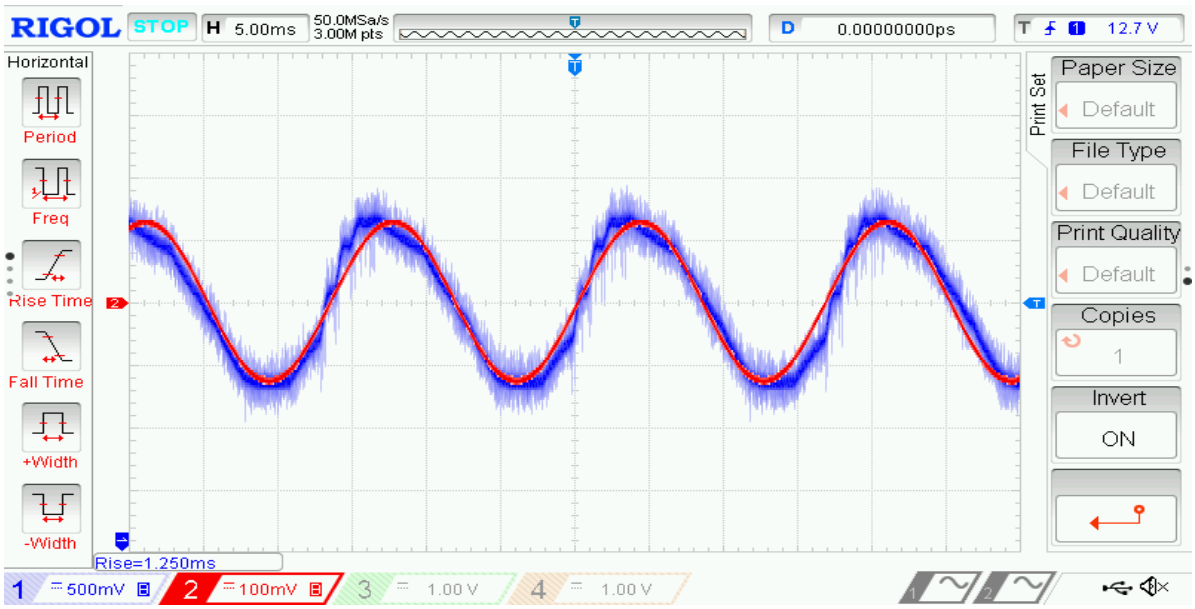

Figure 6.14: Experimental control of 60Hz reference and output voltage of the buck converter.

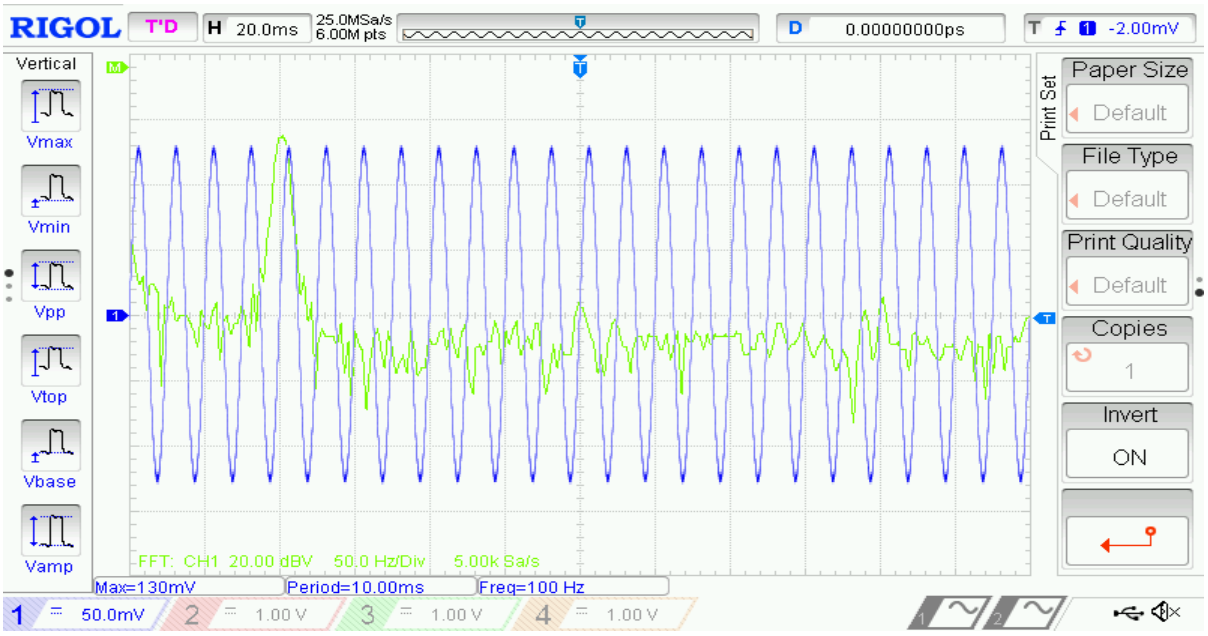

Figure 6.15: Experimental analysis of 60Hz control signal by FFT of the buck converter.

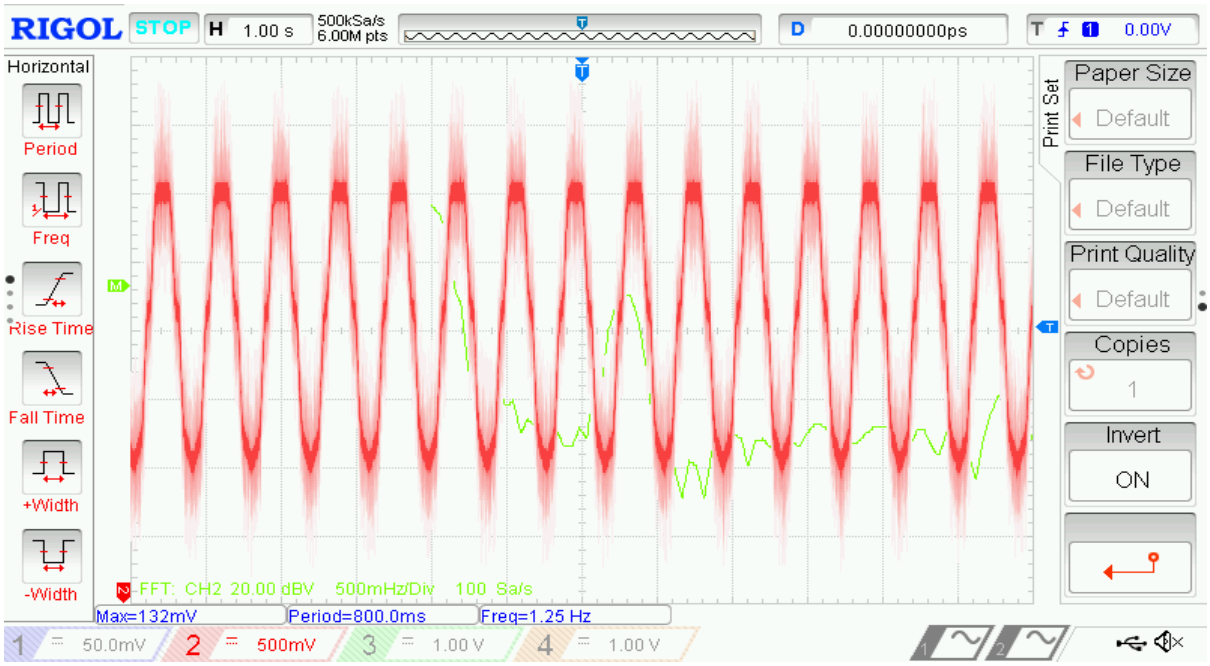

Figure 6.16: Experimental analysis of output voltage by FFT of the buck converter.

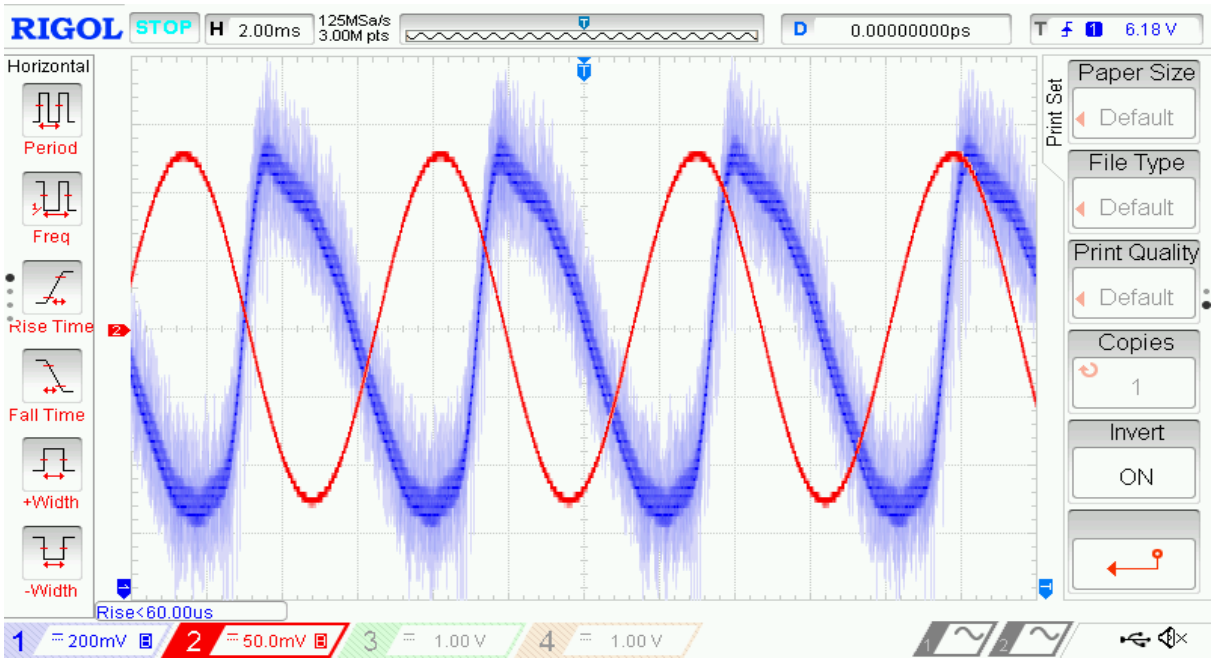

Figure 6.17: Experimental control by 10 KHz at output voltage of the buck converter.

Figure 6.18: Experimental analyzing 10 KHz control signal by FFT of buck converter.

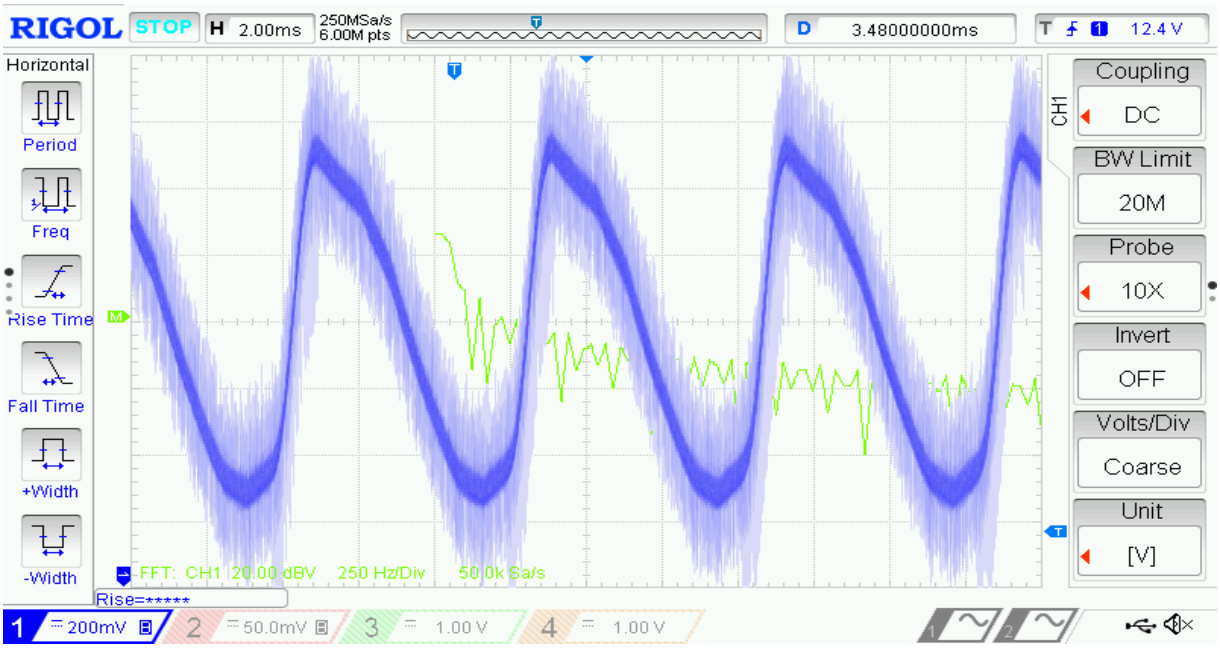

Figure 6.19: Experimental analyzing output voltage signal by FFT of the buck converter.

The experimental verification of the input (control) to output voltage signal by FFT of buck converter is very close to the simulation results.

6.3 Identification of DC-DC Boost Converter

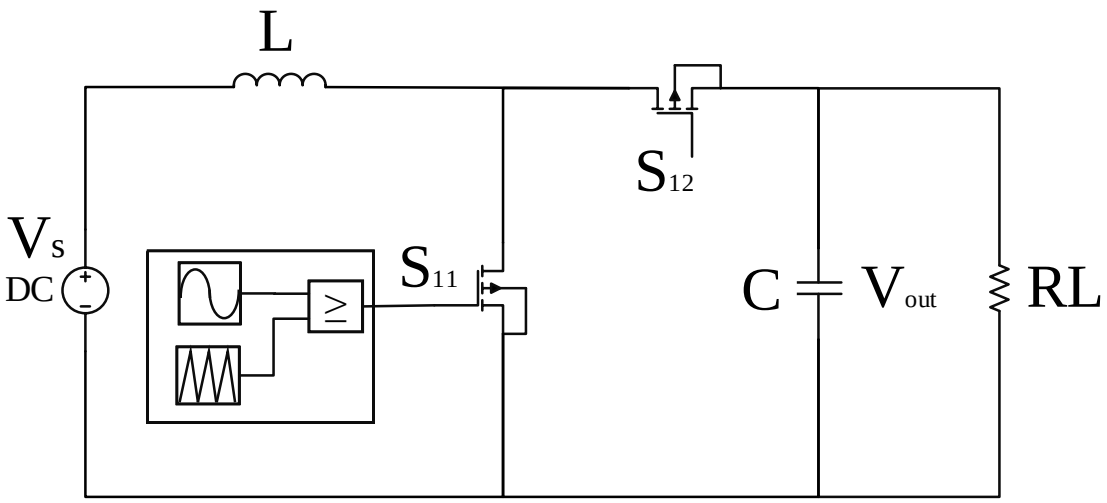

Figure 6.20: DC-DC Boost Converter.

The identification of the boost converter is presented in Fig. 6.21. The boost converter contains an inductor (L), capacitor (C), and resistive load. The input voltage is a constant value. The control signal is combination of a dc voltage added to a sinusoidal a wave at a selected frequency rangr. However, the control signal frequencies are less than the triangular wave frequency. The converter operates in the continuous conduction mode by adjusting the amplitude of the control signal for each application. The results represent the relationship between the control reference signal and the output signal. The input (duty-cycle signal) and the output voltage are displayed on the phasor model of the small signal variation.

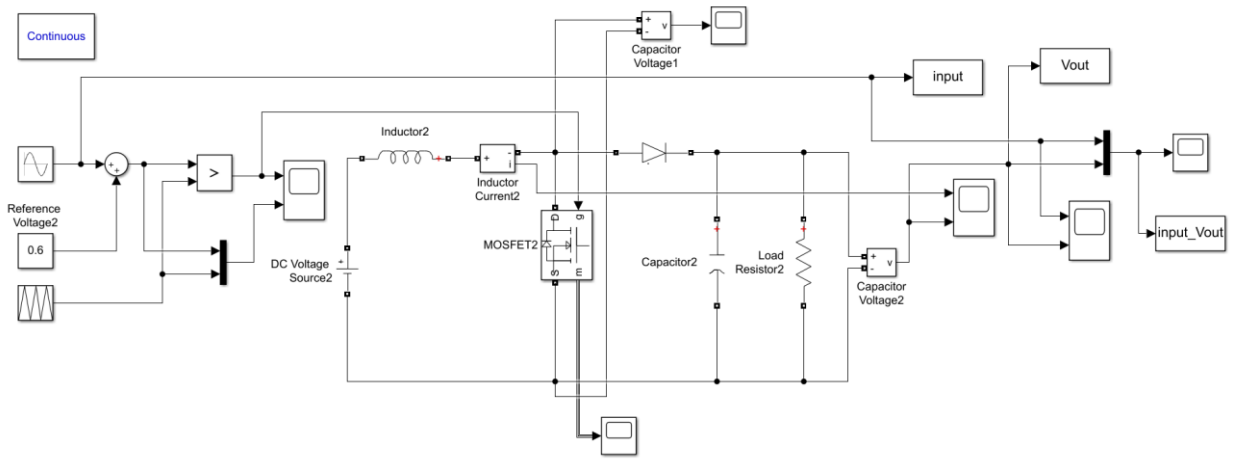

Figure 6.21: DC-DC Boost Converter Matlab Simulink.

6.3.1 Fast Fourier Transform (FFT) Algorithm for Boost Converter

The FFT is applied in the analysis to define the amplitude and phase angle. By using the FFT of the output signal the gain and the phase shift between the input and output signal ws determined as shown in the following figures:

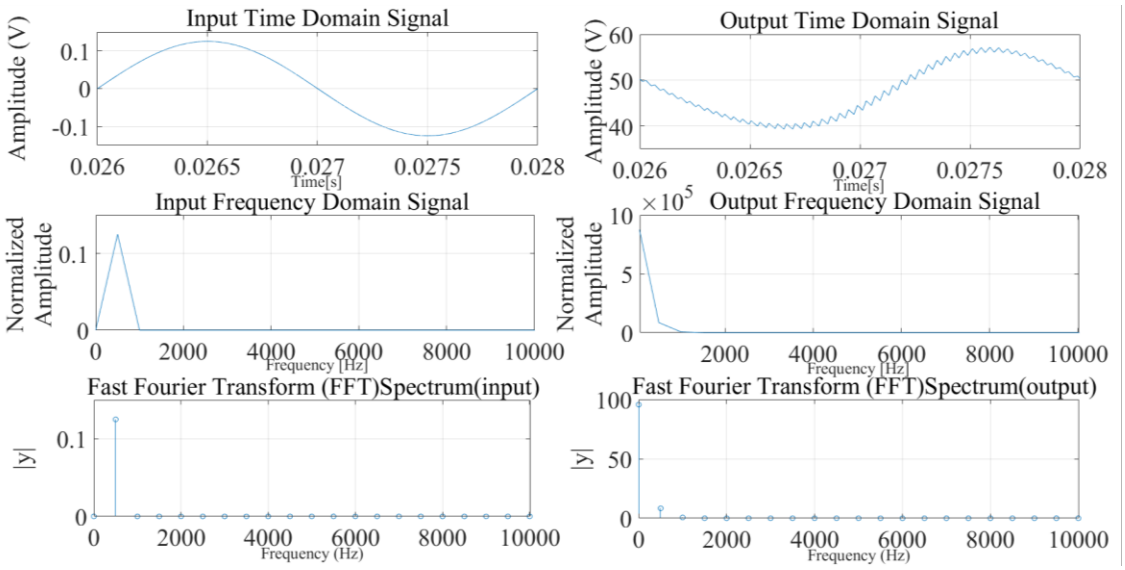

Figure 6.22: Example of the (FFT) analysis for buck converter of 500Hz.

A magnitude and phase shift for each frequency applied was tabulated and is shown in Table 6.2.

Table 6.2: Collected data bode plot for boost converter.

Frequency (Hz)	Magnitude (dB)=20*log( )	Phase shift (degrees)
5	42.4555	-1.5061
10	42.4648	-3.0156
20	42.5014	-6.0584
100	43.3133	-33.1772
200	45.5471	-73.3662
300	45.0749	-140.7821
400	40.5477	-183.5606
500	36.4659	-202.3726
600	33.597	-213.5911
700	31.2051	-222.7427
800	29.8854	-224.9429
900	28.4123	-229.7827
1000	27.162	-233.7191
1500	22.8994	-246.3085
2000	20.2925	-253.2719

Continued Table 6.2: Collected data bode plot for boost converter.

Frequency (Hz)	Magnitude (dB)=20*log( )	Phase shift (degrees)
2500	18.1081	-255.4484
3000	16.7004	-257.3572
3500	15.1509	-258.2636
4000	14.1601	-259.2652
4500	13.6031	-261.0557
4700	13.0189	-263.6907
4800	13.0189	-263.6907
5000	13.0189	-263.6907

6.3.2 Bode Plot Generation for Boost Converter

Using the data of magnitude and phase shift for the boost converter, the Bode plot drawing has a magnitude (∓ 20) in decibel (dB). The frequencies sine function of the control input is $2\pi f$ rad/sec. A frequency range of 5-5K Hz is applied in the Simulink model.

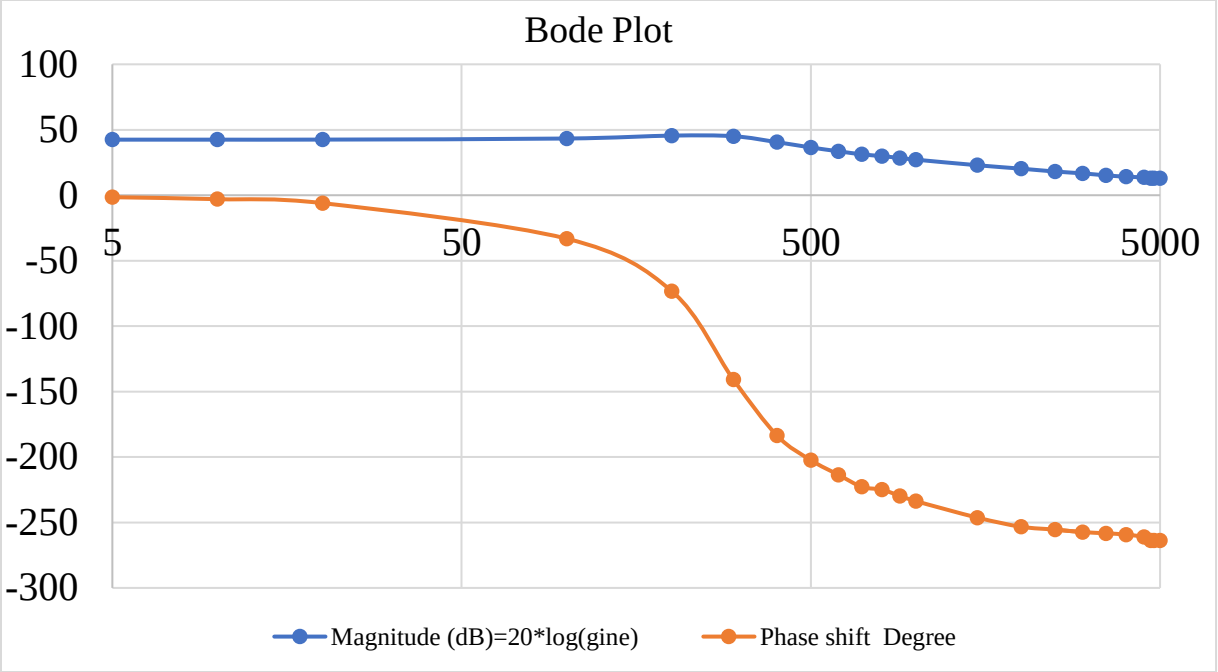

Figure 6.23:Bode Plot of Boost converter Powersim simulation data.

A high-order integer transfer function for the system is derived using the TFEST command on Matlab. A second order system estimated for the system is analyzed for fitting the estimation data by 66.71% of the actual behavior for the system.

$$G(s)_{sose} = \frac{2.786 \times 10^{8}}{s^{2} + 943.4\,s + 2.067 \times 10^{6}}$$

The estimation by using TFEST on Matlab to a third order system that fits the estimation data by 81.21% of the real system as:

$$G(s)_{tose} = \frac{1.116 \times 10^{12}}{s^{3} + 3507\,s^{2} + 5.907 \times 10^{6}\,s + 7.817 \times 10^{9}}$$

The third order transfer function estimated for the system is analyzed with estimation data by 95.82% the real system as:

$$G(s)_{tosez} = \frac{-9.513 \times 10^{9}\,s + 2.761 \times 10^{13}}{s^{3} + 7.563 \times 10^{4}\,s^{2} + 9.698 \times 10^{7}\,s + 2.142 \times 10^{11}}$$

However the fourth order system is estimated that fits of estimation data by 98.09% of the real behavior of the system.

$$G(s)_{sxose} = \frac{-2.469 \times 10^{11}\, s^2 \;+\; 4.4 \times 10^{14}\, s \;+\; 7.544 \times 10^{17}}{s^4 \;+\; 2.067 \times 10^{6}\, s^3 \;+\; 4.351 \times 10^{9}\, s^2 \;+\; 8.503 \times 10^{12}\, s \;+\; 5.675 \times 10^{15}}.$$

The comparison between all the estimated systems for simulation data is made to show the high order equivalent to the original system behavior is shown in the Fig. 6.27.

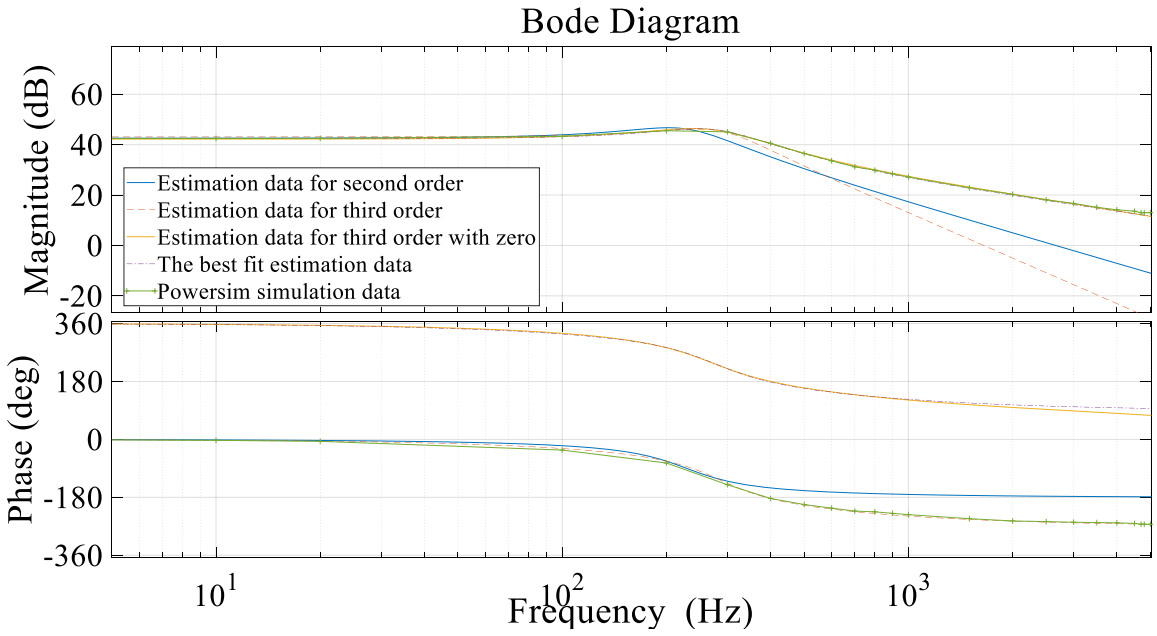

Figure 6.24: Simulated data Bode plot of boost converter and estimation data.

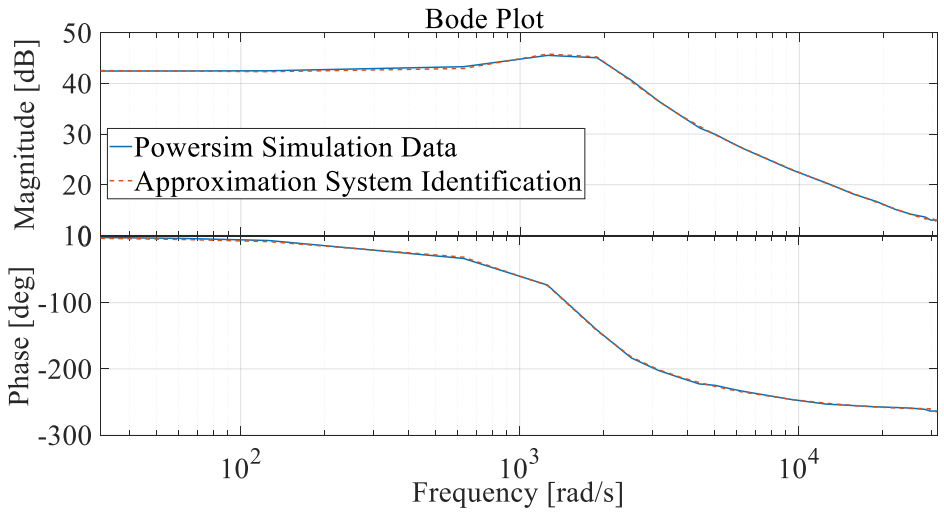

Figure 6.25: Simulation data Bode plot boost converter and approximation data.

The real behavior of the system is represented by the fractional order transfer function by applying Levy's method with resulting estimation error of 4%.

$$G(s)_{FO} =$$

$$\frac{2.5708\times10^{-13}s^{3.25}-1.2387\times10^{-9}s^{2.6}+1.1012\times10^{-9}s^{1.95}+0.00035331s^{1.3}-0.84513s^{0.65}+137.38}{53.669\times10^{-12}s^{3.25}+3.8974\times10^{-10}s^{2.6}+3.1564\times10^{-7}s^{1.95}+3.5464\times10^{-5}s^{1.3}+0.00059335s^{0.65}+1}.$$

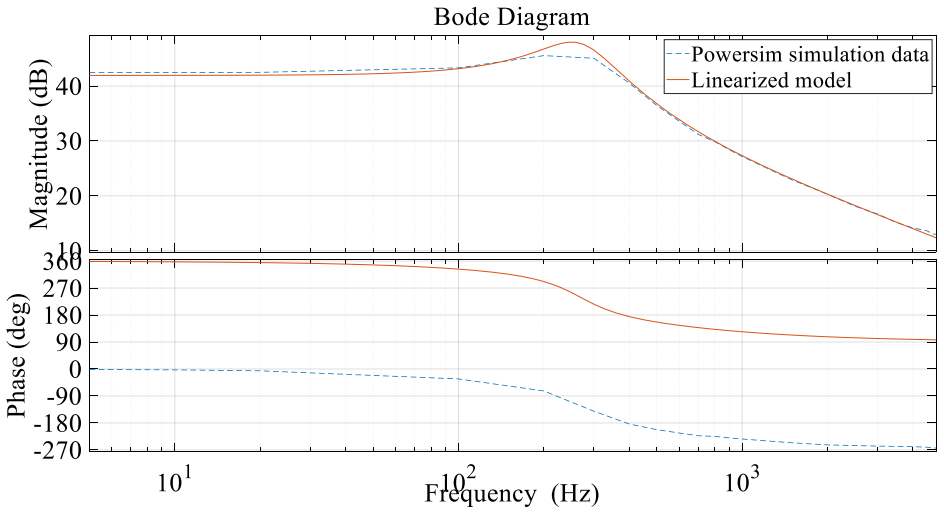

Figure 6.26: Simulation of boost converter actual Bode Plot and FO model.

6.3.3 Controller for the DC-DC Boost Converter

The cascaded PI control of the boost converter is used with an inner and outer loop controller for the converter. Design of the inner-loop for the inductor current is tracking a reference value of the current by define an error variable as:

$$\dot{x}_1 = e(t) = i_{lref} - i_l$$

With an additional state variable defined from the tracking error as:

$$x_1 = \int e(t),$$

$$x_2 = i_l.$$

The state space equations are represented as:

$$\dot{x}_1 = i_{lref} - x_2$$

$$\dot{x}_2 = -\frac{r_l x_2}{L} - \frac{v_o(1-u)}{L}.$$

Converting the state-space equations to a standard LQR form is represented as:

$$\dot{z}_1 = -z_2$$

$$\dot{z}_2 = -\frac{r_l z_2}{L} - \frac{u}{L}.$$

Control input *u* is minimized by the cost function of the LQR:

$$J(t) = \int_0^\infty (z^T Q z + v^2) dt,$$

where Q is symmetrical positive semi-definite matrix. The root locus plot for current control of the boost converter as presented in Chapter 5 is shown in Fig. 5.10.

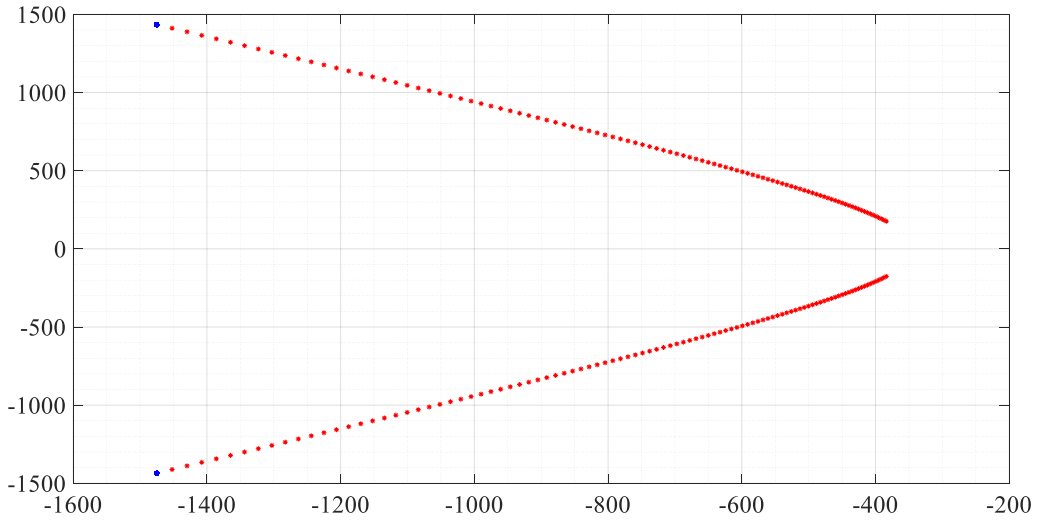

Figure 6.27: Root locus of closed loop poles for boost converter inner-loop cpntroller.

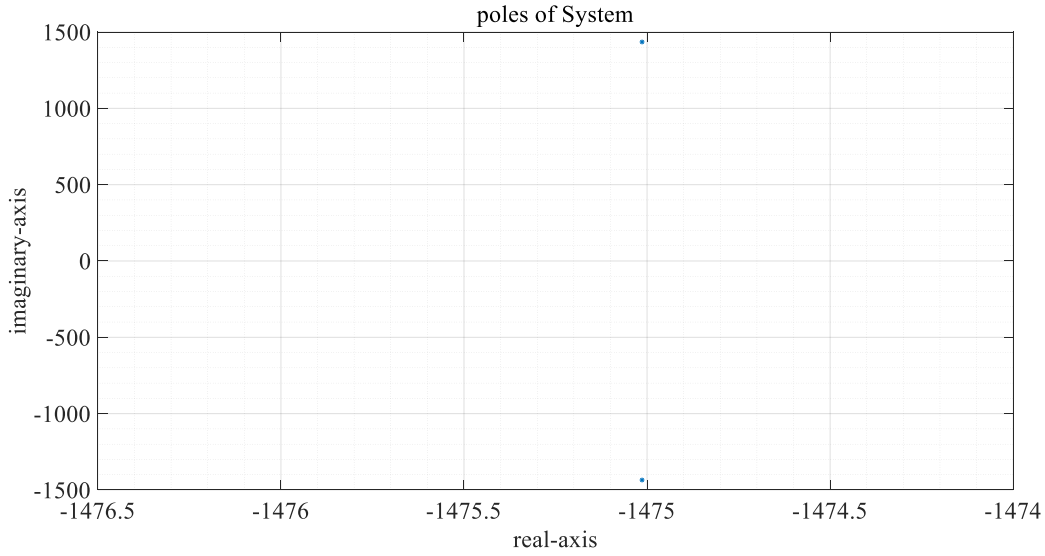

Figure 6.28: Poles of current controller location of the boost converter.

Defining gains for outer-loop controller for the boost converter, the LQR technique is used.

The output error function is represented:

$$\dot{x}_1 = e(t) = V_{ref} - V_{out}$$

A tracking error state variable is added as

$$x_1 = \int e(t),$$

$$x_2 = V_{out},$$

$$\dot{x}_1 = V_{ref} - x_2$$

$$\dot{x}_2 = \frac{(1-u)}{C} i_l - \frac{1}{C\ R_L} x_2.$$

For determining the equation for tracking of the system behavior is

$$\dot{z}_1 = -z_2$$

$$\dot{z}_2 = \frac{v_{in}}{C v_{ref}} u - \frac{1}{C\ R_L} z_2.$$

The control input *u* is minimized by the quadratic cost function :

$$J(t) = \int_0^\infty (z^T Q z + v^2) dt,$$

where Q is symmetrical positive semi-definite matrix. The control for boost converter from Chapter 5 is shown in Fig. 5.11. The corresponding root locus and closed loop poles are shown in Figs. 6-30 and 6.31.

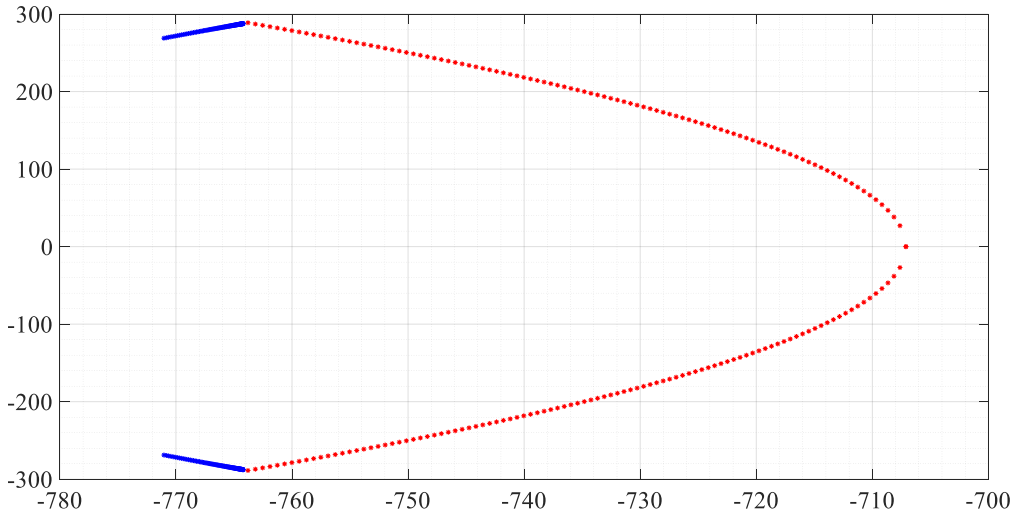

Figure 6.29: Movement of closed loop poles for voltage controller of the boost converter.

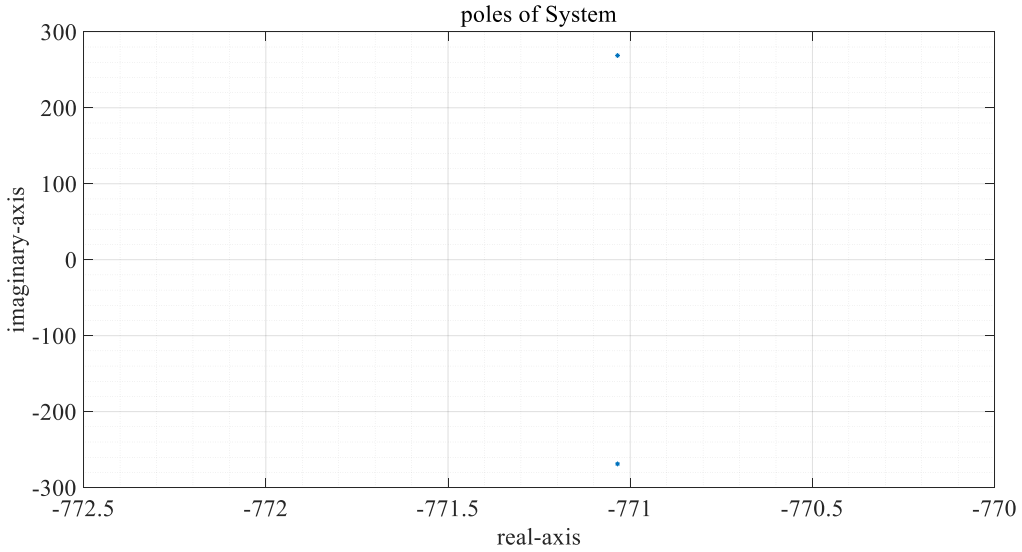

Figure 6.30: Poles of voltage controller location of the boost converter.

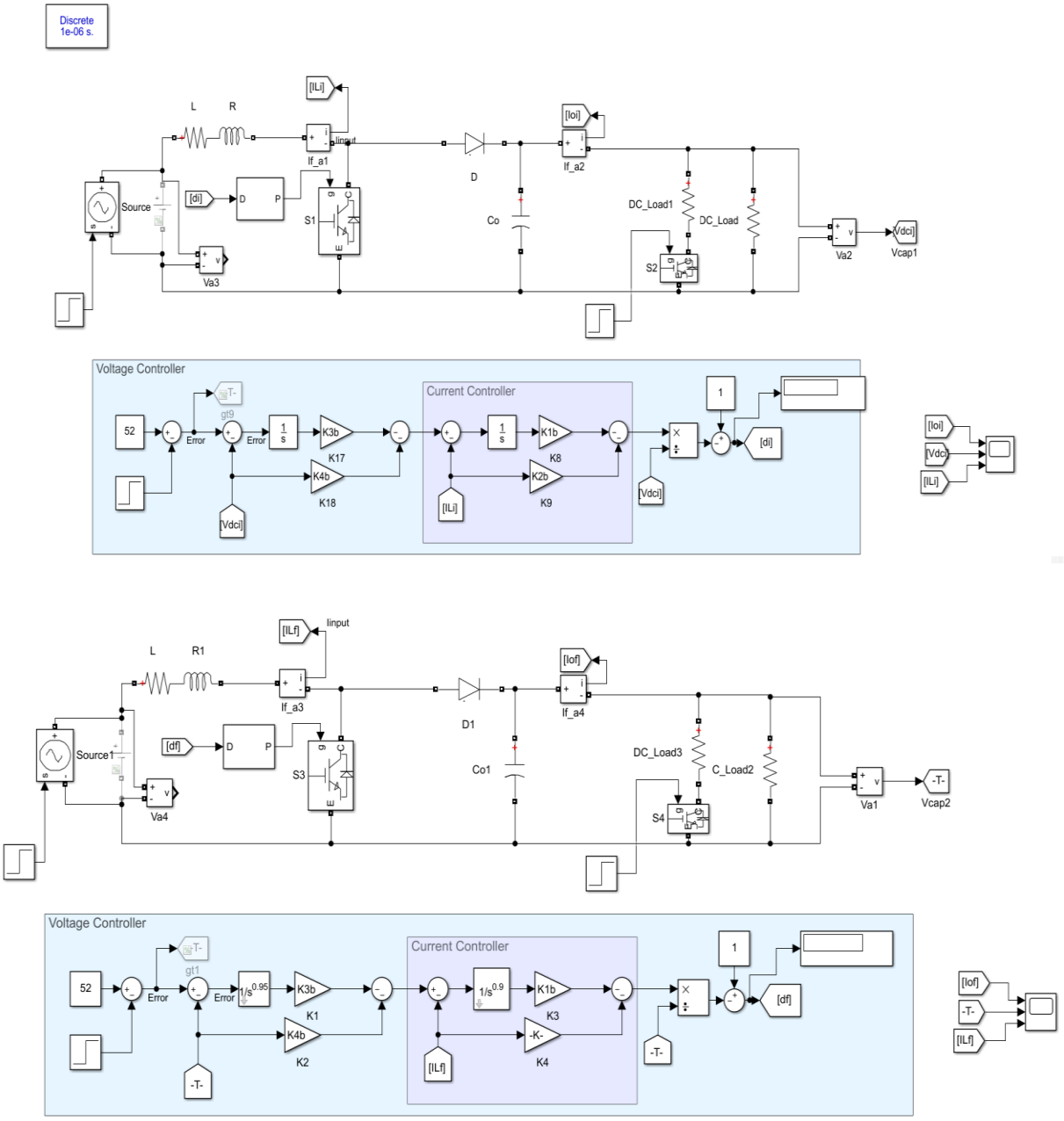

Figure 6.31: Controller configuration for the boost converter.

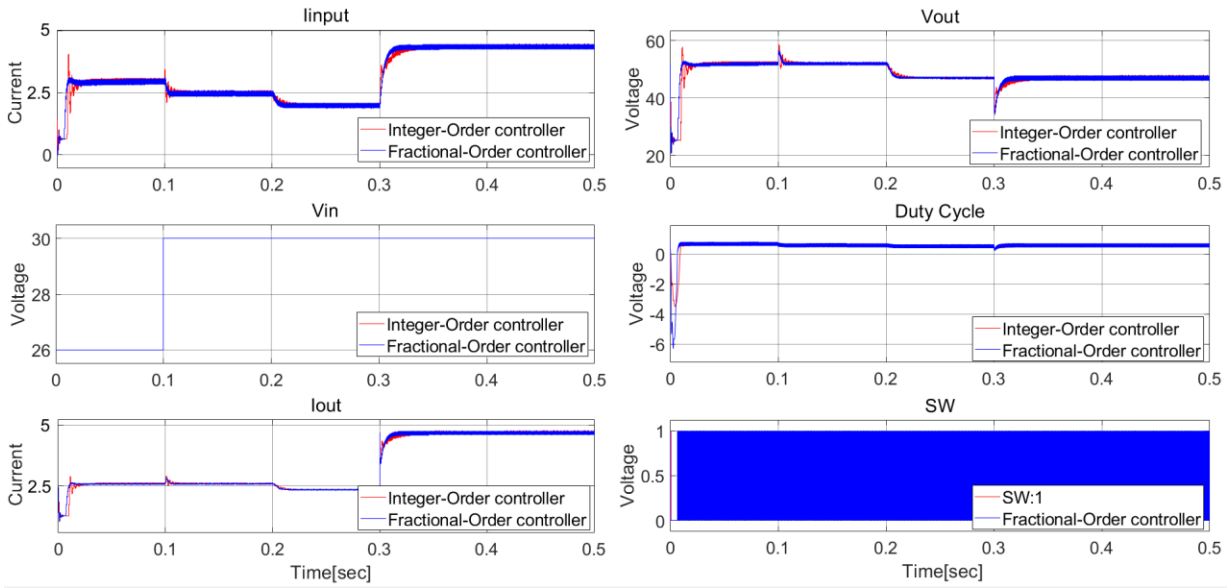

Figure 6.32: Integer-order controller with fractional-order controller for boost converter.

The actual system behavior of the boost converter with a fractional controller has less overshoot and faster response. Disturbances are applied to the system for controlling the output voltage. At 0.1 s the input voltage is increased but the reference output voltage remains at the sa,e value. At 0.2 s, the reference of the output voltage is reduced to have verification of tracking the output value. At 0.3 s the resistive load is decreased for the system to show the performance of the controller shown in Fig. 6.33.

6.3.4 Experimental Reults for Boost Converter

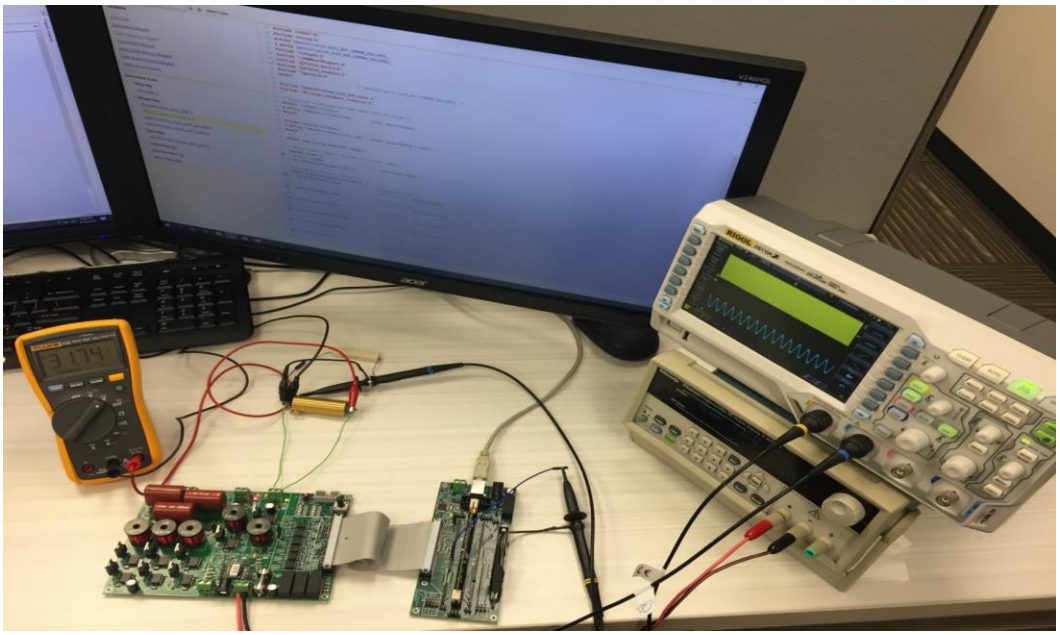

Figure 6.33: Experimental control of the boost converter.

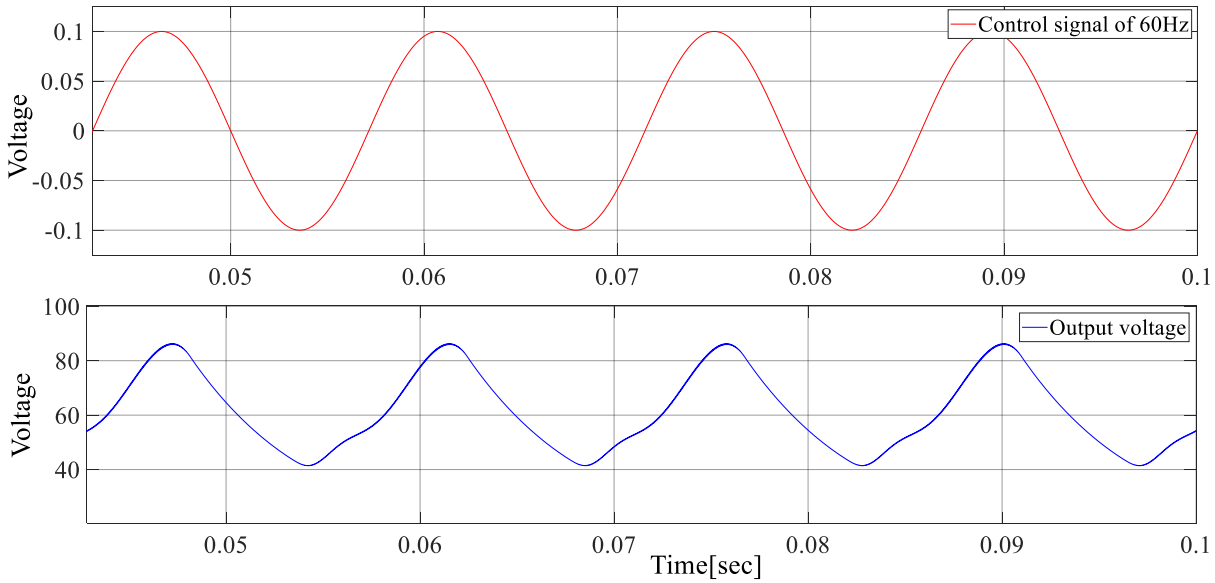

Figure 6.34: Simulation of reference signal at 60Hz and output voltage of the boost converter.

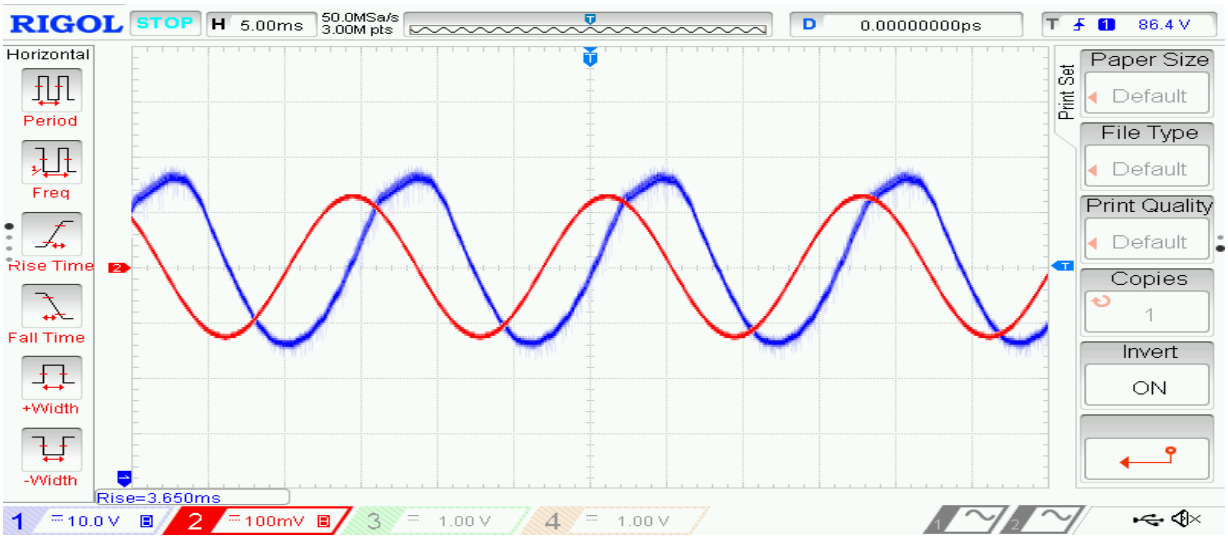

Figure 6.35: Simulation control signal 60Hz and output voltage of the boost converter.

Figure 6.36: Experimental FFT analysis of control signal 60Hz the boost converter.

Figure 6.37: Experimental FFT analysis of output voltage boost converter.

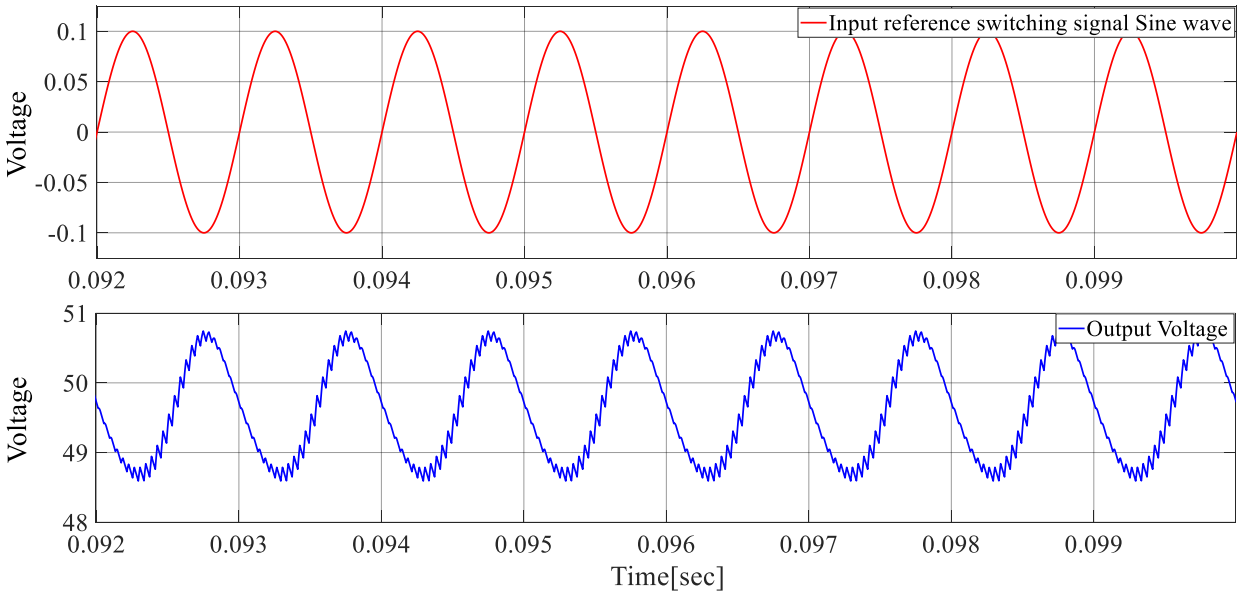

Figure 6.38: Simulation control signal of 100Hz and output voltage boost converter.

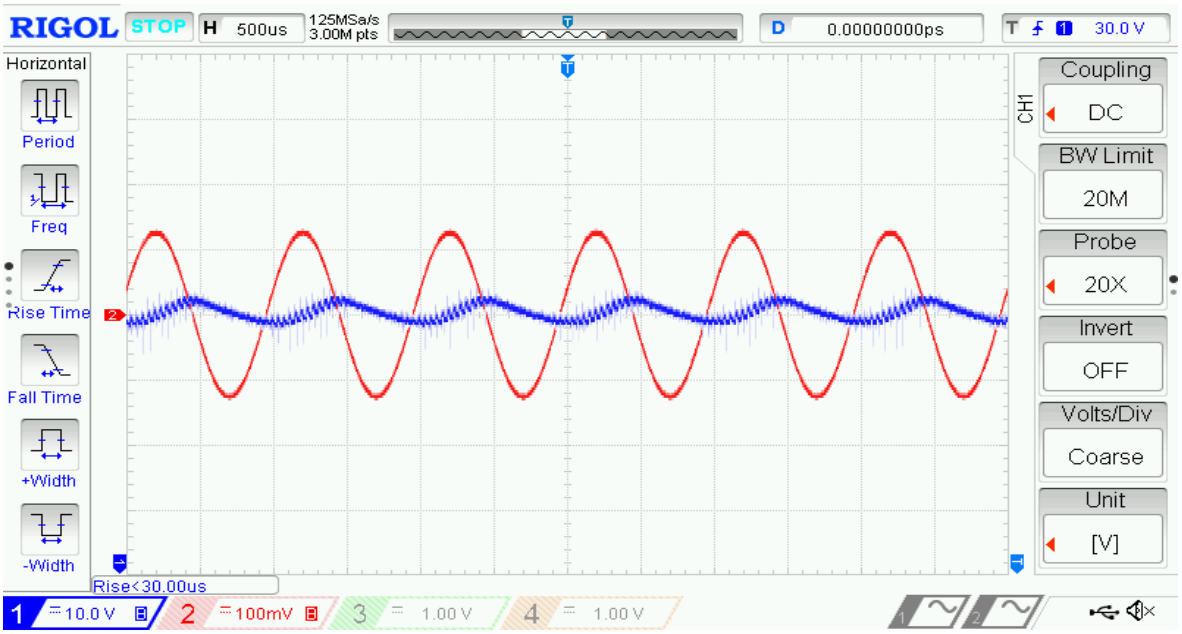

Figure 6.39: Experimental control signal of 100Hz and output voltage boost converter.

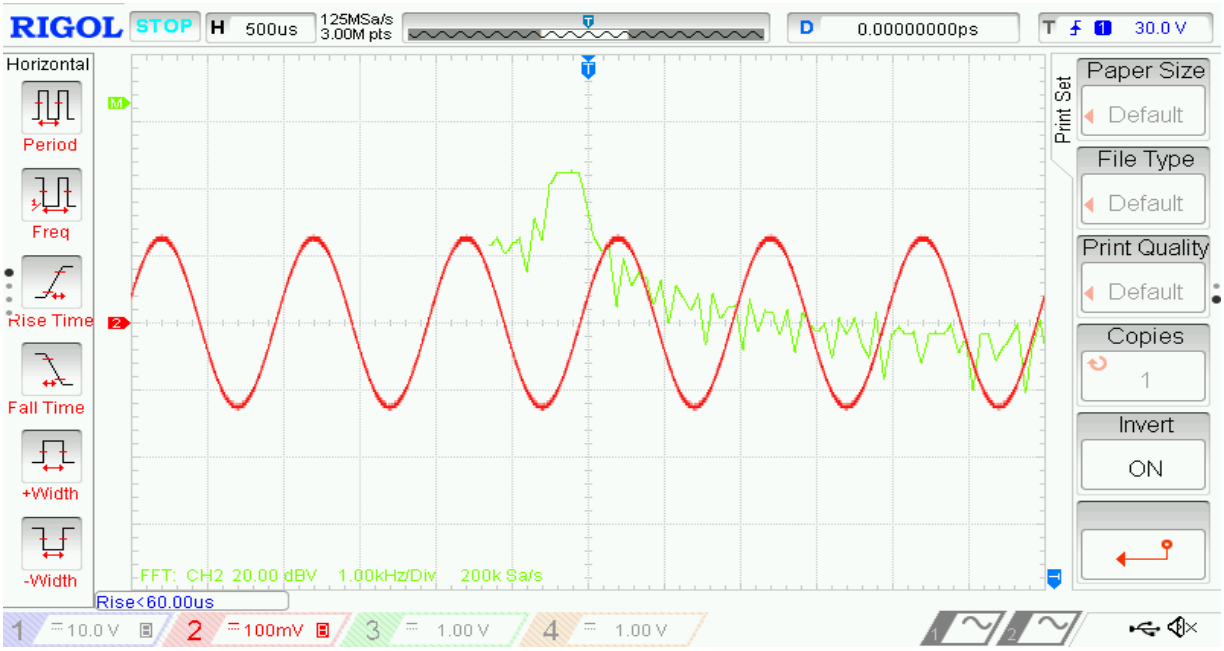

Figure 6.40: Experimentalal FFT analysis of control signal of 100Hz boost converter.

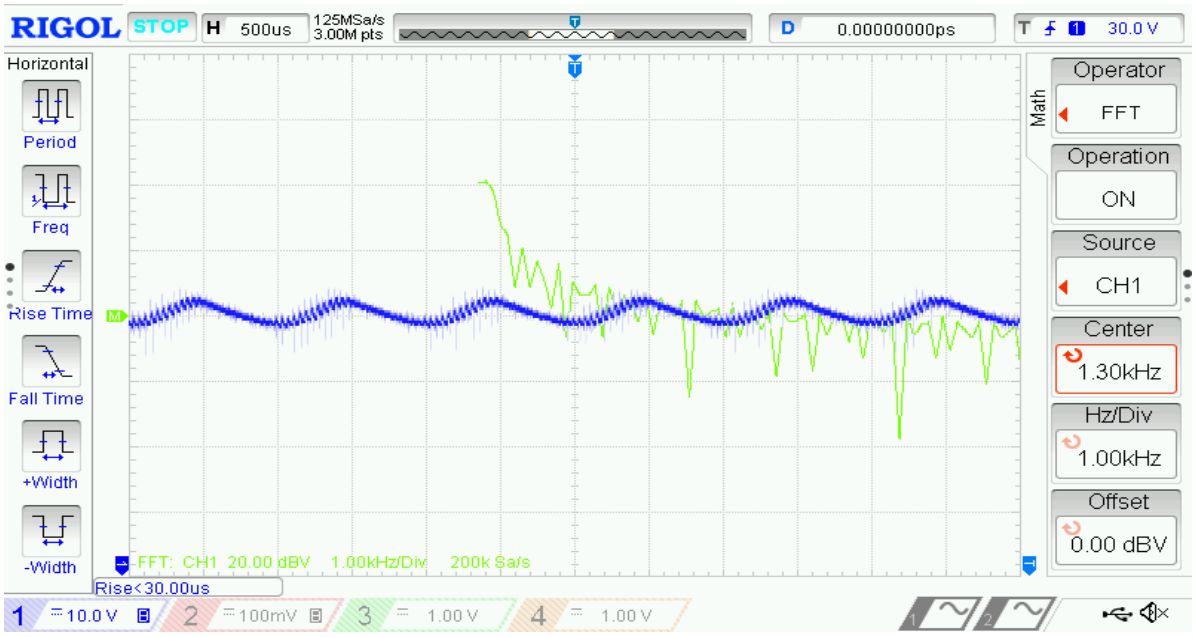

Figure 6.41: Experimental analysis FFT of output voltage boost converter.

Experimental output voltages with FFT analysis of the boost converter is shown in Fig. 6.41 and Fig. 6.42. The experimental analysis of the input (control) and output voltage signal by FFT of the boost converter matches the simulation analysis of the system.

6.4 Identification of a DC-DC Boost Converter with Constant Power Load (CPL)

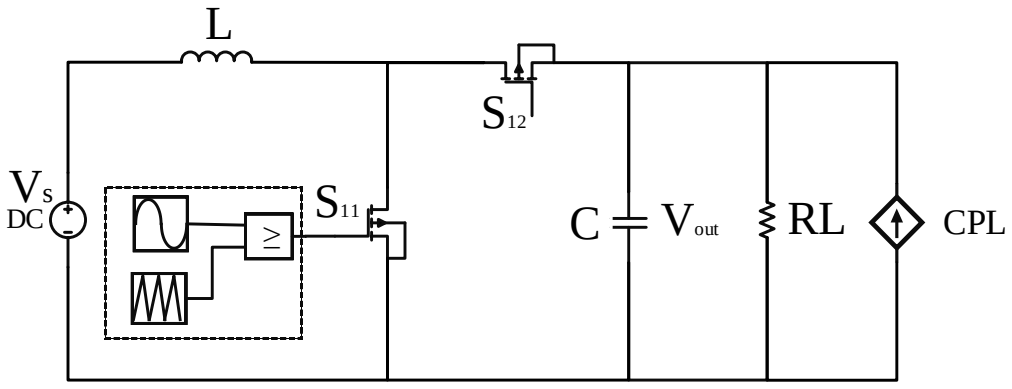

Figure 6.42: DC-DC boost converter with CPL.

The circuit of the boost converter with a constant power load (CPL) is presented that in Figure. 6.43. The system of the boost converter with CPL contains an inductor L, capacitor C,

resistive load and the constant power load. The input voltage on this application is constant value. The control signal is combination of a dc voltage added to a sinusoidal a wave of a selected frequency range. The converter operates in the continuous conduction mode at all time by adjusting the amplitude of the control signal for the application. The results represent the relationship between the control signal and the output voltage.

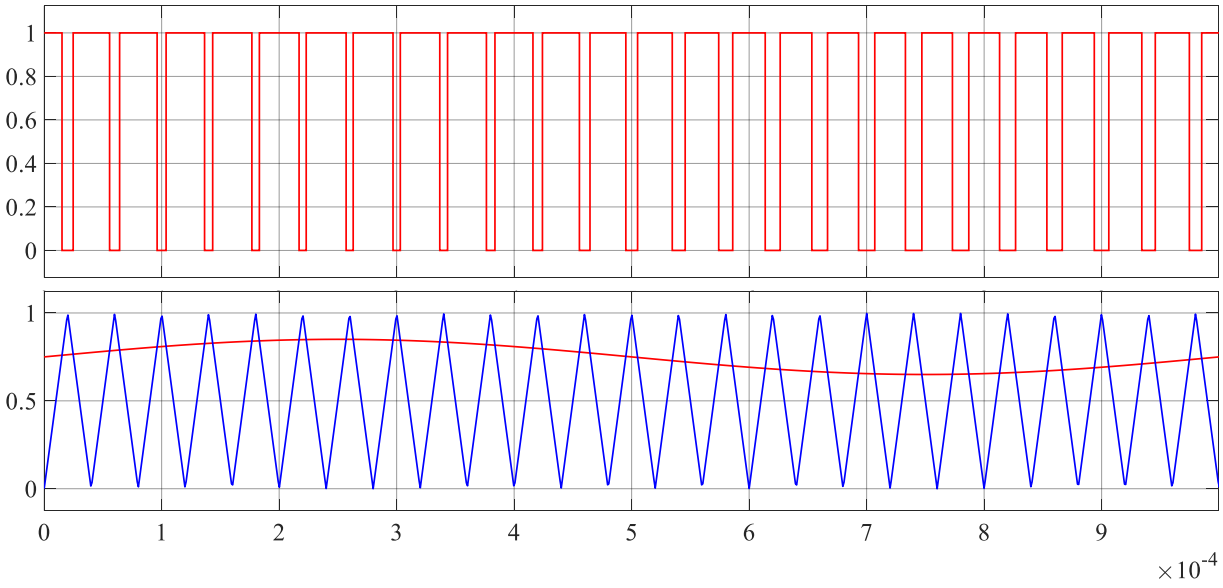

Figure 6.43: Example of control signal for boost converter with CPL at 1000Hz.

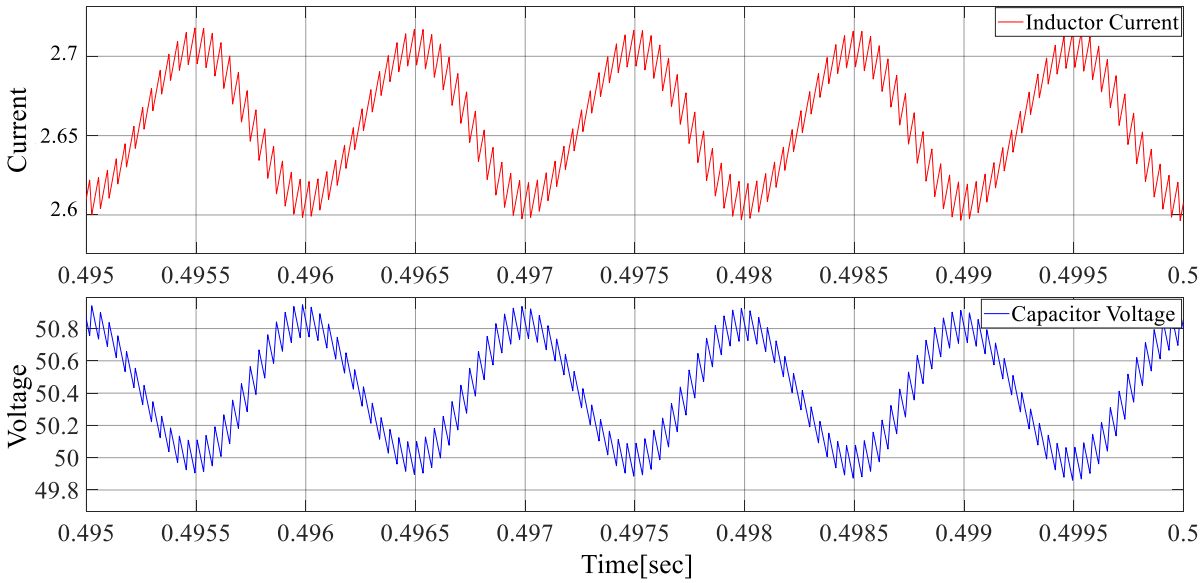

Figure 6.44: Inductor current and capacitor voltage with CPL at 1000Hz.

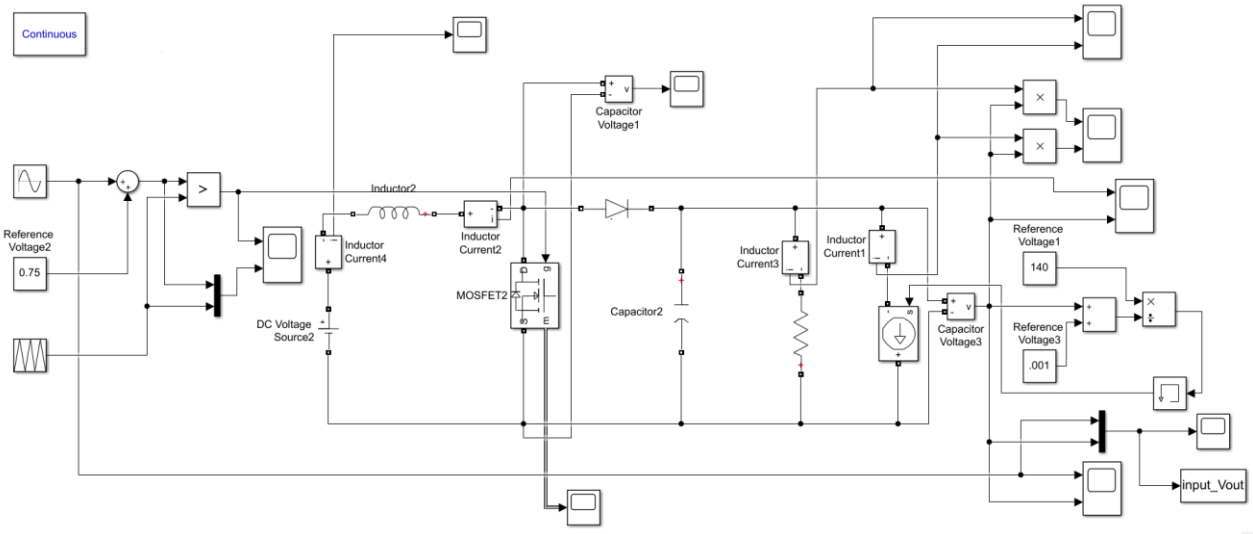

Figure 6.45: DC-DC boost converter with CPL in Matlab-Simulink.

6.4.1 FFT Algorithm for Boost Converter with CPL

The FFT is used to define the amplitude and phase angle for the output signal. A magnitude and phase shift for each frequency is applied to the system that achieved as shown in Table 6.4.

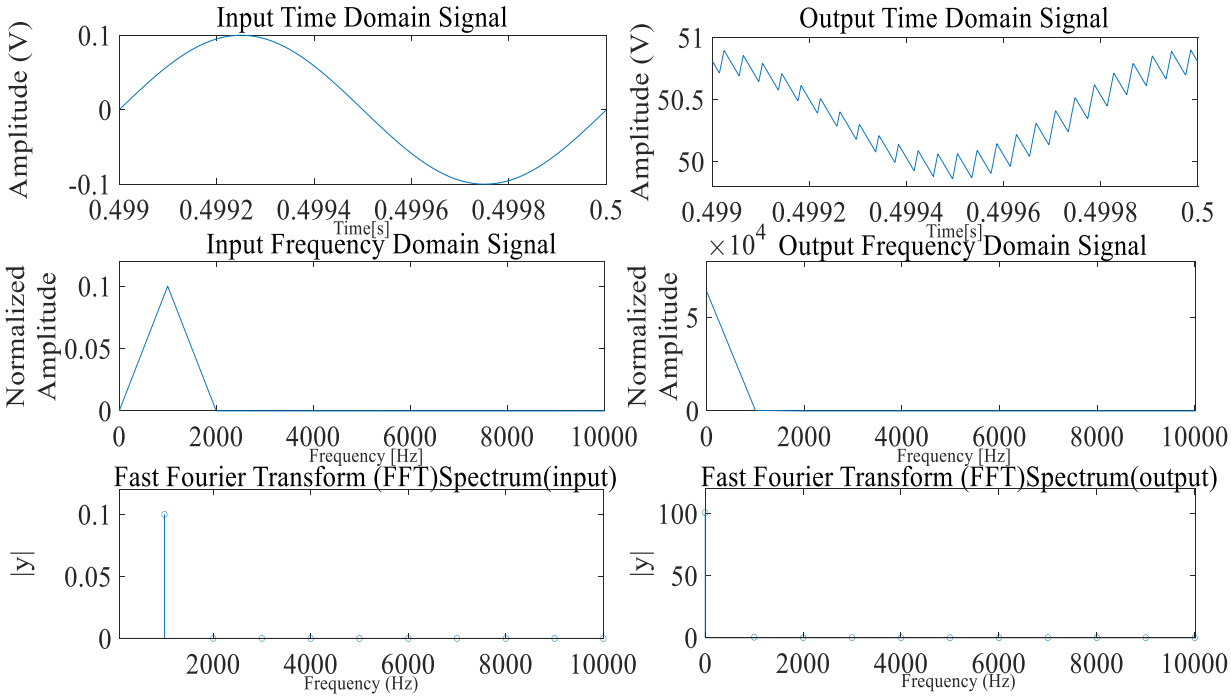

Figure 6.46: Example of FFT analysis for boost converter with CPL of 1000Hz.

Table 6.3: Collected data bode plot for boost with CPL converter.

Frequency(Hz)	Magnitude (dB)=20*log(gine)	Phase shift Degree
1	47.3921	-10.9952
5	47.0526	-22.0885
10	47.6473	-30.7251
15	51.4103	-35.5453
20	53.6425	-46.8761
25	56.854	-52.6526
30	57.3562	-86.1381

Continued Table 6.3: Collected data bode plot for boost with CPL converter.

Frequency(Hz)	Magnitude (dB)=20*log(gine)	Phase shift Degree
40	52.9534	-212.2466
50	45.4137	-226.6947
60	41.4514	-228.2263
75	37.8449	-235.7627
85	35.9335	-241.4321
100	34.8573	-246.9964
150	30.6334	-247.3601
200	28.9137	-256.3521
250	27.84	-259.6278
300	26.1333	-261.425
350	24.7746	-262.295
400	23.5796	-263.5039
450	22.9723	-263.6524
500	21.8184	-264.5572
550	20.7828	-265.2161
600	20.3112	-265.6837

Continued Table 6.3: Collected data bode plot for boost with CPL converter.

Frequency(Hz)	Magnitude (dB)=20*log(gine)	Phase shift Degree
650	19.3166	-266.1577
700	18.6279	-267.236
750	18.0871	-266.1082
800	17.4952	-266.9808
850	17.0051	-266.6152
900	16.475	-267.103
950	15.9756	-268.3574
1000	15.5359	-267.7728
1250	14.6166	-267.464
1500	13.0996	-267.4748
1750	12.7184	-268.8022
2000	12.1755	-268.6971
2250	10.9842	-269.2033
2500	9.1765	-268.8765
2750	8.7891	-268.3201
3000	8.2396	-269.0522
3250	7.5043	-269.3374

Continued Table 6.3: Collected data bode plot for boost with CPL converter.

Frequency(Hz)	Magnitude (dB)=20*log(gine)	Phase shift Degree
3500	6.7154	-269.0346
3750	6.3799	-269.6419
4000	5.7671	-269.0872
4250	5.0017	-269.5761
4500	4.2365	-269.8106
4750	4.1526	-269.0254
5000	4.0012	-269.4579

6.4.2 Bode Plot Generation for Boost Converter with CPL

The open-loop system response to varying frequency inputs (duty cycle) is obtained and data tabulated in Table 6.3. Based on the accuracy of data is obtained of magnitude and phase shift resulting a Bode plot drawing has magnitude (∓ 20) in decibel (dB) and the phase shift in degrees and angular frequency ω. The frequency of the sinusoidal function in the control input of Simulink model is $2\pi f$ rad/sec. The frequency range of (1-5K Hz) applied to the model as shown that in Figure . 6.48.

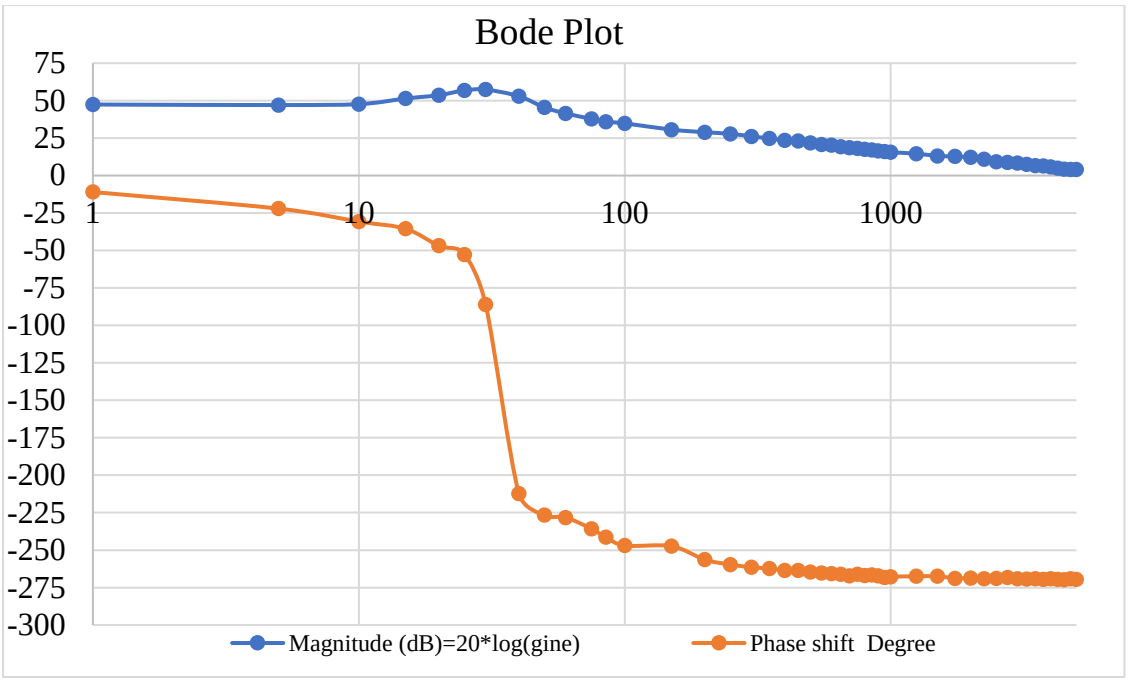

Figure 6.47: Bode Plot of boost with CPL from simulation data.

Comparing the high order transfer function determined with the Matlab command (TFEST) is applied to the frequency response data. A second order system is estimated from the analyzed data that is fitted with estimation accuracy of 58.07% of the actual system behavior as:

$$G(s)_{sose} = \frac{8.65\times10^{6}}{s^{2} + 63.87\, s + 3.413\times10^{4}}.$$

A third order system is estimated from the simulation data that fits to the estimation data by 76.21% of the simulated system,

$$G(s)_{tose} = \frac{2.82\times10^{9}}{s^{3} + 244.4\, s^{2} + 5.374\times10^{4}\, s + 8.981\times10^{6}}.$$

A third order system is estimated for the system with an added zero. It fits the data by 77.96% of the simulated system,

$$G(s)_{tosez} = \frac{-4.669\times10^{6}\, s + 3.797\times10^{9}}{s^{3} + 346.7\, s^{2} + 5.955\times10^{4}\, s + 1.357\times10^{7}}.$$

An eleventh order system is estimated for the analyzed system and has the best fits to the data by 99.28% of the actual system as following:

$$G(s)_{fose} = \frac{-3.837 \times 10^4\, s^{10} + 1.569 \times 10^7\, s^9 - 1.299 \times 10^9\, s^8 + 3.145 \times 10^{11}\, s^7}{s^{11} + 185\, s^{10} + 1.825 \times 10^5\, s^9 + 5.256 \times 10^7\, s^8 + 1.374 \times 10^{10}\, s^7}$$

$$\frac{-8.446 \times 10^{14}\, s^6 + 4.109 \times 10^{16}\, s^5 - 3.298 \times 10^{19}\, s^4 + 1.315 \times 10^{21}\, s^3 - 1.06 \times 10^{23}\, s^2}{+2.848 \times 10^{12}\, s^6 + 2.668 \times 10^{13}\, s^5 + 4.657 \times 10^{16}\, s^4 + 7.913 \times 10^{18}\, s^3 + 6.848 \times 10^{19}\, s^2}$$

$$\frac{+9.548 \times 10^{24}\, s + 6.746e25}{+4.939 \times 10^{22}\, s + 2.543 \times 10^{23}}.$$

The comparison between all the estimated transfer functions for simulation data is shown in Figure. 6.49.

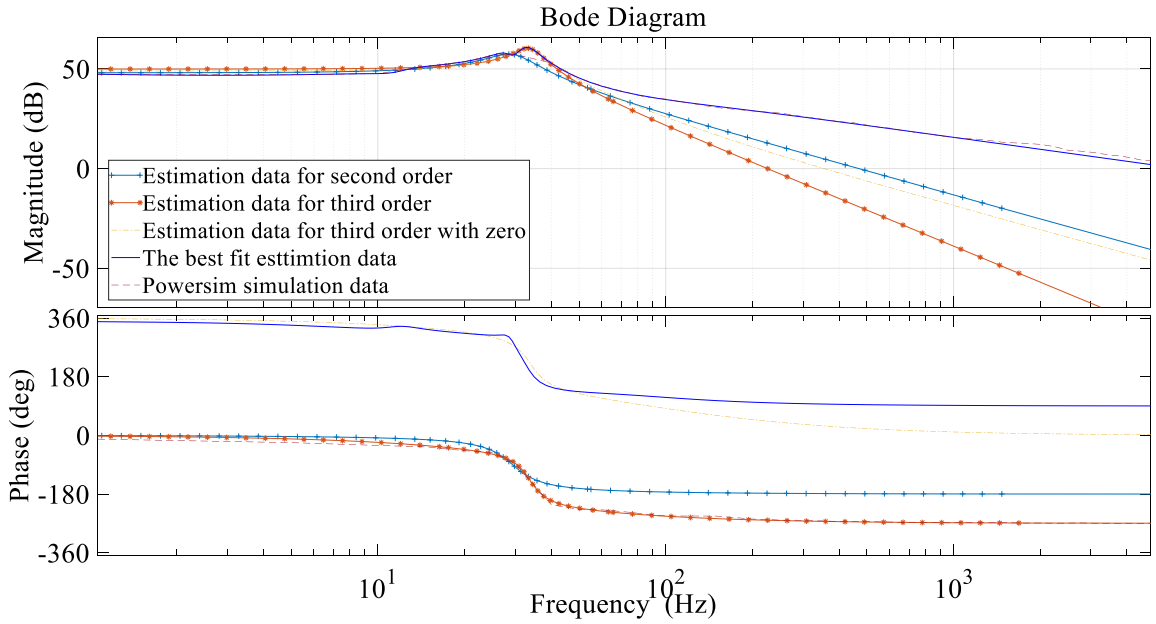

Figure 6.48: Bode plot comparison of the boost converter with CPL data.

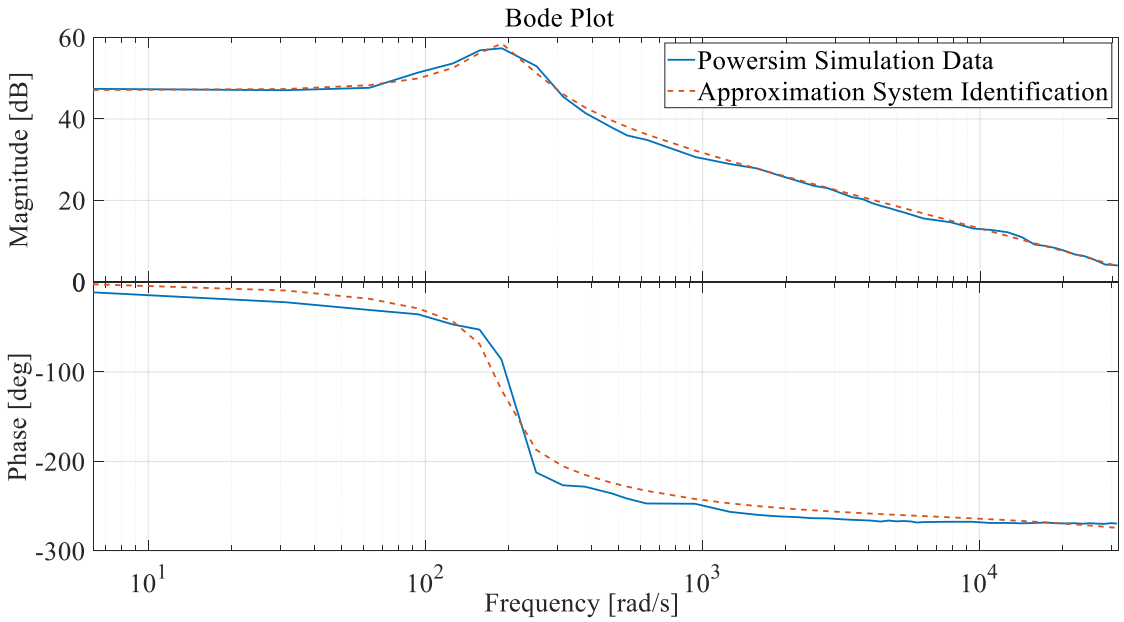

Figure 6.49: Bode plot of boost converter with CPL.

The actual behavior of the system for the fractional order transfer function is derived by applying Levy's method resulting the estimation error is 6% as following:

$$G(s)_{FO} = \frac{6.0463\times10^{-5}s^{1.8} - 1.4803s^{0.9} + 227}{6.425\times10^{-14}s^{3.6} + 1.4168\times10^{-9}s^{2.7} + 8.0277\times10^{-5}s^{1.8} + 7.4832\times10^{-5}s^{0.9} + 1}.$$

6.4.3 Modeling and Analysis of a DC-DC Boost Converter with CPL

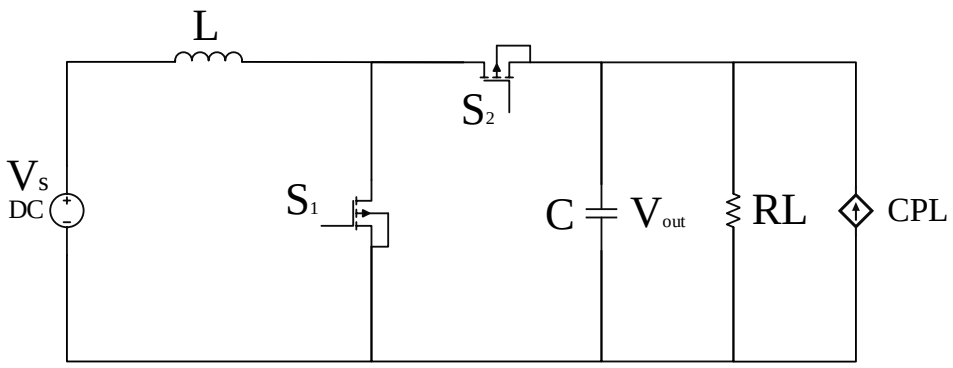

Figure 6.50: Boost converter with CPL.

A dc-dc power converter is constructed by using connection of a boost converter with a constant power load (CPL). The model of the boost converter with CPL is derived to be:

KVL L:

$$V_s = L\,\frac{d_i}{dt} + V_C(1 - S_1)$$

KCL C:

$$i\,(1 - S_1) = C\,\frac{d_v}{dt} + \frac{V_C}{RL} + \frac{P}{V_C}$$

Average Normalized Model

$$x_1 = i\,, x_2 = V_{out}, S_1 = U$$

$$\dot{x}_1 = \frac{V_S}{L} - \frac{x_2(1 - U)}{L}$$

$$\dot{x}_2 = \frac{x_1(1 - U)}{C} - \frac{x_2}{C\,RL} - \frac{P}{C x_2^{\,2}}$$

With state-space equations:

$$A = \begin{bmatrix} 0 & \frac{-(1-U)}{L} \\ \frac{(1-U)}{C} & \frac{-1}{CRL} - \frac{P}{Cx_2^2} \end{bmatrix}, \qquad B = \begin{bmatrix} \frac{x_2}{L} \\ \frac{-x_1}{C} \end{bmatrix}, \qquad C = [0 \quad 1], \qquad D = [0]$$

The conventional linearized transfer function is:

$$G(s)_{Linearized} = \frac{-2.677\text{e}04\,\text{s} + 7.738\text{e}06}{s^2 + 25.15\,s + 3.72e04}.$$

The actual system is compared with the linearized system as a Bode plot and is shown in Figure. 6.51.

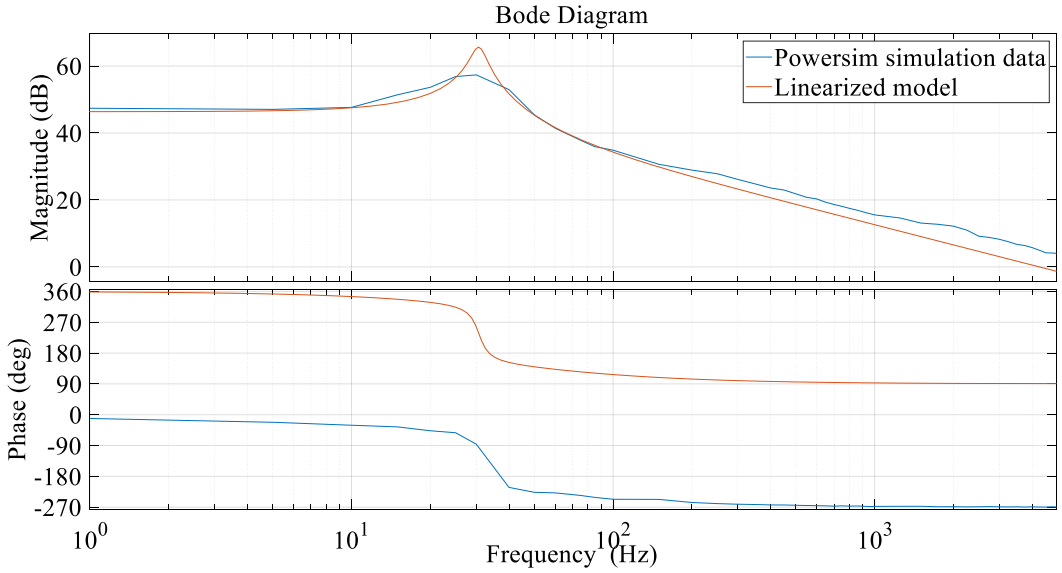

Figure 6.51: Bode plot comparison of boost converter with CPL (actual data and linearized model).

6.4.4 Controller for the DC-DC Boost Converter with CPL

The cascaded controller is used for the boost converter with an inner and outer loop controller for the converter. The error variable is defined as:

$$\dot{x}_1 = e(t) = i_{lref} - i_l$$

and the a new state variable is defined from the tracking error as:

$$x_1 = \int e(t),$$

$$x_2 = i_l\,.$$

The state-space equations are represented as:

$$\dot{x}_1 = i_{lref} - x_2$$

$$\dot{x}_2 = -\frac{r_l x_2}{L} - \frac{v_o(1-u)}{L}$$

Converting the state-space equations to standard LQR is represented as following:

$$\dot{z}_1 = -z_2$$

$$\dot{z}_2 = -\frac{r_l z_2}{L} - \frac{u}{L}$$

The controller input *u* is minimized by the quadratic cost function

$$J(t) = \int_0^\infty (z^T Q z + v^2)dt,$$

where Q is a symmetric positive semi-definite matrix. The root locus of the boost converter is provided in Fig. 6.53.

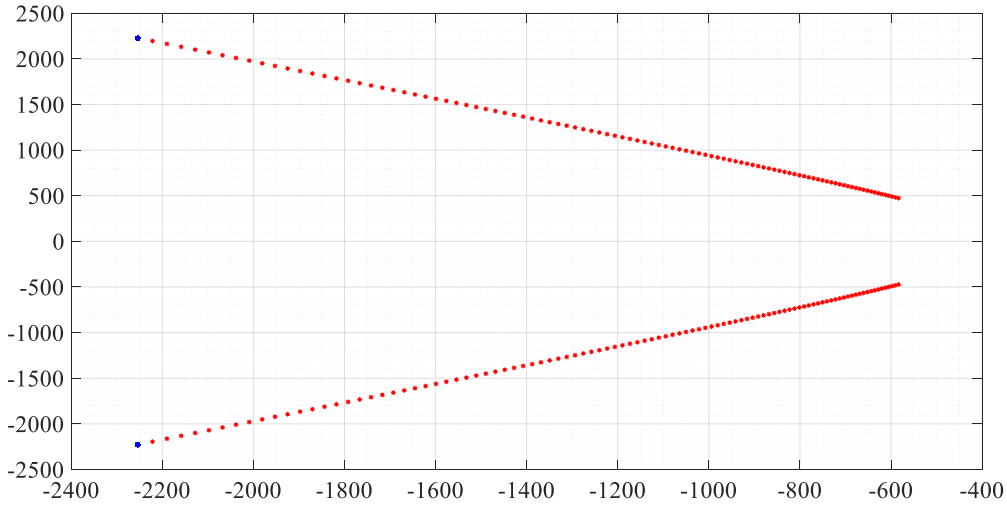

Figure 6.52: Movement of closed loop poles for current control loop of the boost with CPL.

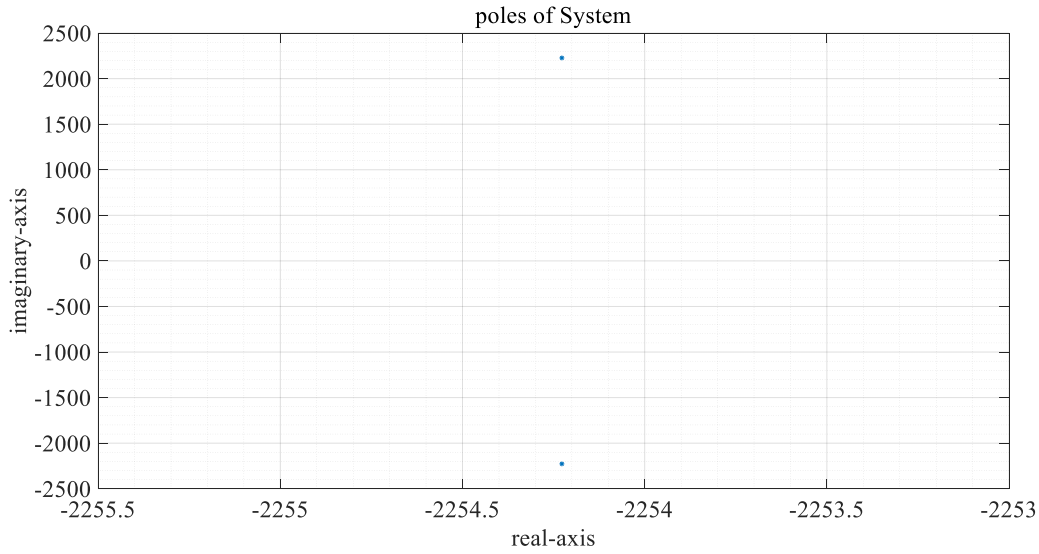

Figure 6.53: Poles of current control loop location of the boost with CPL.

Define the gains for outer loop to control the output voltage of the boost converter by using the LQR technique. The new state variable is represented as:

$$\dot{x}_1 = e(t) = V_{ref} - V_{out}.$$

Consideration the tracking error,

$$x_1 = \int e(t),$$

$$x_2 = V_{out},$$

$$\dot{x}_1 = V_{ref} - x_2$$

$$\dot{x}_2 = \frac{(1-u)}{C} i_l - \frac{1}{C\ R_L} x_2 - \frac{P}{C x_2}$$

Determining the tracking of the system behavior as following:

$$\dot{z}_1 = -z_2$$

$$\dot{z}_2 = \frac{v_{in}}{C v_{ref}} u - \frac{1}{C\ R_L} z_2 - \frac{P}{C z_2}$$

The controller of the input *u* minimizes the quadratic cost function:

$$J(t) = \int_0^\infty (z^T Q z + v^2) dt$$

where Q is a symmetric positive semi-definite matrix. The control for boost converter is shown in Figure. 6.55.

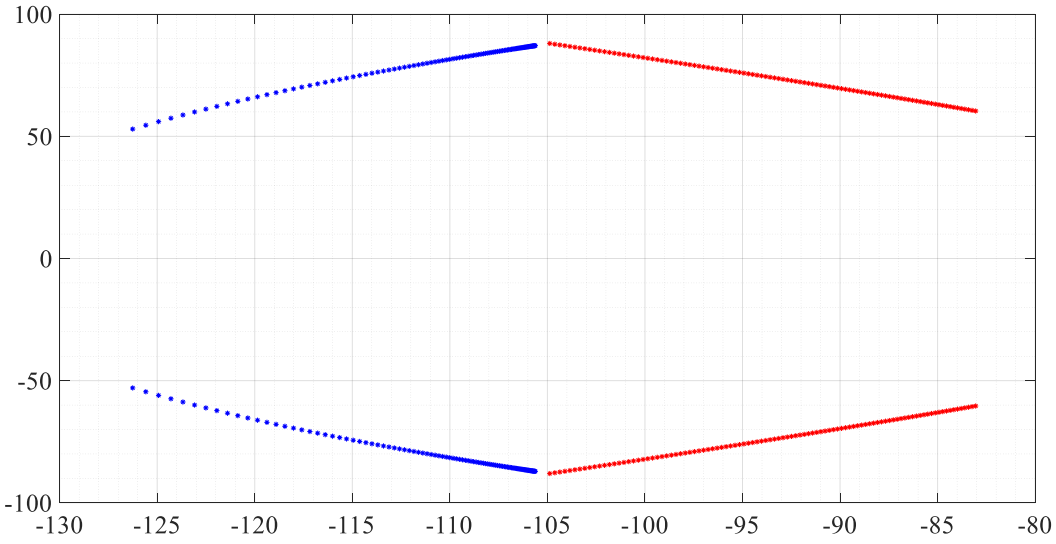

Figure 6.54: Movement of closed loop poles for voltage controller of the boost with CPL.

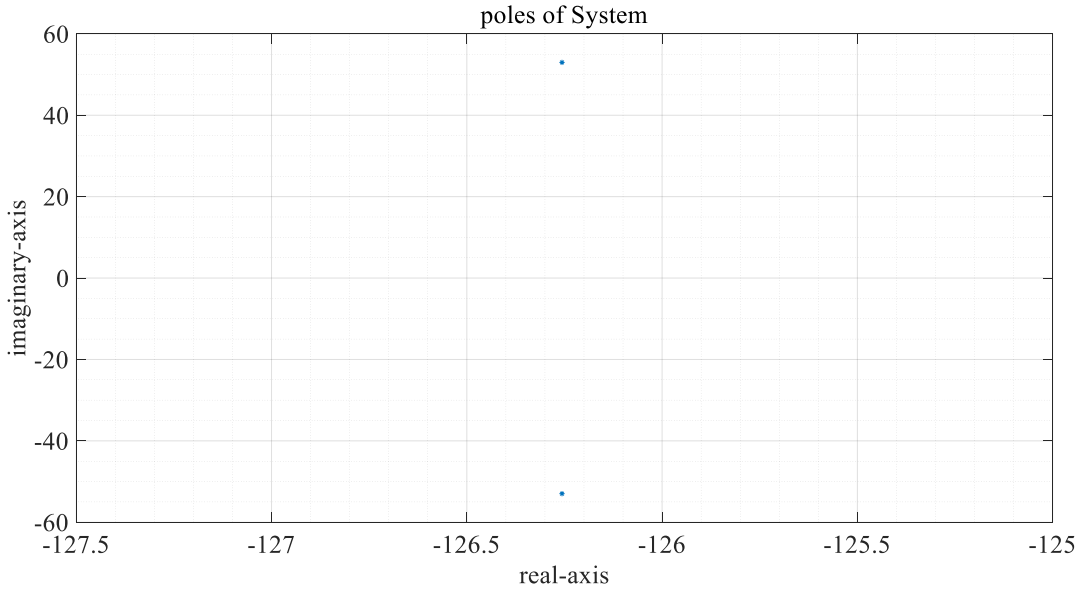

Figure 6.55: Poles of voltage controller location of the boost with CPL.

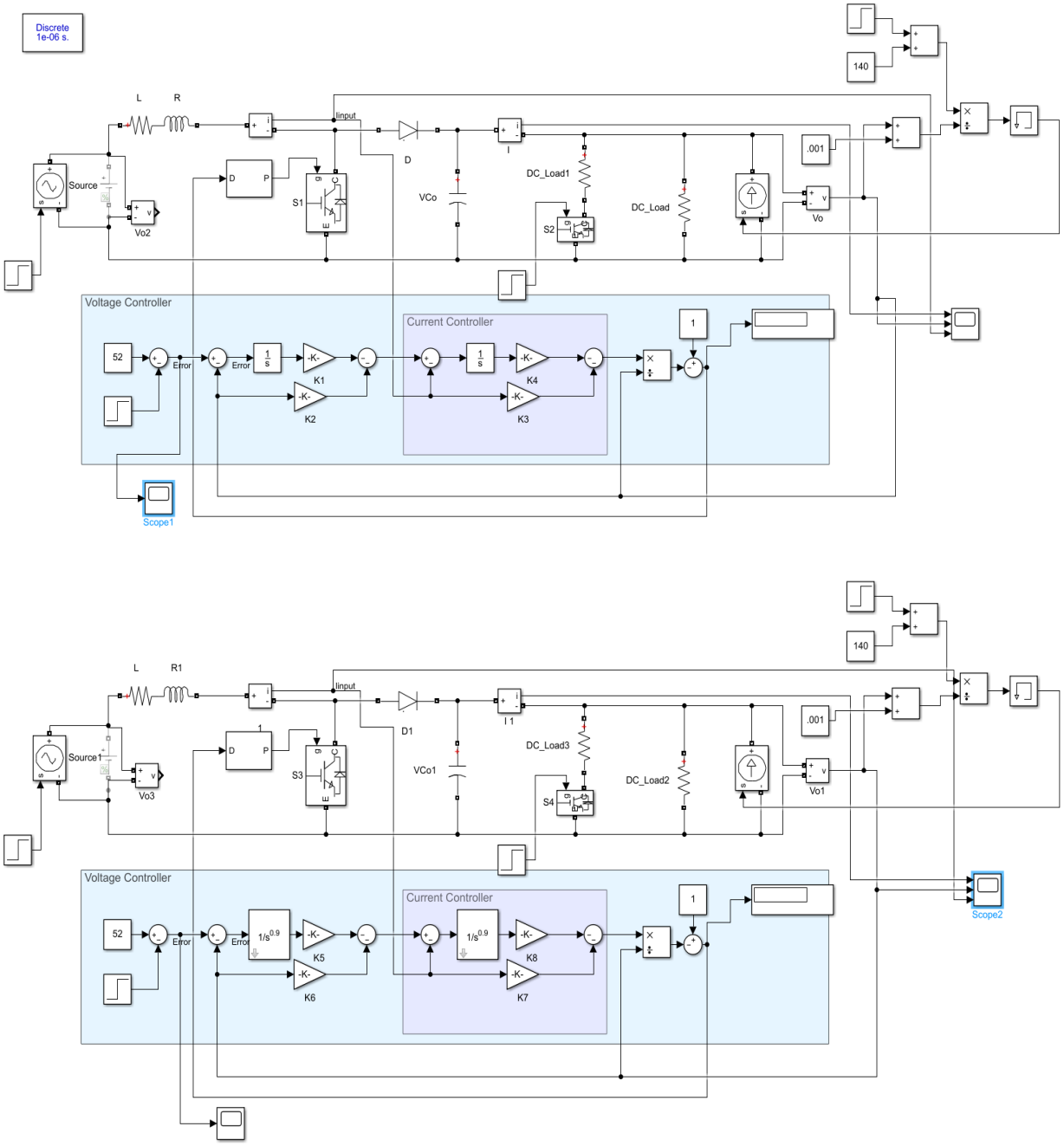

Figure 6.56: Integer-Order controller with fractional-order controller for boost with CPL.

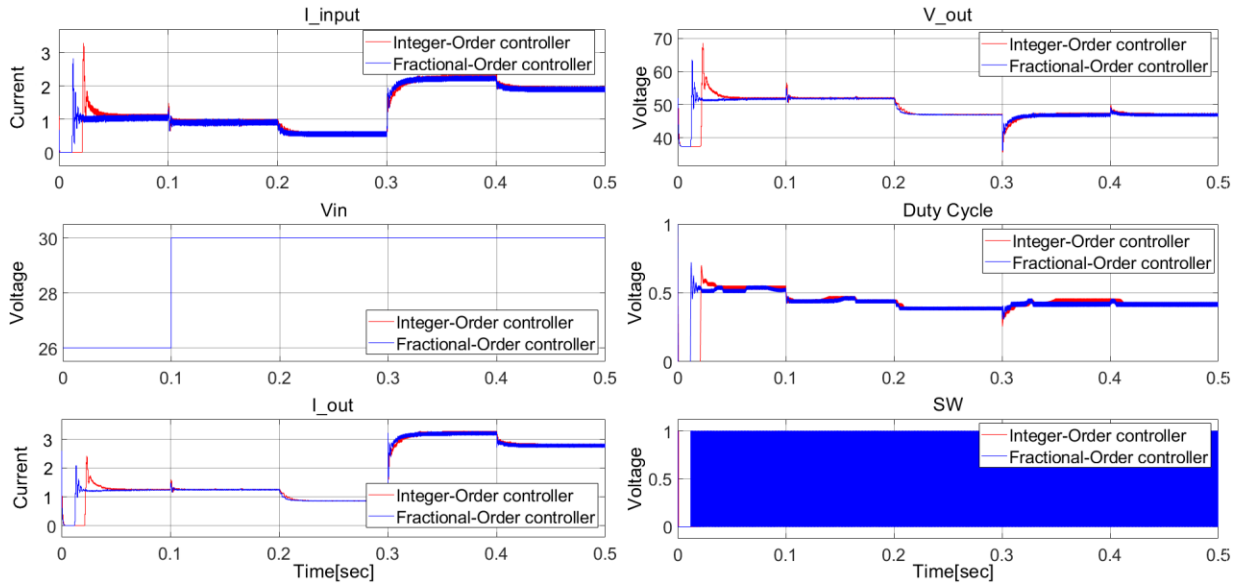

Figure 6.57: Fractional order controller and integer-order controller for boost with CPL.

The actual system behavior of the boost converter with CPL with the fractional controller has less overshoot and faster response. Disturbances are applied for the systems for controlling the output voltage. At 0.1 s, the input voltage is increased but the output voltage remains at the expected value. At 0.2 s, the reference of the output voltage is reduced to have verification of tracking the output value. At 0.3 s, the resistive load is decreased top 0.4 of the value of the constant power load. The system performance with the controller is shown in Fig. 6.58.

6.5 Identification of a Boost-Buck Converter Circuit

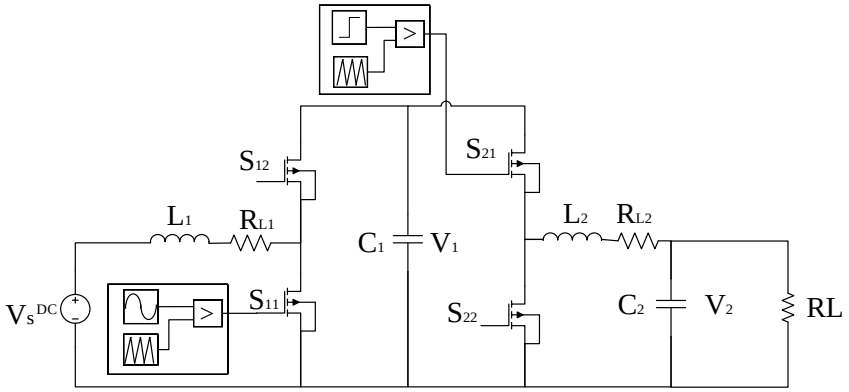

Figure 6.58: Boost-buck frequency response simulation.

The system used in this experimental part is a cascaded boost and buck converter. The objective behind this study is to develop the FO control for a boost converter with a CPL and controlling non-minimum phase fractional-order system. The research additionally shows new methods for modeling and examining converters. The procedure presents the actual system boost converter with CPL boost buck converter. The cascade boost-buck converter has two controller switches. The cascade boost-buck converter is considered as one system. The system is represented by a fractional order transfer function. The boost converter PWM switching is shown in Fig. 6.60. The PWM structure for the buck converter is shown in Fig. 6.61. The output signal taken from the output voltage over the load of the system. The voltage output ripples of frequency is determined between 5-5KHz.

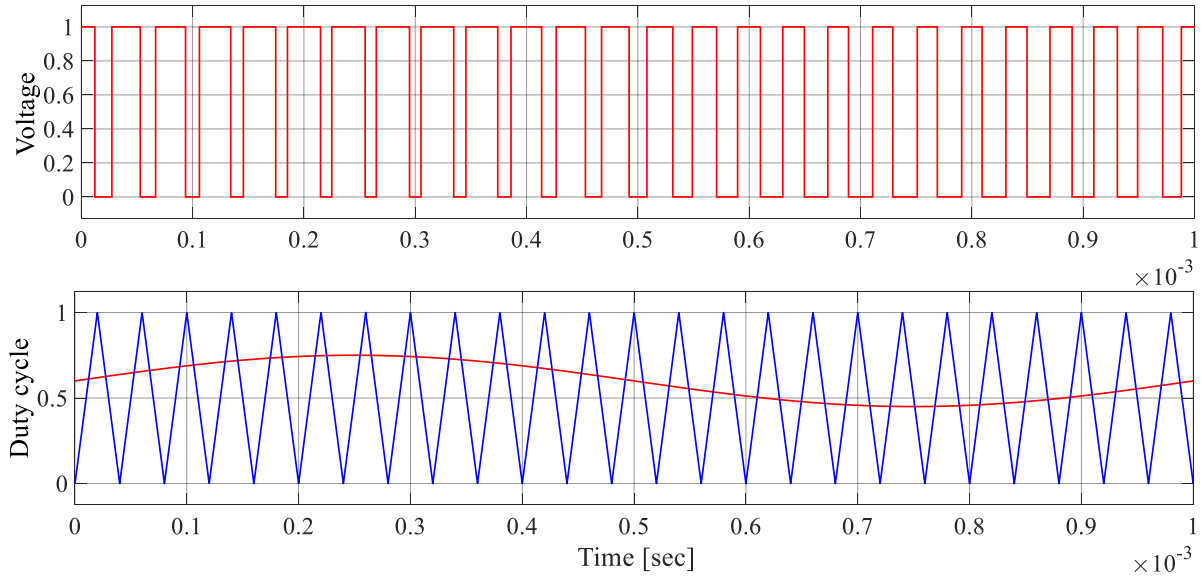

Figure 6.59: Switching input for boost converter.

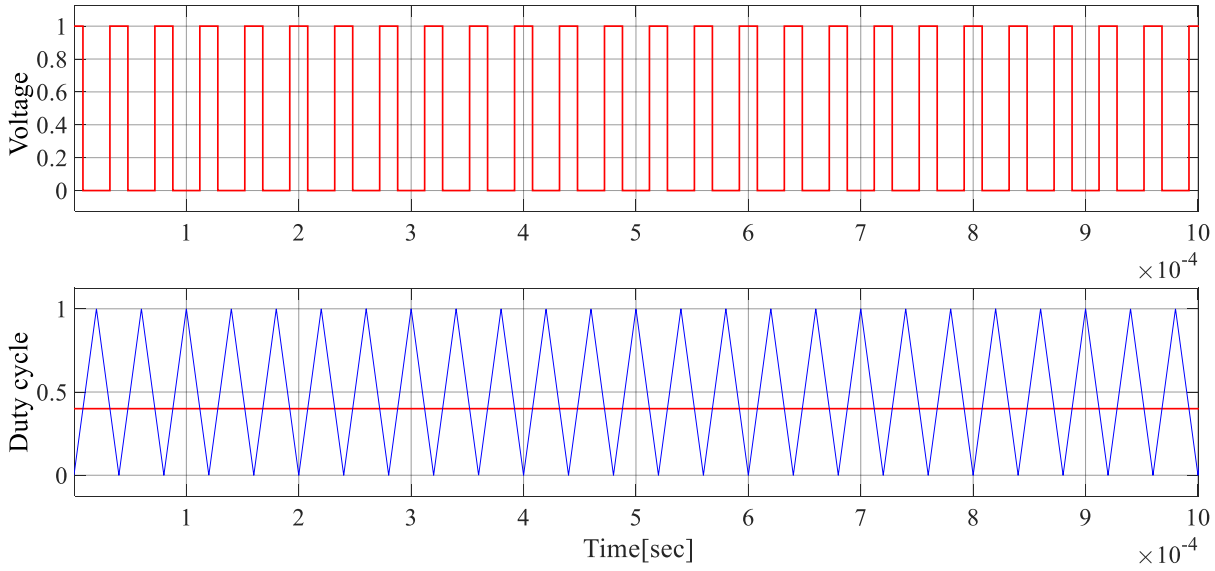

Figure 6.60: Switching input for buck converter.

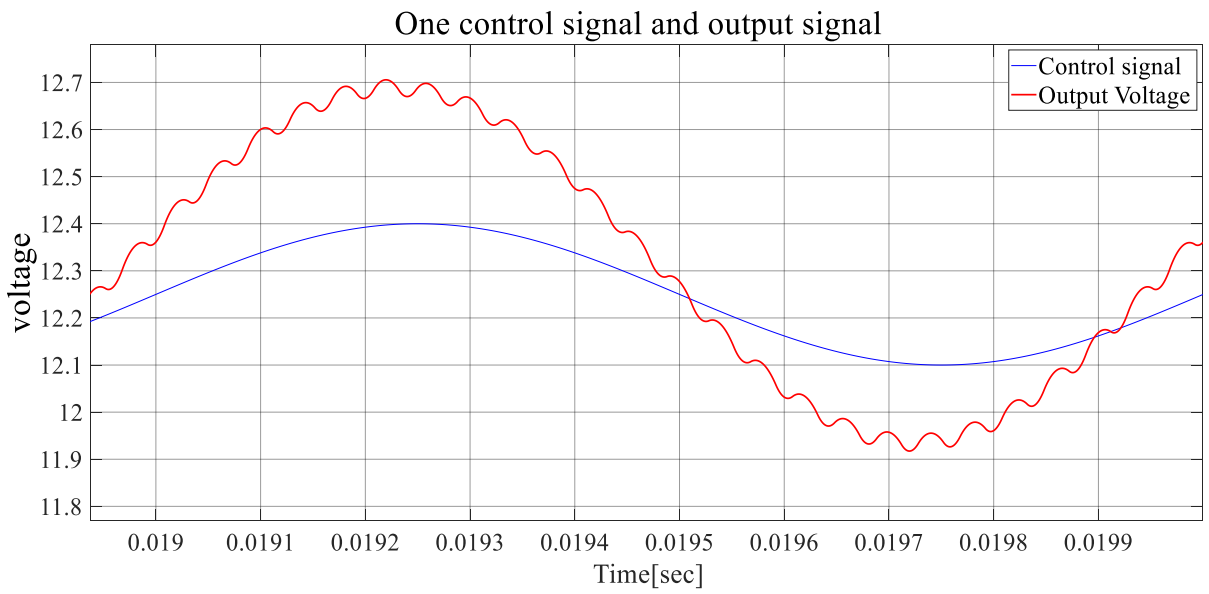

Figure 6.61: Input-Output frequency response of boost-buck converter.

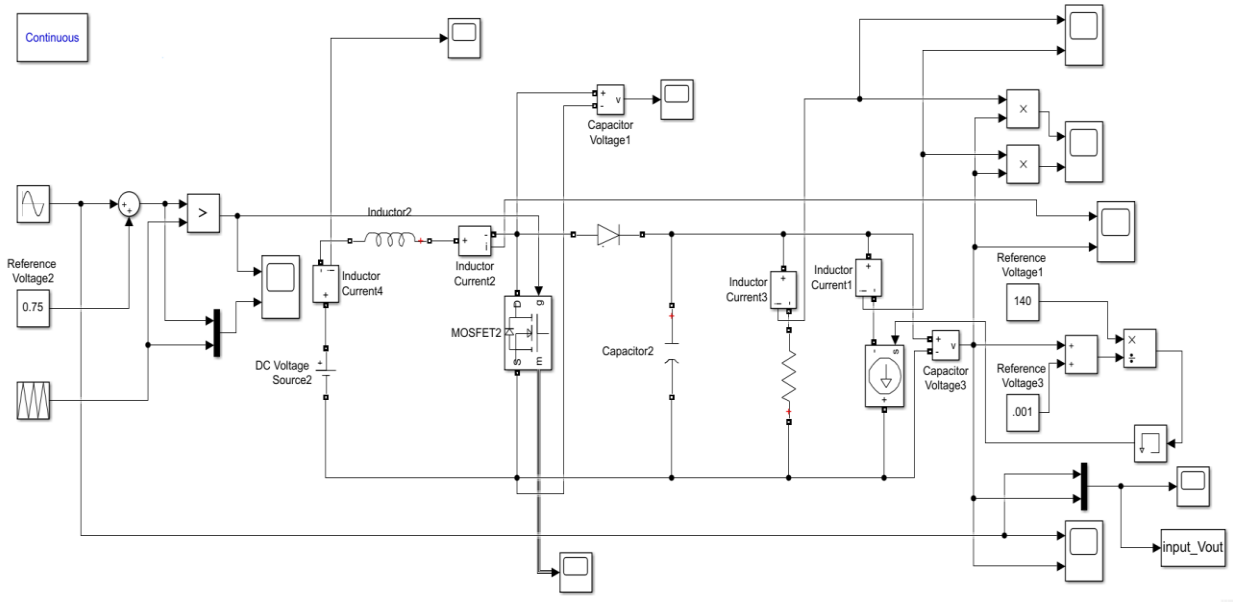

Figure 6.62: Boost-buck Matlab simulation.

The magnitude and phase shift of the system is represented in Table 6.4 by using the previously defined methods.

Table 6.4: Data of Bode plot for boost-buck converter.

Frequency (Hz)	Magnitude (dB)=20*log( )	Phase shift (degrees)
50	26.6144	-25.9991
100	27.0115	-51.5781
200	28.6012	-100.997
300	30.9423	-159.5464
400	29.4158	-230.1422
500	24.4035	-275.7914
600	19.9116	-301.6907
700	16.2372	-319.0664
800	13.1326	-332.1507
900	10.4446	-342.4006
1000	8.0431	-351.0239
1500	-1.3096	-378.7302
2000	-8.1307	-395.1614
2500	-13.5589	-405.0542
3000	-17.4309	-416.5254
3500	-21.7178	-454.032
4000	-22.9075	-465.3801

Continued Table 6.4: Data of Bode plot for boost-buck converter.

Frequency (Hz)	Magnitude (dB)=20*log( )	Phase shift (degrees)
4500	-27.4369	-491.8412
5000	-29.1813	-490.2091

In Fig. 6. 64 shows the bode plot from the observed data.

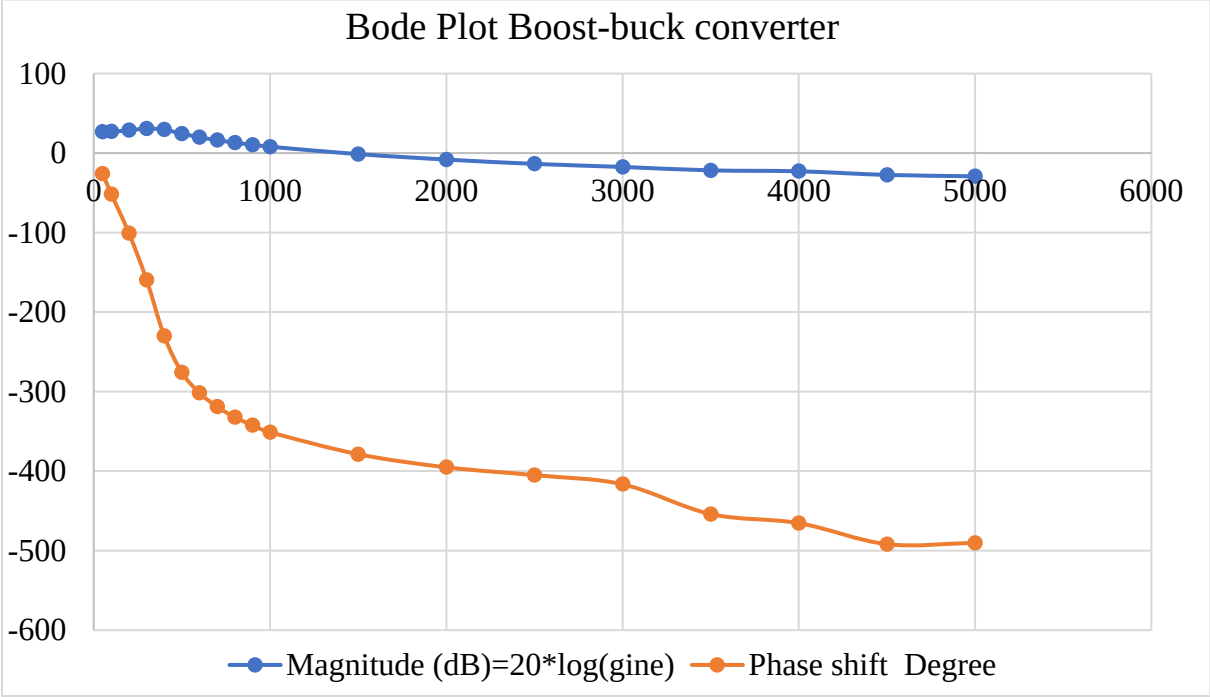

Figure 6.63: Bode plot of boost-buck converter form collected simulation data.

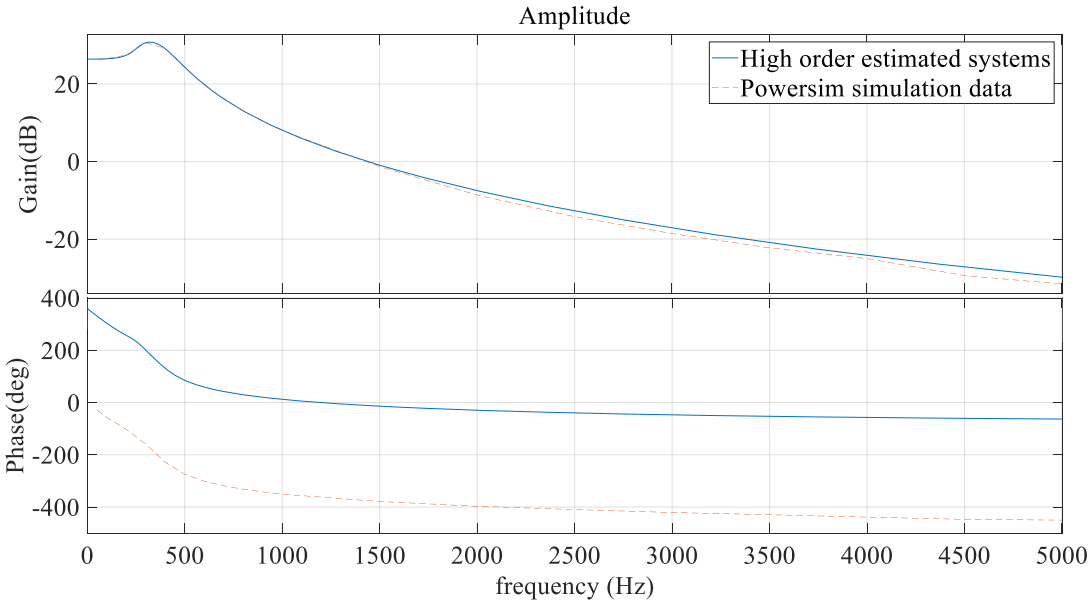

Figure 6.64: Bode plot of boost-buck simulation data and estimated system.

Hence, the transfer function for the estimated system in integer order generated by using Matlab command (TFEST).

$$G(s)=\frac{-8.453e11s^4-3.431e16s^3+2.806e19s^2-2.381e22s+1.837e26}{s^7+5.062e04s^6+5.242e08s^5+2.028e12s^4+5.706e15s^3+1.007e19s^2+1.148e22s+8.687e24}$$

Zeros and poles for the high order system show a non-minimum phase system as below with poles in the left hand side.

z =

1.0e+04 *

-4.1412 + 0.0000i

0.1879 + 0.0000i

-0.0529 + 0.1586i

-0.0529 - 0.1586i

```
p =
  1.0e+04 *
 -3.8180 + 0.0000i
 -0.8097 + 0.0000i
 -0.1875 + 0.0000i
 -0.0706 + 0.2185i
 -0.0706 - 0.2185i
 -0.0527 + 0.1601i
 -0.0527 - 0.1601i
```

6.5.1 Modeling and Analysis of a DC-DC Boost-Buck Converter

A multi-variable dc-dc power converter is constructed by using a cascaded boost and buck converter. Fig. 6. 69 shows the boost-buck circuit.

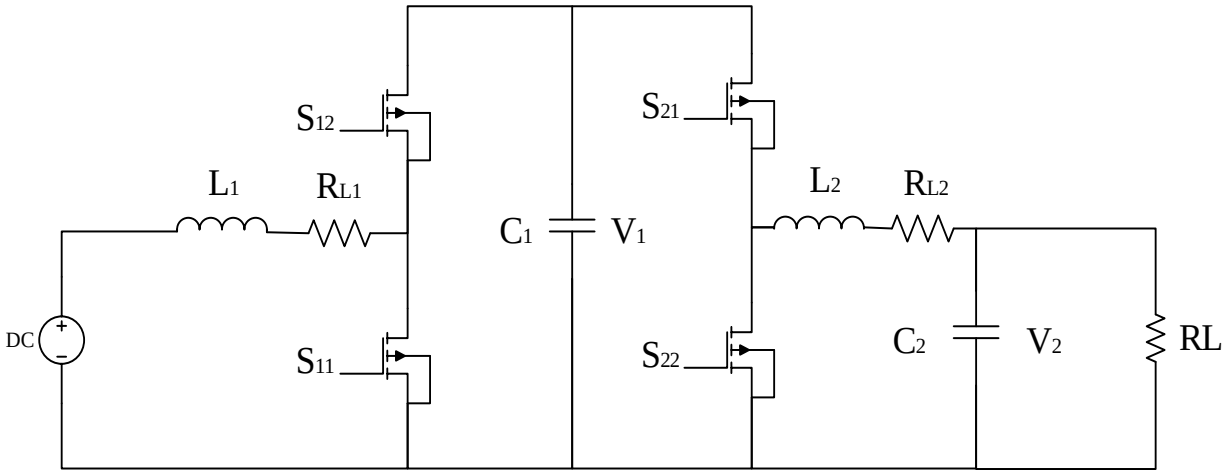

Figure 6.65: Boost-buck circuit.

The model of the converter is derived to be:

KVL L1:

$$V_s = L_1 \frac{d_{i1}}{dt} + R_{L1} i_1 + V_1 (1 - S_{11})$$

KCL C1:

$$i_1\left(1-S_{11}\right)=C_1\frac{dv_1}{dt}+i_2S_{21}$$

KVL L2:

$$V_1S_{21}=L_2\frac{di_2}{dt}+R_{L2}i_2+V_2$$

KCL C2:

$$i_2=C_2\frac{dv_2}{dt}+\frac{V_2}{RL}$$

Average normalized Model

$$x_1=i_1,x_2=V_1,x_3=i_2,x_4=V_2,S_{11}=U_1,S_{21}=U_2$$

$$\dot{X}_1=\frac{V_s}{L_1}-\frac{R_{L1}x_1}{L_1}-\frac{x_2\left(1-U_1\right)}{L_1}$$

$$\dot{X}_2=\frac{x_2\left(1-U_1\right)}{C_1}-\frac{x_3U_2}{C_1}$$

$$\dot{X}_3=\frac{x_2U_2}{L_2}-\frac{R_{L2}x_3}{L_2}-\frac{x_4}{L_2}$$

$$\dot{X}_4=\frac{x_3}{C_2}-\frac{x_4}{C_2RL}$$

A state space model and controller inputs is given by:

$$A=\begin{bmatrix} \frac{-R_{L1}}{L_1} & \frac{-(1-U_1)}{L_1} & 0 & 0 \\ \frac{(1-U_1)}{C_1} & 0 & \frac{-U_2}{C_2} & 0 \\ 0 & \frac{U_2}{L_2} & \frac{-R_{L2}}{L_2} & \frac{-1}{L_2} \\ 0 & 0 & \frac{1}{C_2} & \frac{-1}{C_2 RL} \end{bmatrix}$$

$$B=\begin{bmatrix} \frac{x_2}{L_1} & 0 \\ \frac{-x_1}{C_1} & \frac{-x_3}{C_1} \\ 0 & \frac{x_2}{L_2} \\ 0 & 0 \end{bmatrix}$$

$$C=\begin{bmatrix} 0 & 1 & 0 & 0 \\ 0 & 0 & 0 & 1 \end{bmatrix}$$

$$D=\begin{bmatrix} 0 & 0 \\ 0 & 0 \end{bmatrix}$$

The linearized transfer function is

$$G(s)_{\text{linearized}} = \frac{\text{-9.276e11 s + 1.657e15}}{s^4 + 1.096e04 s^3 + 3.345e07 s^2 + 7.083e10 s + 7.857e13}$$

The zero and poles are:

z =

1.7857e+03

```
p =
  1.0e+03 *
 -0.6882 + 2.1813i
 -0.6882 - 2.1813i
 -1.9720 + 0.0000i
 -7.6159 + 0.0000i
```

The actual system is compared with the linearized system as shown in Figure 6.68.

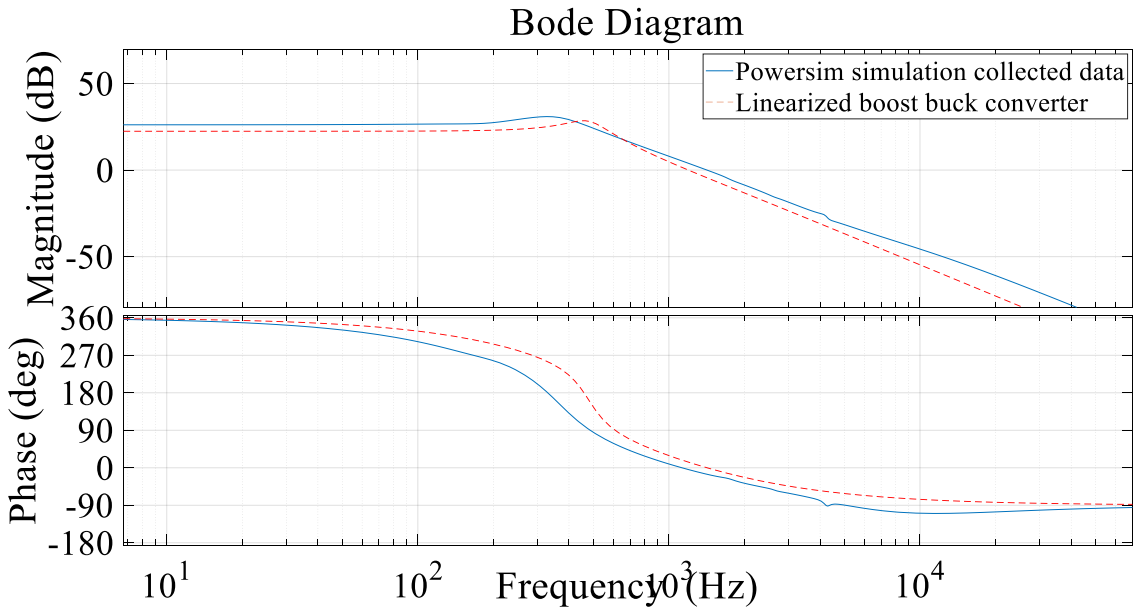

Figure 6.66: Bode plot for boost-buck of actual versus linearized data.

The fractional-order transfer function is compared with the real system characteristic behavior is shown in the Figure 6.72.

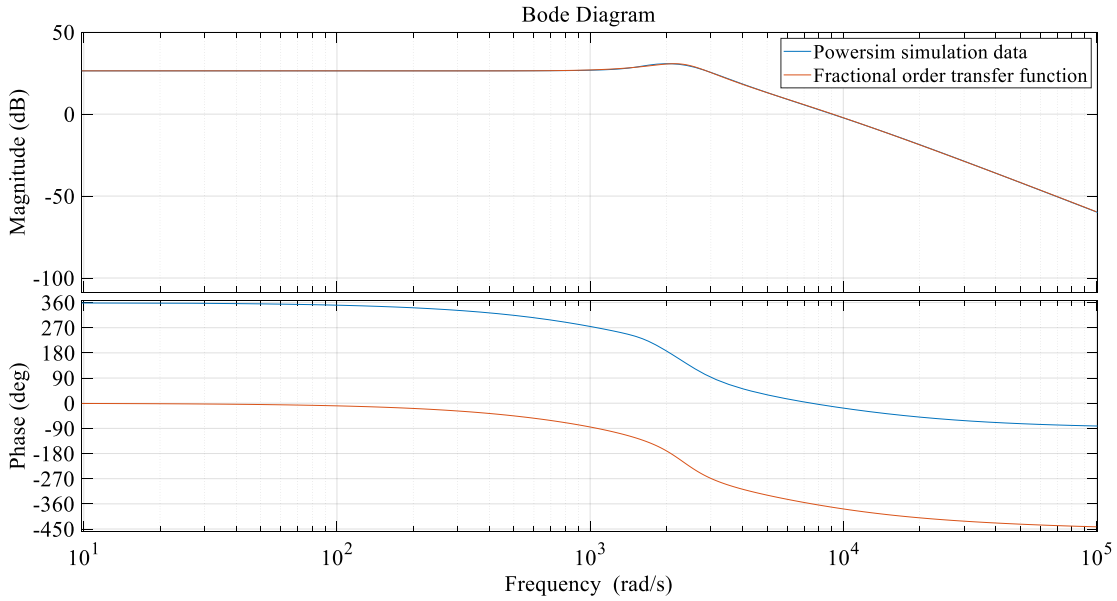

Figure 6.67: Bode plot for boost-buck actual versus fractional order.

The Levy identification method is used to find the fractional order system. It is compared with converter data is shown in Fig. 6.68. The fractional-order transfer function is equivalent to the actual system as:

$$G(s)_{fo} = \frac{-0.0011301s + 0.03882s^{0.8} - 0.54057s^{0.6} + 3.7922s^{0.4} - 13.322s^{0.2} + 18.58}{-3.6463e-05s + 0.0029157s^{0.8} - 0.041271s^{0.6} + 0.25783s^{0.4} - 0.7878s^{0.2} + 1}$$

6.5.2 PI Controller for the DC-DC Boost-buck Converter

The main objective of this research applies fractional order system identification method to find the actual behavior of the system and to design controllers for each stage of boost-buck converter to assure a stable system as shown in Figure 6.69. The controller is designed based on the both an integer order and fractional order models for comparison purposes.

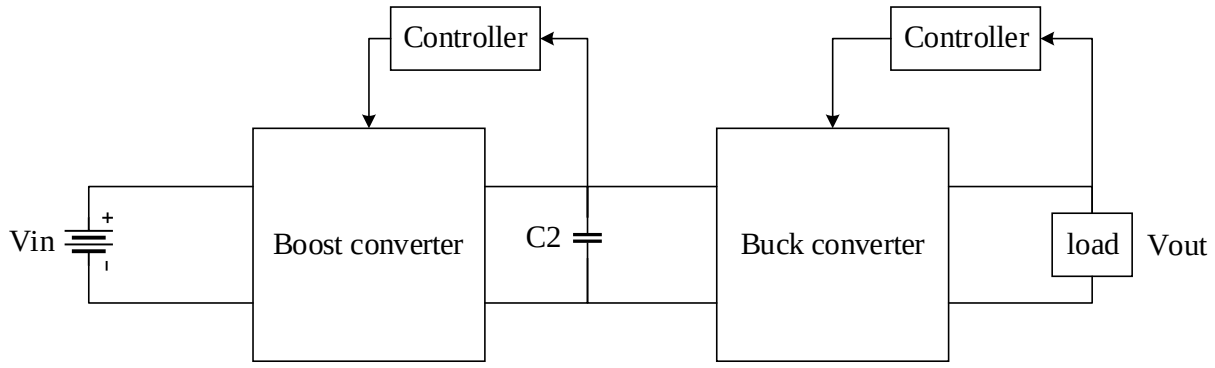

Figure 6.68: System block diagram of boost-buck converter.

The controller of the boost converter stage is used an inner and outer loop. The current state variable is represented as:

$$\dot{x}_1 = e(t) = i_{lboref} - i_{lbo}$$

where the reference inductor current for the boost converter and i_{lbo} is for the boost converter inductor. The state variable is defined from the tracking error as:

$$x_1 = \int e(t),$$

$$x_2 = i_{lbo}.$$

The state-space equations are represented as:

$$\dot{x}_1 = i_{lboref} - x_2$$

$$\dot{x}_2 = -\frac{r_{lbo}x_2}{L} - \frac{v_o(1-u)}{L}$$

Converting the state-space equations to standard LQR is represented as following:

$$\dot{z}_1 = -z_2$$

$$\dot{z}_2 = -\frac{r_l z_2}{L} - \frac{u}{L}$$

For controlling input u is minimized by the quadratic cost function:

$$J(t) = \int_0^\infty (z^T Q z + v^2) dt$$

where Q is a symmetric positive semi-definite matrix. The root locus for boost converter as shown in Fig. 6.70.

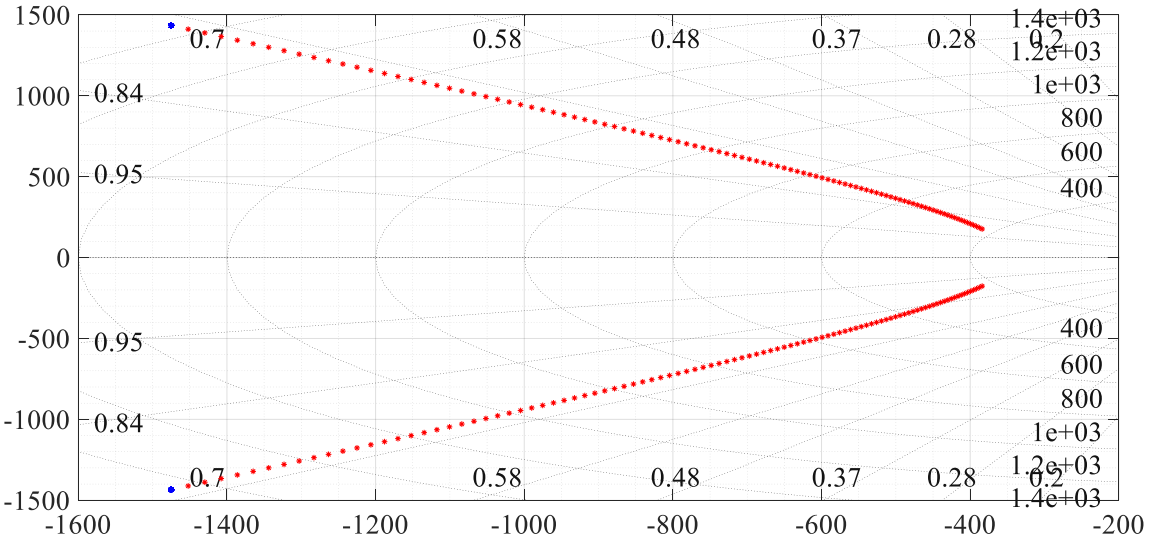

Figure 6.69: Movement of closed loop poles current controller of boost-buck converter.

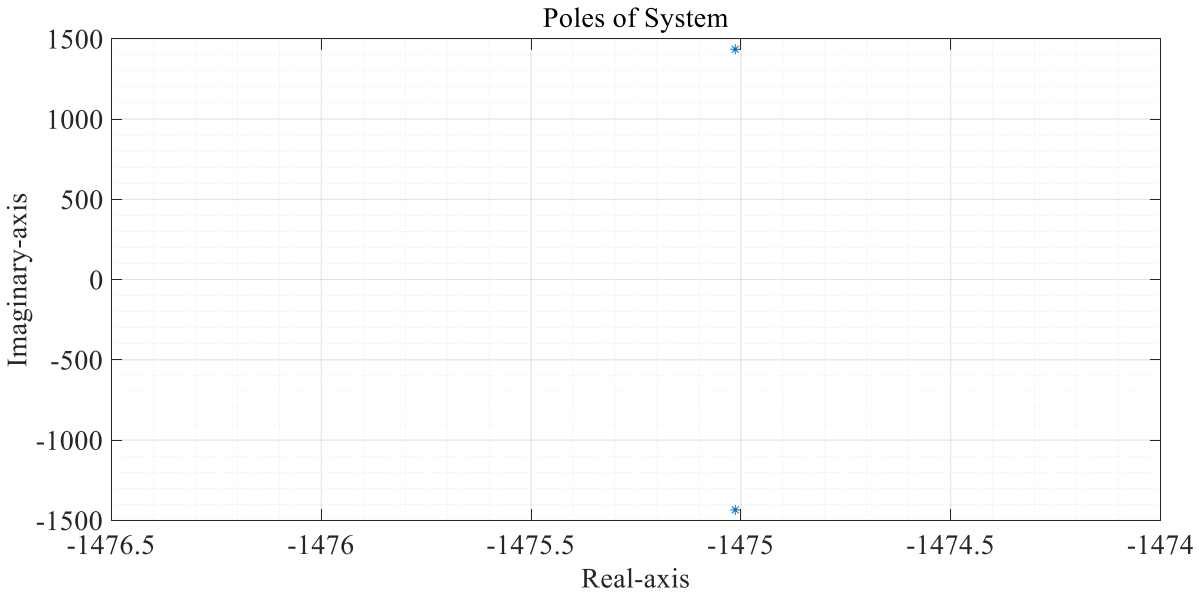

Figure 6.70: Poles of current controller location boost-buck converter.

Define the gains for outer-loop to control the output voltage of the boost converter. An error is defined as:

$$\dot{x}_1 = e(t) = V_{ref} - V_{out}$$

A new tracking error state-variable is added as

$$x_1 = \int e(t),$$

$$x_2 = V_{out},$$

$$\dot{x}_1 = V_{ref} - x_2$$

$$\dot{x}_2 = \frac{(1-u)}{C} i_l - \frac{1}{C\,R_L} x_2.$$

For determining the tracking of the system behavior:

$$\dot{z}_1 = -z_2$$

$$\dot{z}_2 = \frac{v_{in}}{C v_{ref}} u - \frac{1}{C\ R_L} z_2$$

The control input *u* is minimized by quadratic cost function

$$J(t) = \int_0^\infty (z^T Q z + v^2) dt$$

where Q is a symmetric positive semi-definite matrix. The control for boost converter is shown in Fig. 6.72.

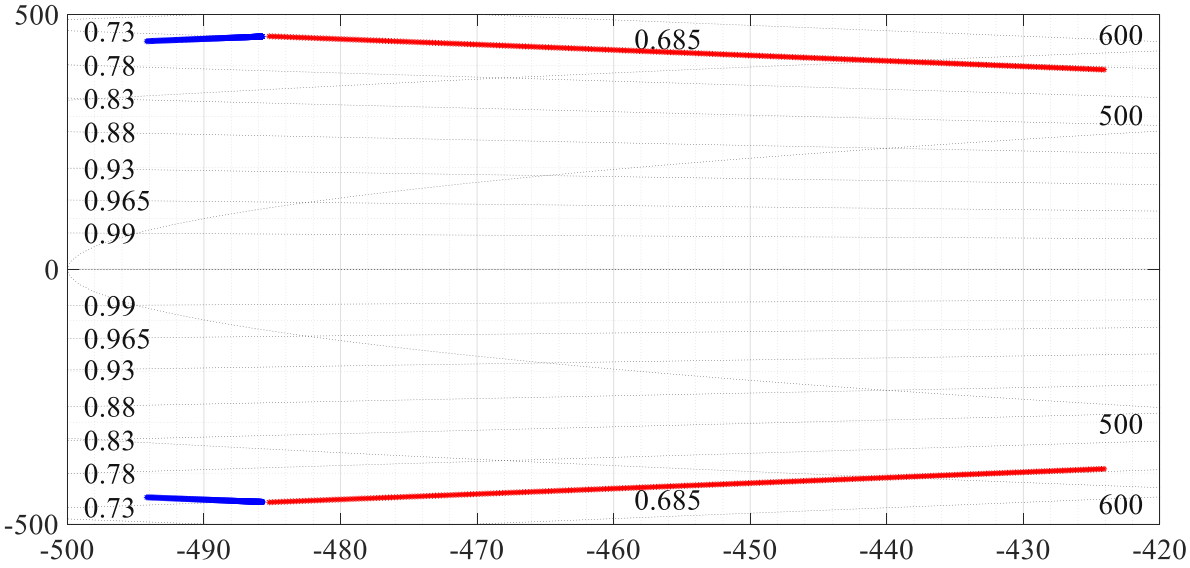

Figure 6.71: Movement of closed loop poles for voltage controller of the boost-buck converter.

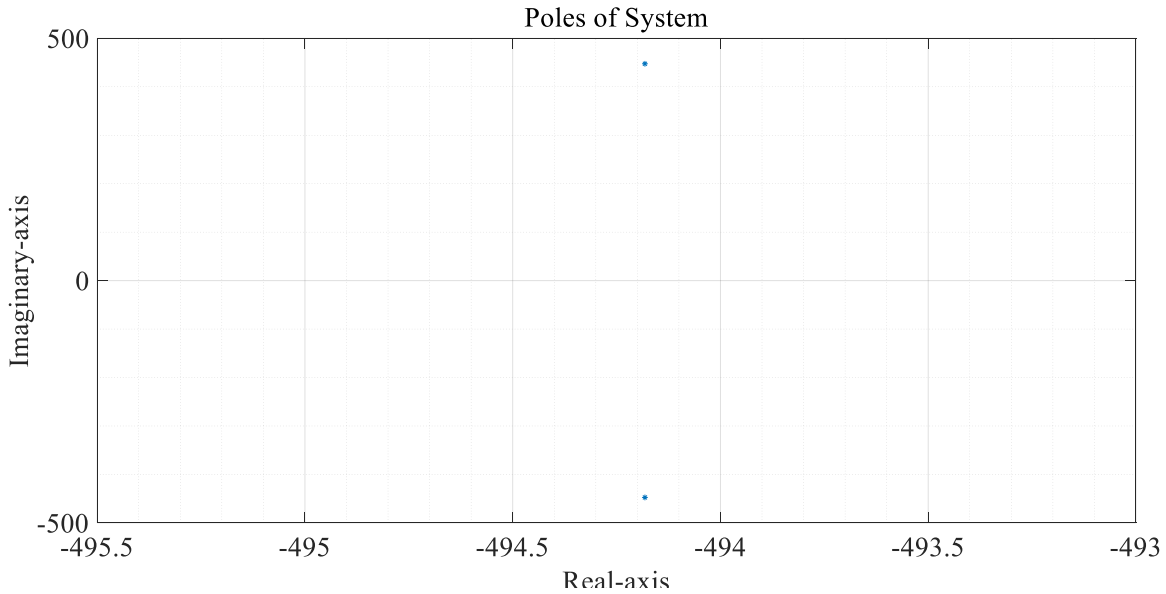

Figure 6.72: Poles of voltage controller location of the boost-buck converter.

The gains for controlling the output voltage of the buck stage uses a new state variable as:

$$\dot{x}_1 = e(t) = V_{ref} - V_{out}.$$

The tracking error has a new state-variable defined as

$$x_1 = \int e(t),$$

$$x_2 = i_l,$$

$$x_3 = V_{out},$$

$$\dot{x}_1 = V_{ref} - x_3$$

$$\dot{x}_2 = \frac{1}{C}x_2 - \frac{1}{C\,R_L}x_3$$

$$\dot{x}_3 = -\frac{rL}{L}x_2 - \frac{1}{L}x_3 + \frac{V_{in}}{L}u$$

Tracking of the system behavior is:

$$\dot{z}_1 = -z_3$$

$$\dot{z}_2 = \frac{1}{C} z_2 - \frac{1}{C\,R_L} z_3$$

$$\dot{z}_3 = -\frac{rL}{L} z_2 - \frac{1}{L} z_3 + \frac{V_{in}}{L} u$$

For control input *u* is minimized by the quadratic cost function:

$$J(t) = \int_0^\infty (z^T Q z + v^2) dt$$

where Q is a symmetric positive semi-definite matrix . The closed-loop control for buck converter is showing in Figure 6.74.

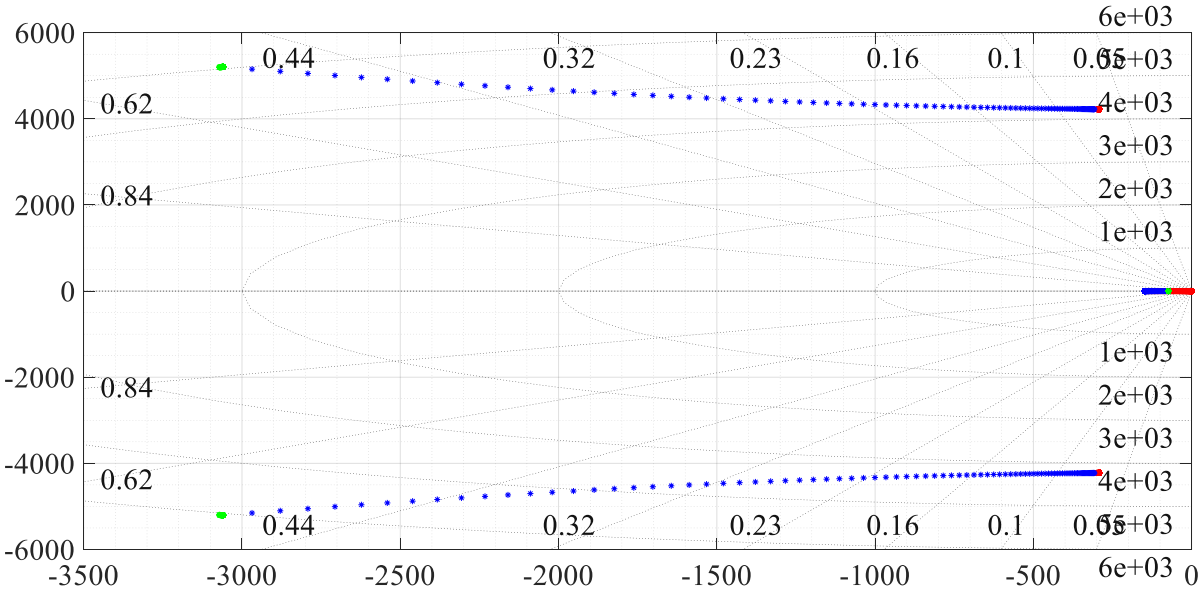

Figure 6.73: Movement of poles in LQR boot-buck converter.

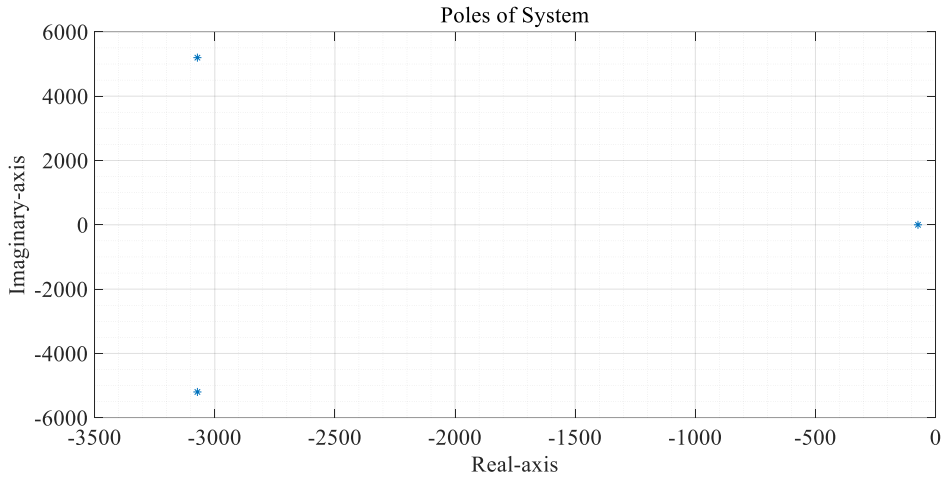

Figure 6.74: Poles of the boost-buck System.

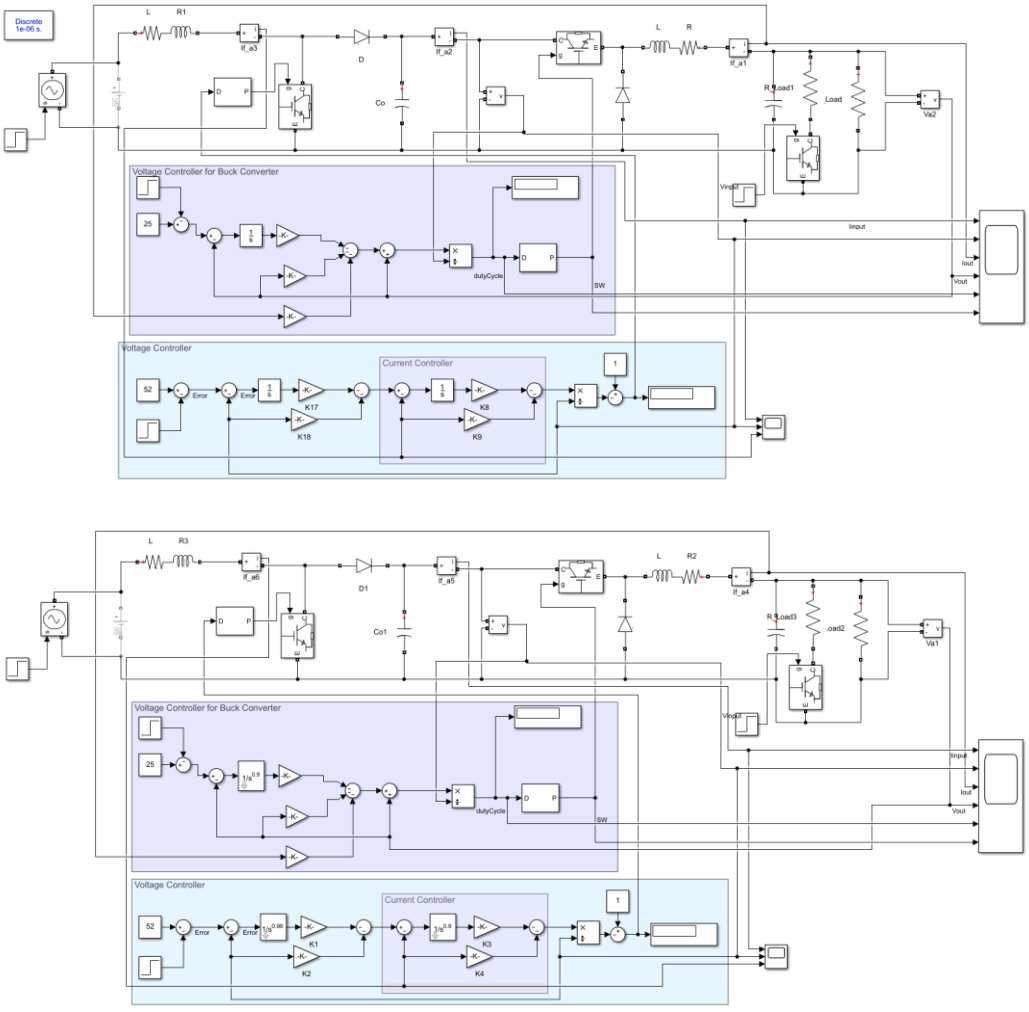

Figure 6.75: Simulation fractional-order, integer-order controller of boost-buck converter.

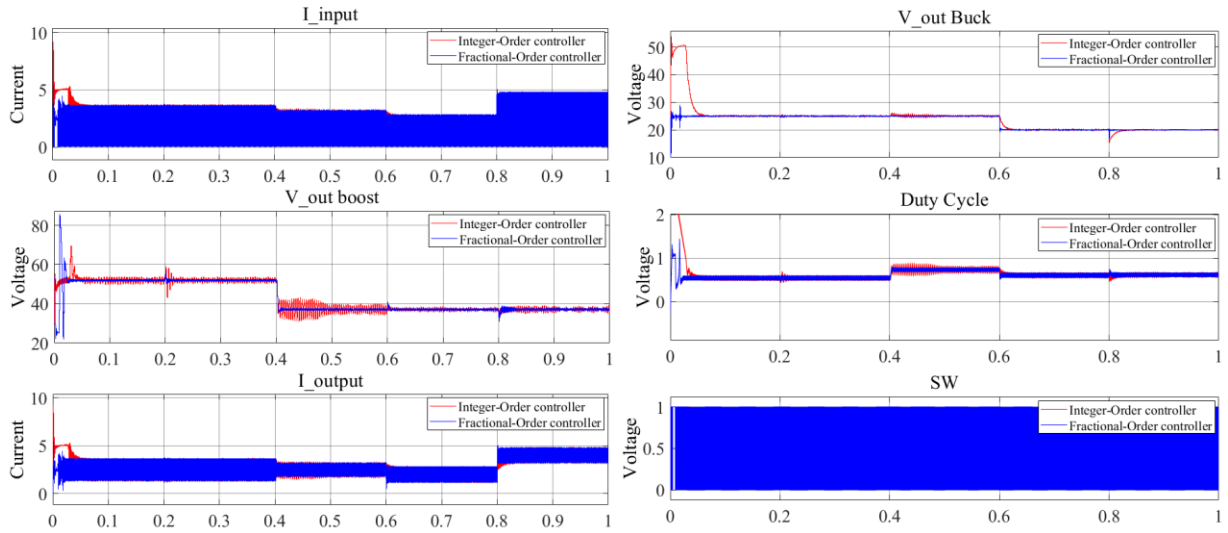

Figure 6.76: Simulation result for fractional and integer order controller of boost-buck converter.

The actual system behavior of the cascaded boost-buck converter with the fractional controller has less overshoot and faster response. Disturbances are applied to the systems for controlling the output voltage. At 0.2 s, the input voltage of the boost sage is reduced but the output voltage remains at the expected value. At 0.4 s, the reference of the output voltage of the boost stage is reduced to have verification of tracking the output value. At 0.6 seconds, the reference of the output voltage of the buck stage is reduced to have verification of tracking the output value. At the 0.6 seconds, the resistive load is decreased and the system performance of the controller is shown in Fig. 6.77.

6.5.3 Experimental Part for the DC-DC Boost-Buck Converter

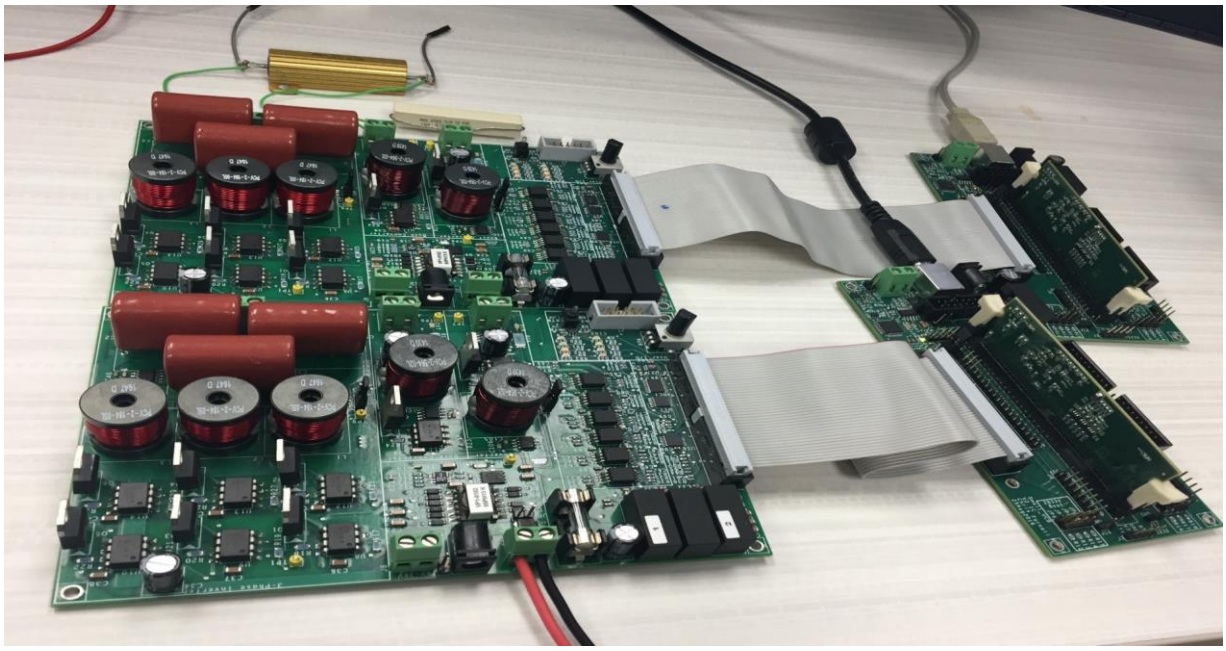

Figure 6.77: Experiment of identify and control boost-buck converter.

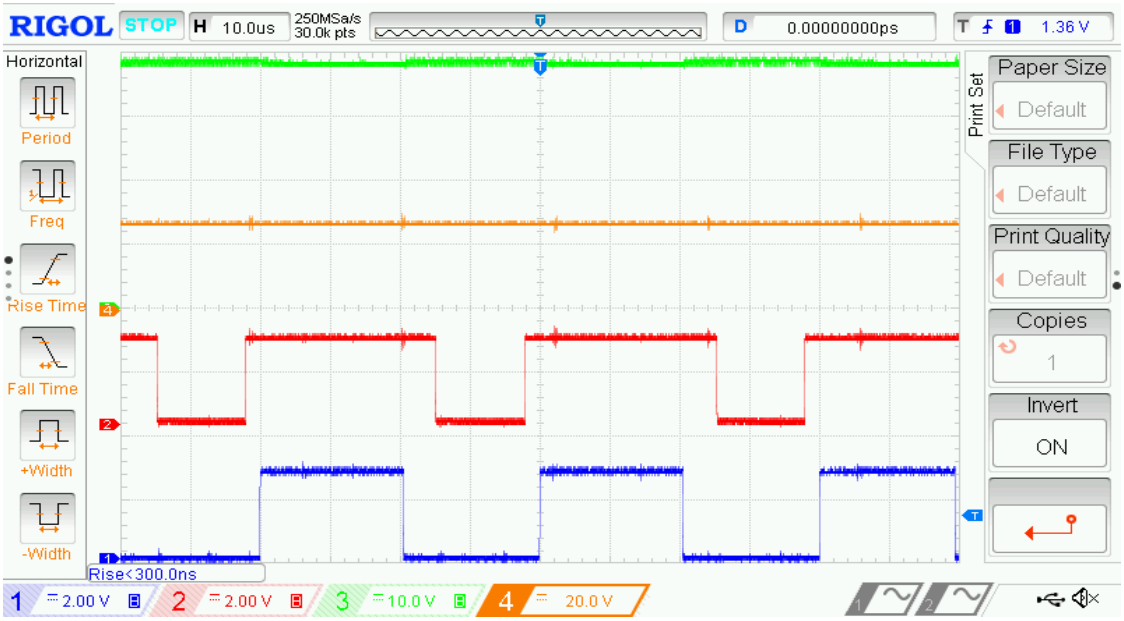

Figure 6.78: Open loop switching and voltages output of boost-buck converter.

The open-loop response for the boost stage switching is around 50% to boost the input voltage for double value. However, the buck switch reduces the output voltage around 70%.

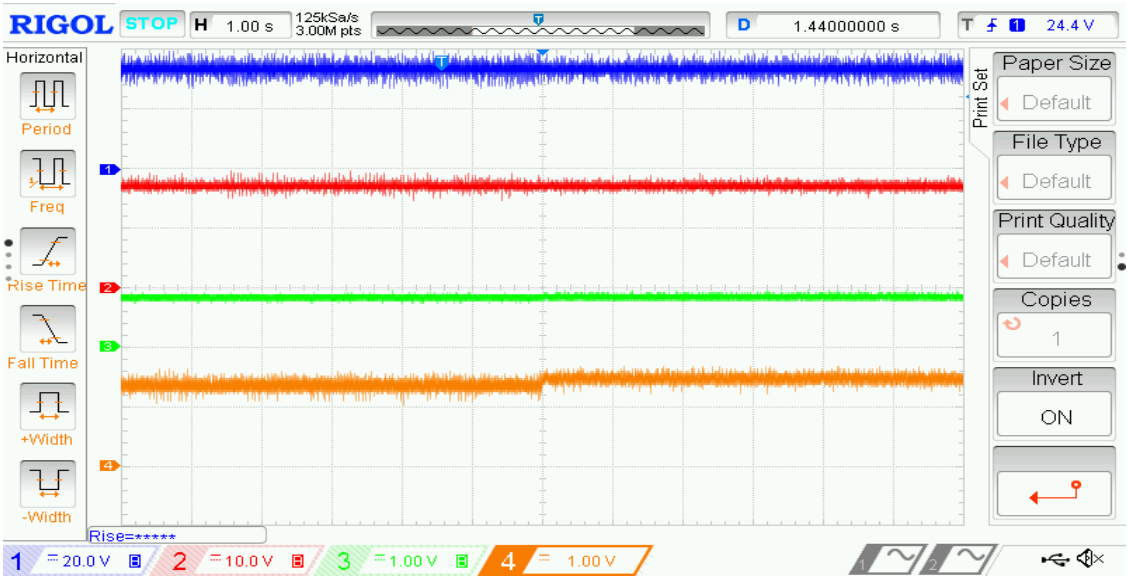

Figure 6.79: Experimental result of output voltages and currents of boost-buck converter.

The result for controlling the system output voltage matches the simulation results. Also applying change for the resistive load the system is stable and the voltage is tracking the reference value for the output voltage.

6.6 Identification of a DC-DC Interleaved Boost Converter with (CPL)

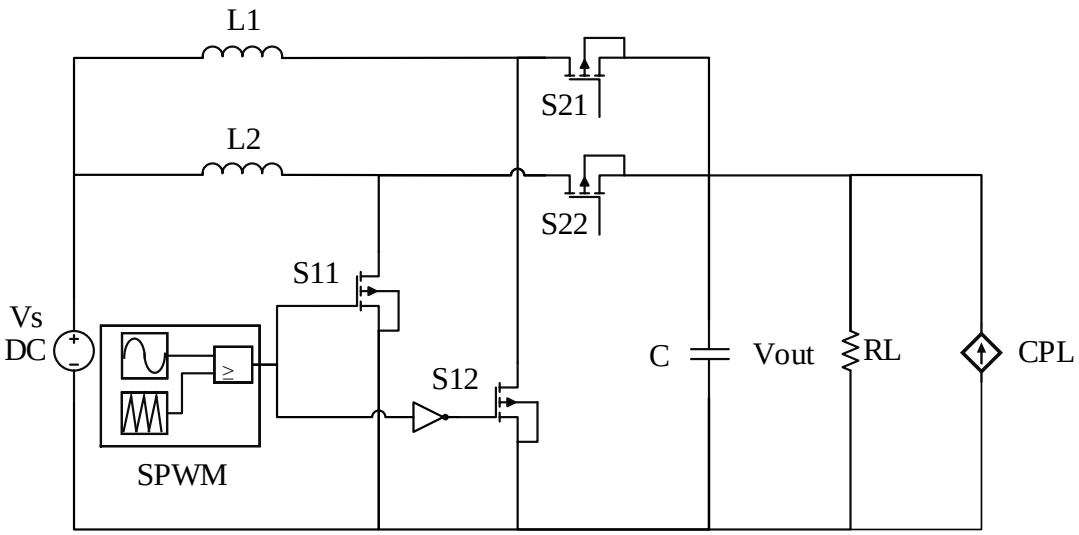

Figure 6.80: DC-DC interleaved boost Converter with CPL.

The interleaved boost Converter with CPL circuit design is presented in Figure 6. 81.

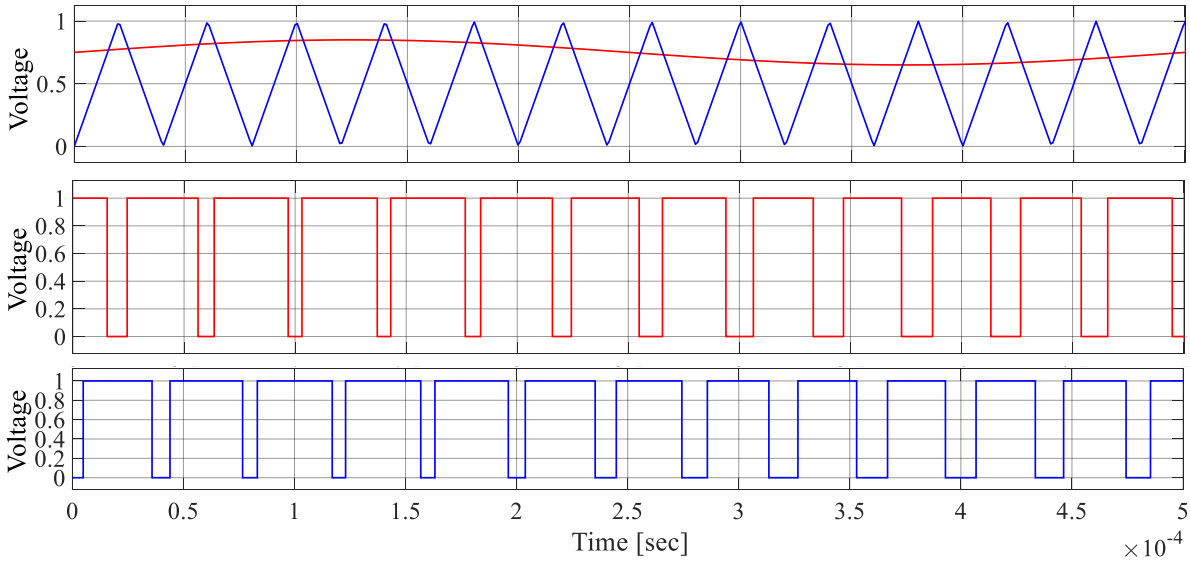

Figure 6.81: Control signals for interleaved boost converter with CPL of 2000Hz.

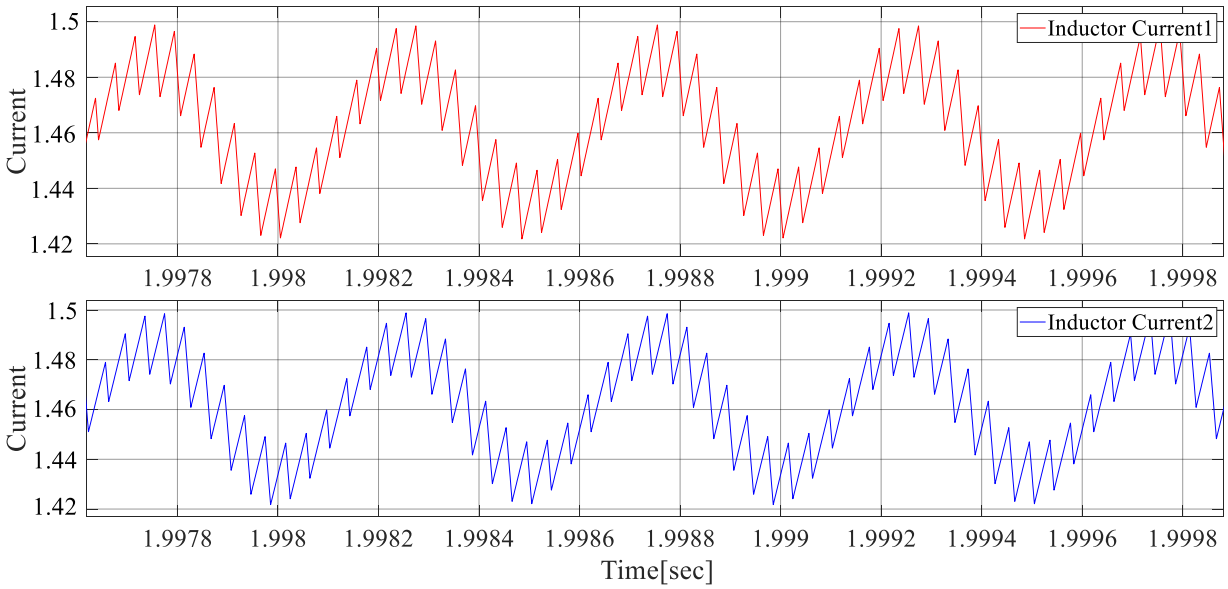

Figure 6.82: Inductor current signal for interleaved boost converter with CPL of 2000Hz.

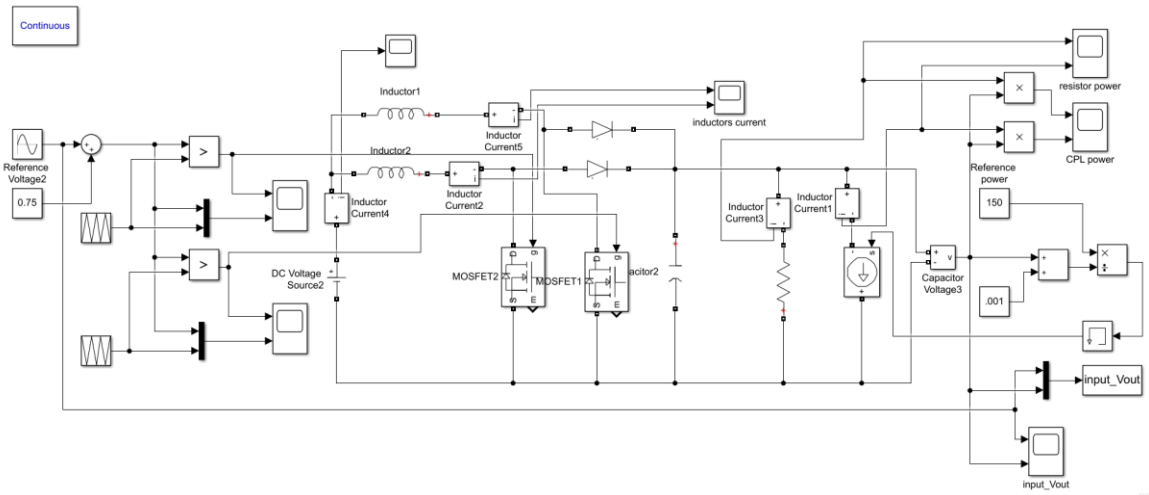

Figure 6.83: DC-DC Interleaved Boost Converter with CPL Matlab Simulink.

6.6.1 Fast Fourier Transform (FFT) Algorithm for Interleaved Boost Converter with (CPL)

The FFT applied to define the amplitude and phase angle for the output signal to determine amplitude and phase angle of input signal.

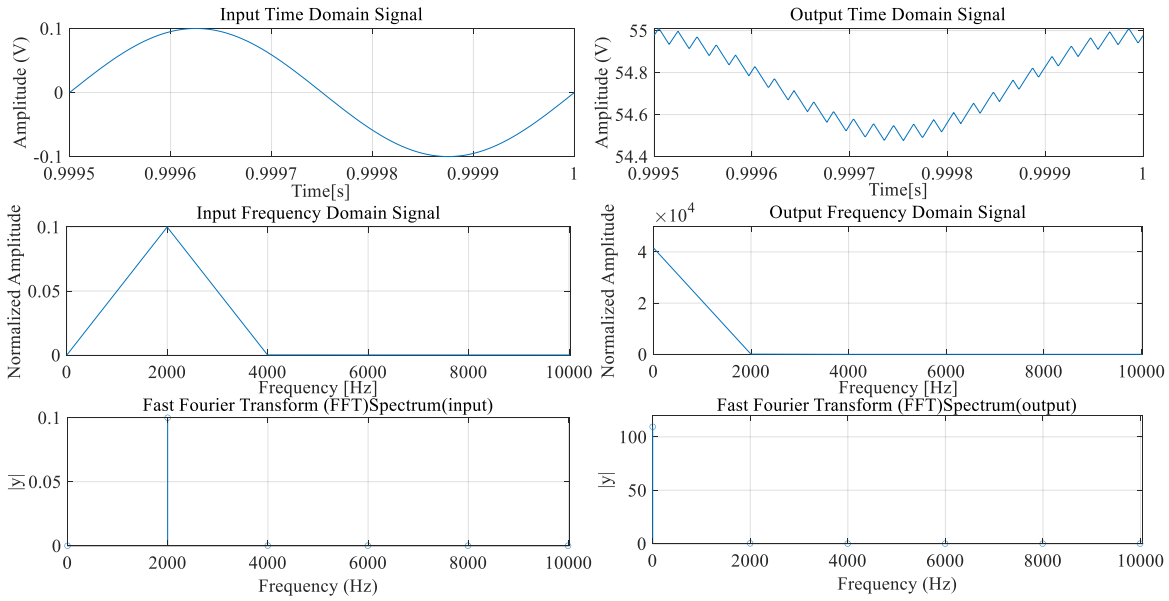

Figure 6.84: FFT analysis of interleaved boost converter with CPL of 2000Hz.

The magnitude and phase shift for each frequency is applied for the system obtained as shown in the Table 6.5:

Table 6.5: Collected data of bode plot for Interleaved Boost Converter with CPL.

Frequency(Hz)	Magnitude (dB)=20*log( )	Phase shift (degrees)
1	47.9018	-1.1225
5	48.0829	-5.802
10	48.6301	-13.5089
25	48.9811	-28.6078
30	54.6687	-87.3775
35	53.8314	-129.7308
50	49.9931	-176.6309

Continued Table 6.5: Collected data of bode plot for Interleaved Boost Converter with CPL.

75	43.0618	-214.1855
325	23.0879	-261.7982
350	22.3709	-263.8613
400	21.1952	-264.9893
450	20.1376	-266.5506
500	19.1868	-268.1228
550	18.3581	-268.707
600	17.589	-269.6024
650	16.8806	-270.4099
700	16.2368	-270.8058
750	15.6348	-271.4044
800	15.0701	-271.8631
850	14.5405	-272.147
900	14.046	-272.5913
950	13.5701	-272.8576
1000	13.128	-273.0826
1250	11.1963	-274.1456
1500	9.5991	-274.8814

Continued Table 6.5: Collected data of bode plot for Interleaved Boost Converter with CPL.

Frequency(Hz)	Magnitude (dB)=20*log( )	Phase shift (degrees)
1750	8.2625	-275.3563
2000	7.1124	-275.6909
2250	6.0837	-275.994
2500	5.1873	-276.2134
2750	4.3514	-276.4246
3000	3.5577	-276.3014
3250	2.8382	-276.853
3500	2.2168	-276.8672
3750	1.6018	-276.9843
4000	1.01	-276.7598
4250	0.5309	-277.0524
4500	0.0831	-277.1601
4750	-0.527	-277.3
5000	-0.819	-277.2365

6.6.2 Bode plot generation for Interleaved Boost Converter with CPL

Based on the accuracy of data obtained of magnitude and phase shift, the resulting Bode plot has magnitude (∓ 20) in decibels (dB) and the phase shift represented in degrees. The

frequency of the sine waveform in the control input of Simulink model is 2πf rad/sec. The frequency range of (50-5K Hz) applied to the model as showing in Fig. 6.91.

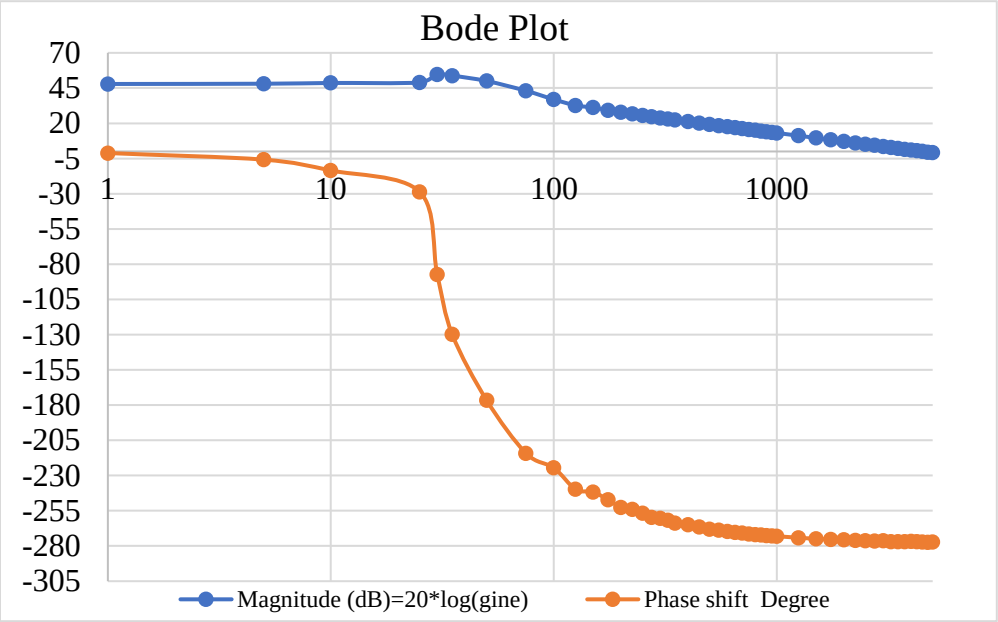

Figure 6.85: Bode plot of interleaved boost converter with CPL form obtained data.

The higher order transfer function of the system is estimated by using TFEST on Matlab to the frequency response collected data of the real system. Third order system is estimated for the actual system is fits the estimation data by 79.34%.

$$G(s)_{tose} = \frac{2.82 \times 10^9}{s^3 + 244.4\, s^2 + 5.374 \times 10^4\, s + 8.981 \times 10^6}$$

A fourth order system is estimated by using TFEST command fits the estimation data by 77.75%

$$G(s)_{fose} = \frac{2.6 \times 10^{12}}{s^4 + 928\, s^3 + 2.884 \times 10^5\, s^2 + 4.969 \times 10^7\, s + 9.126 \times 10^9}$$

The fourth order system is estimated with an added zero that fits the data by 79.34% of the actual behavior.

$$G(s)_{fosez} = \frac{3.188 \times 10^{9}\,\mathrm{s} - 9.894 \times 10^{10}}{\mathrm{s}^4 + 209.4\,\mathrm{s}^3 + 4.316 \times 10^{4}\,s^2 + 7.125 \times 10^{6}\,s - 4.493 \times 10^{8}}$$

A seventeenth order system fits the data by 99.43% the actual system.

$$G(s)_{sose} = \frac{1.984 \times 10^{27}\,\mathrm{s}^{11} - 6.144 \times 10^{29}\mathrm{s}^{10} + 6.462 \times 10^{32}\mathrm{s}^{9} - 1.056 \times 10^{35}\mathrm{s}^{8}}{\mathrm{s}^{17} + 1.1557 \times 10^{5}\,\mathrm{s}^{16} + 1.082 \times 10^{9}\,s^{15} + 1.0031 \times 10^{14}\,s^{14} + 2.4 \times 10^{17}s^{13}}$$

$$\frac{+4.892 \times 10^{37}\,\mathrm{s}^{7} - 1.586 \times 10^{40}\mathrm{s}^{6} + 1.739 \times 10^{42}\mathrm{s}^{5} - 4.934 \times 10^{44}\mathrm{s}^{4}}{5.69 \times 10^{22}\,\mathrm{s}^{12} + 1.566 \times 10^{24}\,\mathrm{s}^{11} + 1.73 \times 10^{28}\,s^{10} + 2.618 \times 10^{30}\,s^{9} + 2.023 \times 10^{33}s^{8}}$$

$$\frac{+4.892 \times 10^{37}\,\mathrm{s}^{7} - 1.586 \times 10^{40}\mathrm{s}^{6} + 1.739 \times 10^{42}\mathrm{s}^{5} - 4.934 \times 10^{44}\mathrm{s}^{4}}{1.638 \times 10^{35}\,\mathrm{s}^{7} + 9.072 \times 10^{37}\,\mathrm{s}^{6} + 8.476 \times 10^{38}\,s^{5} + 1.569 \times 10^{42}\,s^{4} + 6.24 \times 10^{43}s^{3}}$$

$$\frac{+1.675 \times 10^{46}\,\mathrm{s}^{3} - 1.965 \times 10^{48}\mathrm{s}^{2} + 7.214 \times 10^{49}\mathrm{s} + 8.357 \times 10^{50}}{4.725 \times 10^{45}\,\mathrm{s}^{2} + 4.204 \times 10^{47}\,\mathrm{s} + 3.275 \times 10^{48}}.$$

The comparison between the estimated systems to simulation data shows the high order equivalent to the original system behavior as shown in Fig. 6. 92.

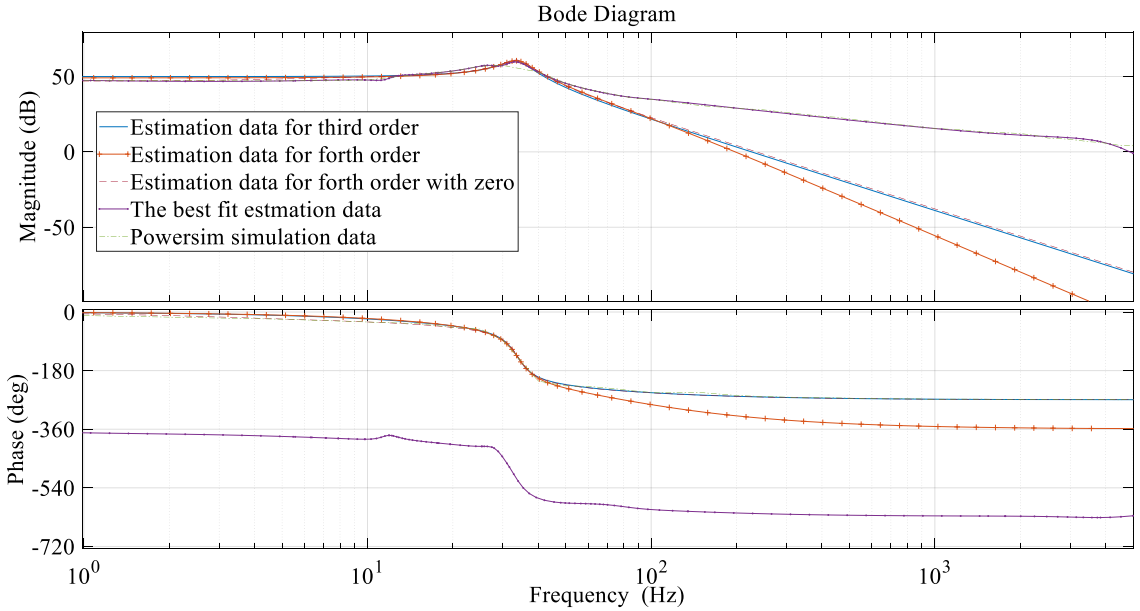

Figure 6.86: Bode plot of the interleaved boost converter with CPLVs estimation data.

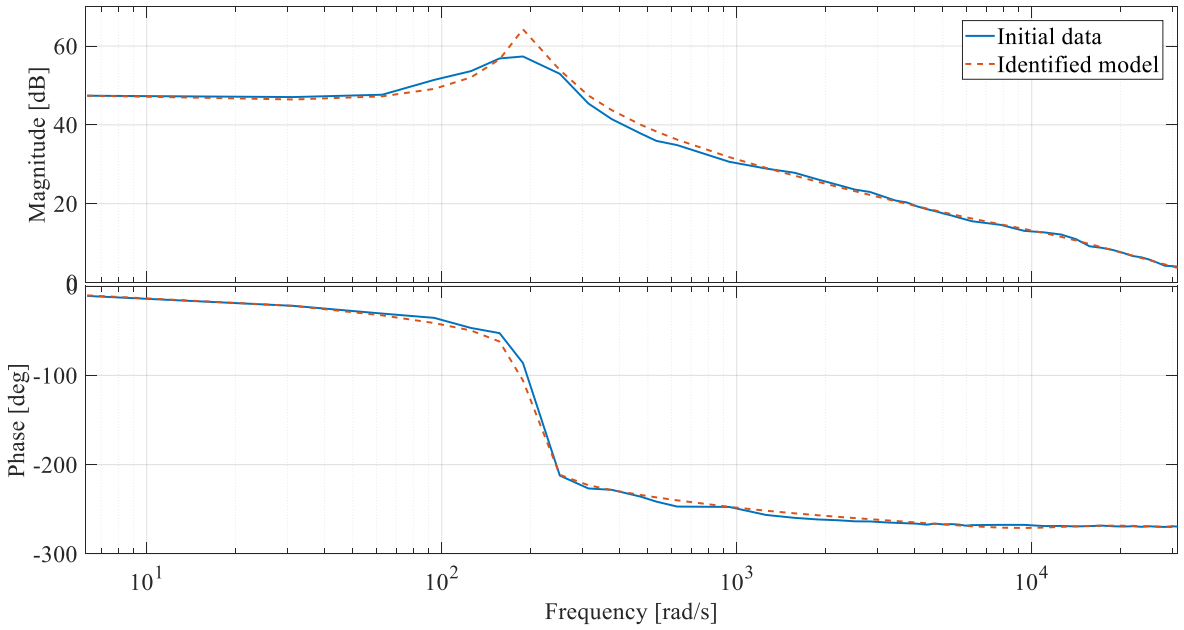

Figure 6.87: Bode Plot of interleaved boost converter with CPL

The real behavior of the system represented by fractional order transfer function using Levy's method with resulting the approximation error of 6%.

$$G(s)_{FO} = \frac{-2.185 \times 10^{-6} s^{2.2} + 0.0010762 s^{1.76} - 0.11674 s^{1.32} + 4.873 s^{0.88} - 69.475 s^{0.44} + 296.25}{4.761510^{-8} s^{2.64} + 6.259510^{-6} s^{2.2} + 0.00028662 s^{1.76} + 0.0041792 s^{1.32} + 0.02002 s^{0.88} + 0.084919 s^{0.44} + 1}.$$

6.6.3 Modeling and Analysis of a DC-DC Interleaved Boost Converter with (CPL)

DC-to-DC power converter is constructed by using connection of Boost converters and CPL load. The model of the converter is derived to be:

KVL L:

$$V_s = L_1 \frac{d_{i_1}}{dt} + V_C(1 - S_{11})$$

$$V_s = L_2 \frac{d_{i_2}}{dt} + V_C(1 - S_{12})$$

KCL C:

$$i_1(1-S_{11})+i_2(1-S_{12})=C\frac{d_v}{dt}+\frac{V_C}{RL}+\frac{P}{V_C}$$

Average Normalized Model

$$x_1=i\,,x_2=V_{out},x_3=\frac{V_s}{(1-U)},S_{11}=S_{12}=U$$

$$\dot{x}_1=\frac{V_S}{L_1}-\frac{x_3(1-U)}{L_1}$$

$$\dot{x}_2=\frac{V_S}{L_2}-\frac{x_3(1-U)}{L_2}$$

$$\dot{x}_3=\frac{x_1(1-U)}{C}+\frac{x_2(1-U)}{C}-\frac{x_3}{C\,RL}-\frac{P}{Cx_3^2}$$

Equilibrium Point and State space model:

$$A=\begin{bmatrix}0 & 0 & \frac{-(1-U)}{L_1}\\ 0 & 0 & \frac{-(1-U)}{L_2}\\ \frac{(1-U)}{C} & \frac{(1-U)}{C} & \frac{-1}{C\,RL}+\frac{P}{Cx_3^2}\end{bmatrix}$$

$$B=\begin{bmatrix}\frac{x_3}{L_1}\\ \frac{x_3}{L_2}\\ \frac{-(x_1+x_2)}{C}\end{bmatrix},C=[0\quad 0\quad 1],D=[0]$$

The linearized transfer function is:

$$G(s)_{Linearized}=\frac{-2.204\times10^4s^2\ +\ 9.375\times10^6s\ \ +\ 3.052\times10^{-8}}{s^3+\ 26.63\,s^2\ +\ 4.185\times10^4s\ \ +\ 3.738\times10^{-10}}.$$

The actual system is compared with the linearized system. The resulting Bode plot resonant peak is shown in Fig. 6.89.

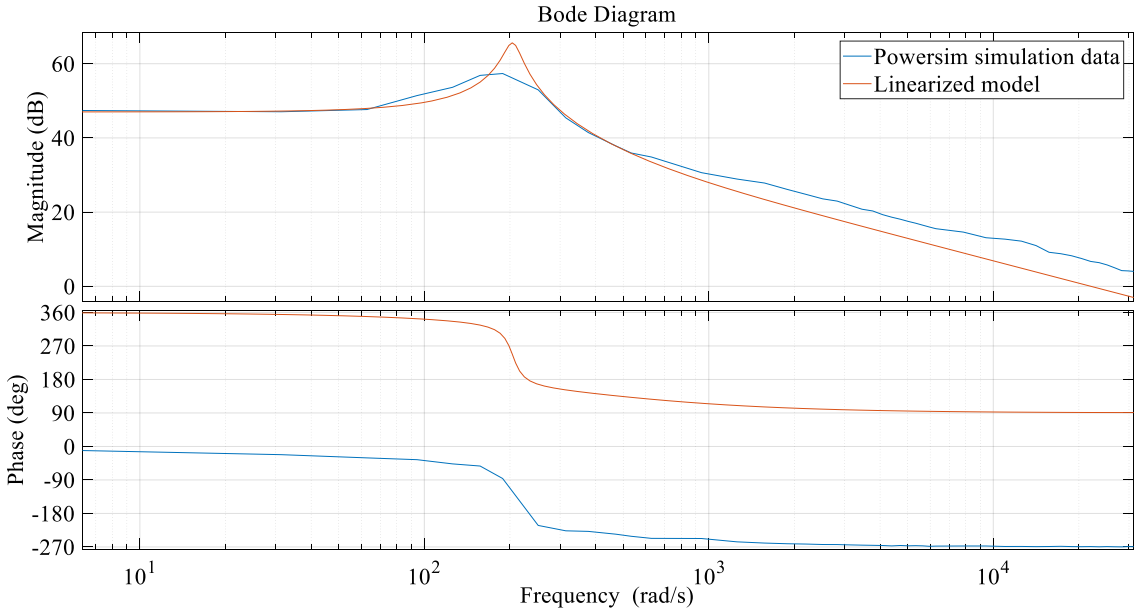

Figure 6.88: Bode plot of interleaved boost converter with CPL

6.6.4 Controller for the DC-DC Interleaved Boost with CPL Converter

The cascaded control is used for controlling the interleaved boost converter with the CPL The error variable is represented as:

$$\dot{x}_1 = e(t) = i_{lref} - (i_{l1} + i_{l2})$$

the new state variable is defined for the tracking error as:

$$x_1 = \int e(t),$$

$$x_2 = (i_{l1} + i_{l2}).$$

The state-space equations are represented as:

$$\dot{x}_1 = i_{lref} - x_2$$

$$\dot{x}_2 = -\frac{r_{l1}x_2}{L} - \frac{r_{l2}x_2}{L} - \frac{v_o(1-u)}{L}$$

Converting the state-space equations are represented as following:

$$\dot{z}_1 = -z_2$$

$$\dot{z}_2 = -\frac{r_{l1}z_2}{L} - \frac{r_{l2}z_2}{L} - \frac{u}{L}$$

For control input u is minimized by the cost function:

$$J(t) = \int_0^\infty (z^T Q z + v^2)dt$$

where Q is a symmetric positive semi-definite matrix, The current controller for interleaved boost with CPL converter is showing in Figure. 6.90.

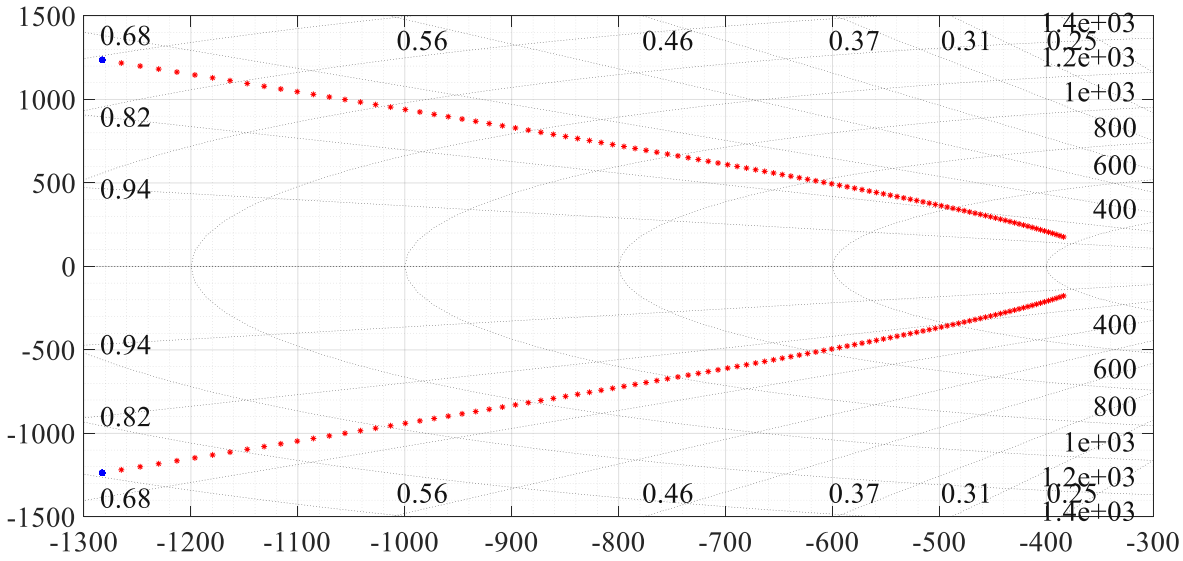

Figure 6.89: Movement of closed loop poles current controller (interleaved boost with CPL).

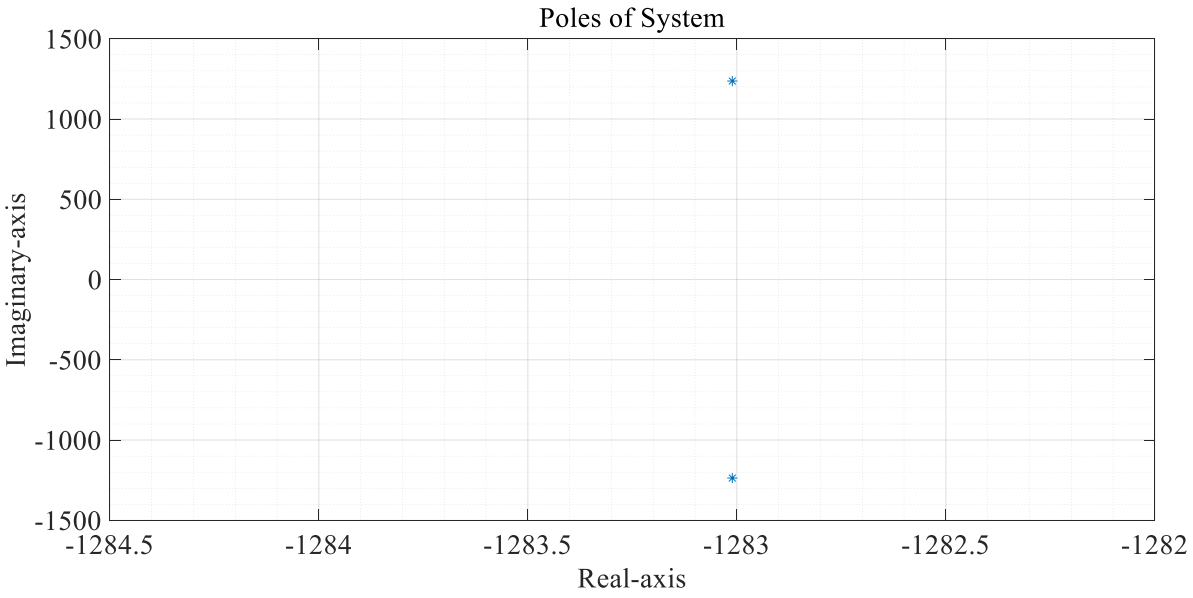

Figure 6.90: Poles of current controller location of interleaved boost converter with CPL.

Defining the gains of outer loop to control the output voltage boost converter, the LQR design technique is used. For a new state variable is defined as:

$$\dot{x}_1 = e(t) = V_{ref} - V_{out}$$

with tracking error,

$$x_1 = \int e(t),$$

$$x_2 = V_{out},$$

$$\dot{x}_1 = V_{ref} - x_2$$

$$\dot{x}_2 = \frac{(1-u)}{C} i_{ltotal} - \frac{1}{C\,R_L} x_2 - \frac{P}{Cx_2}.$$

The tracking of the system behavior is:

$$\dot{z}_1 = -z_2$$

$$\dot{z}_2 = \frac{v_{in}}{C v_{ref}} u - \frac{1}{C\ R_L} z_2 - \frac{P}{C z_2}$$

For control input u is minimized by quadratic cost function

$$J(t) = \int_0^\infty (z^T Q z + v^2) dt$$

where Q is a symmetric positive semi-definite matrix. The control for boost converter is shown in Figure. 6.92.

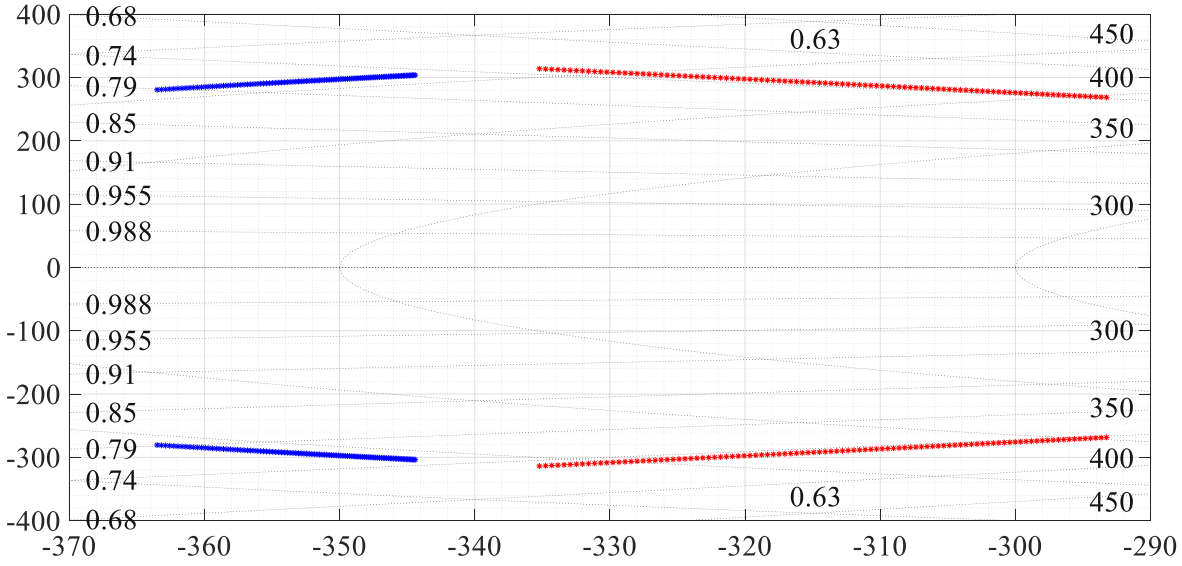

Figure 6.91: Closed loop poles location of voltage controller interleaved boost with CPL.

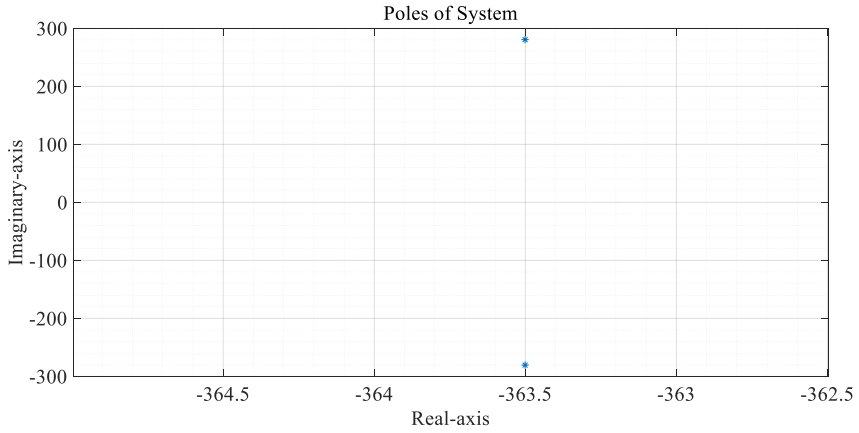

Figure 6.92: Poles of voltage controller location of interleaved boost converter with CPL.

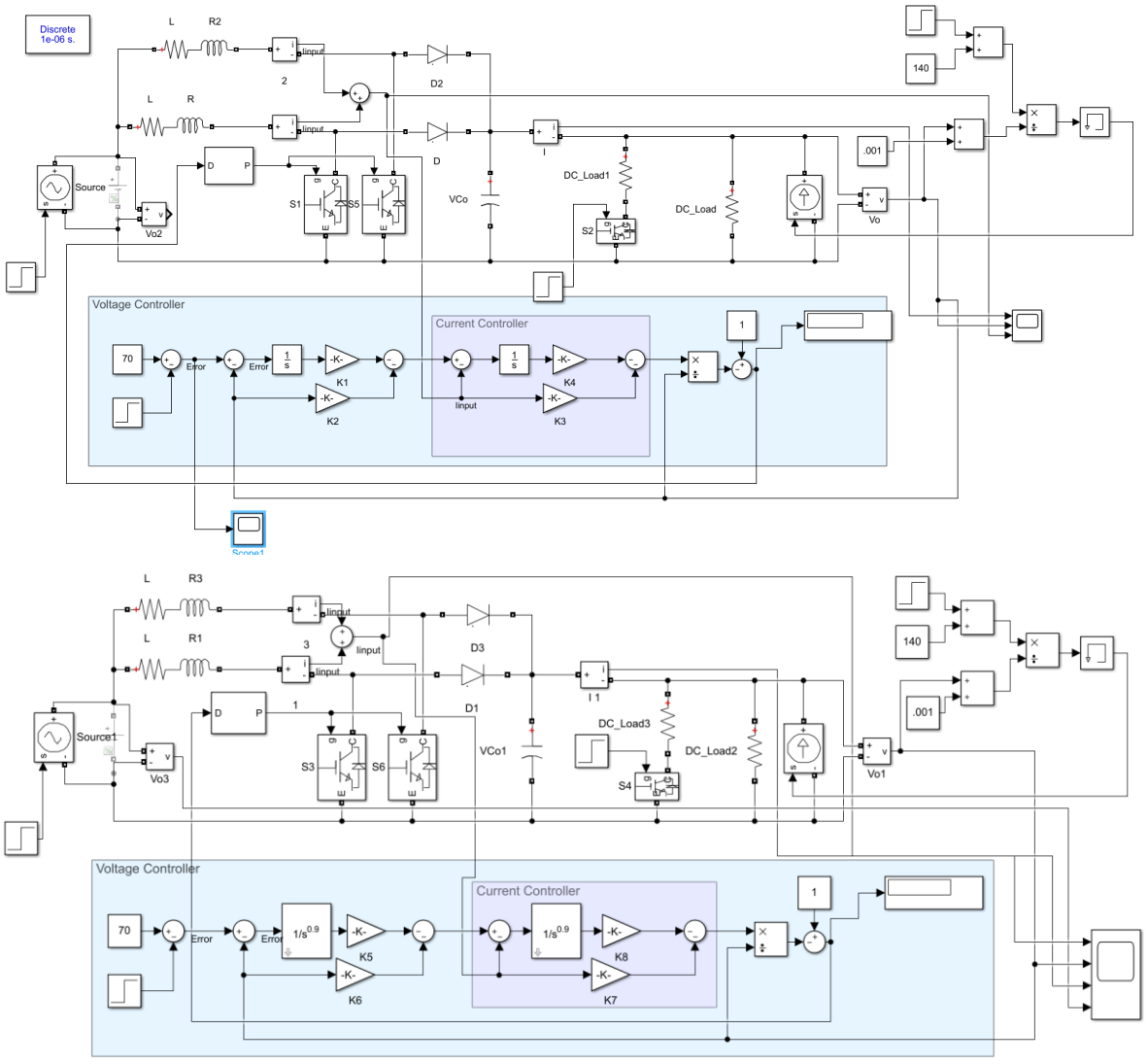

Figure 6.93: Simulation design of fractional-order versus integer-order controller of interleaved boost converter with CPL.

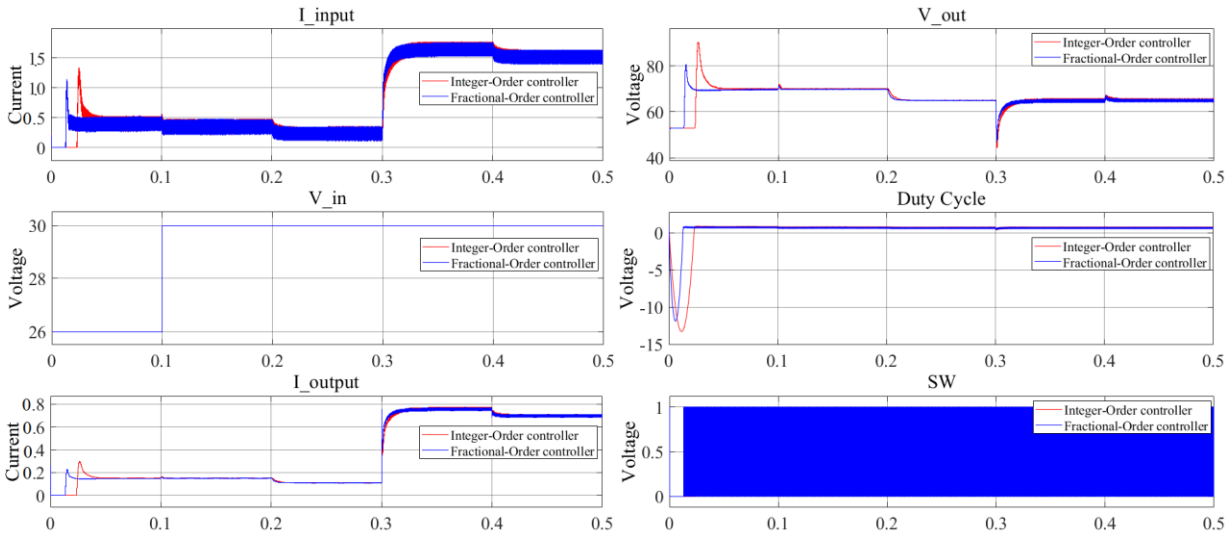

Figure 6.94: Simulation result Fractional Order controller-Integer order controller of interleaved boost converter with CPL.

The actual system behavior of the interleaved boost converter with a CPL using the fractional controller has less overshoot and faster response. Disturbances are applied to the system for controlling the output voltage. At 0.1 s, the input voltage is reduced but the output voltage remains at the expected value. At 0.2 seconds, the reference of the output voltage of the boost stage is reduced to verify the tracking the output value. At 0.3 seconds, the resistive load is decreased such that the tracking performance of the controller is shown in Fig. 6.95.

7 Conclusion

The research developed a new method for modelling switched-mode power electronic dc-dc converters, By employing fractional order calculus, a modified describing function (MDF) method was developed that provides a systematic way to determine an accurate representation of the converter dynamics such that an improved feedback control design can be implemented. The method is primarily motivated by the challenges seen with boost converters however the experimental results showed benefits to buck and boost-buck converters. In addition, the nonlinear behavior of constant power loads was also demonstrated with the new fractional order MDF technique. Examples of constant power loads in LED lighting and computer loads such a data centers. Constant power loads exhibit a destabilizing characteristic on the overall dc-dc converter operation because of an incremental negative impedance characteristic. As constant power loads become more prevalent in electric utility operations, the types of loads will tend towards dominating the dynamic response of electric utility operations. Consequently, the importance of this research is demonstrated through the improved capability to stabilize dc-dc converters that have constant power loads.

Future work will focus on improved implementation methods of fractional order controllers. The disadvantage of the methods developed in this research is the increased numerical processing needed for fractional order systems. Improved off-line analysis and real-time fractional order computational methods are needed to support future deployment of advanced dc-dc converter technologies.

Reference

[1] R. Kurel, *Investigation of electrical characteristics of SiC based complementary JBS structures*. Tallinn University of Technology Press, 2005.

[2] A. Gavrijaševa, *Coin Validation by Electromagnetic, Acoustic and Visual Features*. TUT Press, 2015.

[3] M. A. Meyers, *Dynamic behavior of materials*. John wiley & sons, 1994.

[4] I. Schäfer and K. Krüger, "Modelling of lossy coils using fractional derivatives," *J. Phys. D. Appl. Phys.*, vol. 41, no. 4, p. 45001, 2008.

[5] S. Das and I. Pan, *Fractional order signal processing: introductory concepts and applications*. Springer Science & Business Media, 2011.

[6] I. Podlubny, "Fractional differential equations, vol. 198 of Mathematics in Science and Engineering." Academic Press, San Diego, Calif, USA, 1999.

[7] D. Cafagna, "Fractional calculus: A mathematical tool from the past for present engineers [Past and present]," *IEEE Ind. Electron. Mag.*, vol. 1, no. 2, pp. 35–40, 2007.

[8] K. Oldham and J. Spanier, *The fractional calculus theory and applications of differentiation and integration to arbitrary order*. Elsevier, 1974.

[9] I. Podlubny, "Fractional-order systems and PI/sup/spl lambda//D/sup/spl mu//-controllers," *IEEE Trans. Automat. Contr.*, vol. 44, no. 1, pp. 208–214, 1999.

[10] K. S. Miller and B. Ross, *An introduction to the fractional calculus and fractional differential equations*. Wiley, 1993.

[11] J. C. Prajapati and A. K. Shukla, "Decomposition of generalized Mittag-Leffler function and its properties," *Adv. Pure Math.*, vol. 2, no. 01, p. 8, 2012.

[12] V. B. L. Chaurasia and S. C. Pandey, "On the fractional calculus of generalized Mittag-Leffler function," *Sci. Ser. A Math. Sci.*, vol. 20, pp. 113–122, 2010.

[13] A. K. Shukla and J. C. Prajapati, "On a generalization of Mittag-Leffler function and its properties," *J. Math. Anal. Appl.*, vol. 336, no. 2, pp. 797–811, 2007.

[14] Y. Chen, I. Petras, and D. Xue, "Fractional order control-a tutorial," in *2009 American control conference*, 2009, pp. 1397–1411.

[15] A. K. Mahmood and B. F. Mohammed, "Design optimal fractional order PID controller utilizing particle swarm optimization algorithm and discretization method," *Int. J. Emerg.*

Sci. Eng., vol. 1, no. 10, pp. 87–92, 2013.

[16] S. Das, *Functional fractional calculus*. Springer Science & Business Media, 2011.

[17] R. L. Magin, *Fractional calculus in bioengineering*, vol. 2, no. 6. Begell House Redding, 2006.

[18] C. A. Monje, Y. Chen, B. M. Vinagre, D. Xue, and V. Feliu-Batlle, *Fractional-order systems and controls: fundamentals and applications*. Springer Science & Business Media, 2010.

[19] S. Das and I. Pan, "Basics of fractional order signals and systems," in *Fractional Order Signal Processing*, Springer, 2012, pp. 13–30.

[20] H. Sheng, Y. Chen, and T. Qiu, *Fractional processes and fractional-order signal processing: techniques and applications*. Springer Science & Business Media, 2011.

[21] B. M. Vinagre and V. Feliu, "Optimal fractional controllers for rational order systems: a special case of the Wiener-Hopf spectral factorization method," *IEEE Trans. Automat. Contr.*, vol. 52, no. 12, pp. 2385–2389, 2007.

[22] B.-S. Rayleigh, "JW The theory of sound, Reprint of 2nd Ed.(1894)." Dover Publications, New York, NY, USA, 1945.

[23] R. S. Barbosa, J. A. T. Machado, I. M. Ferreira, and J. K. Tar, "Dynamics of the fractional-order Van der Pol oscillator," in *Second IEEE International Conference on Computational Cybernetics, 2004. ICCC 2004.*, 2004, pp. 373–378.

[24] Y. Li, Y. Chen, and I. Podlubny, "Mittag–Leffler stability of fractional order nonlinear dynamic systems," *Automatica*, vol. 45, no. 8, pp. 1965–1969, 2009.

[25] J.-C. Trigeassou, N. Maamri, J. Sabatier, and A. Oustaloup, "A Lyapunov approach to the stability of fractional differential equations," *Signal Processing*, vol. 91, no. 3, pp. 437–445, 2011.

[26] P. Shah and S. Agashe, "Design and optimization of fractional PID controller for higher order control system," in *International conference of IEEE ICART*, 2013, pp. 588–592.

[27] D. Matignon, "Generalized fractional differential and difference equations: stability properties and modelling issues," in *Mathematical Theory of Networks and Systems symposium*, 1998, pp. 503–506.

[28] D. Matignon, "Stability properties for generalized fractional differential systems," in *ESAIM: proceedings*, 1998, vol. 5, pp. 145–158.

[29] C. Bonnet and J. R. Partington, "Coprime factorizations and stability of fractional

differential systems," *Syst. Control Lett.*, vol. 41, no. 3, pp. 167–174, 2000.

[30] A. Dzielinski and D. Sierociuk, "Adaptive feedback control of fractional order discrete state-space systems," in *International conference on computational intelligence for modelling, control and automation and international conference on intelligent agents, web technologies and internet commerce (cimca-iawtic'06)*, 2005, vol. 1, pp. 804–809.

[31] S. GUERMAH, S. DJENNOUNE, and M. BETTAYEB, "State-space analysis of linear fractional-order systems," *J. Eur. des systèmes Autom.*, vol. 42, no. 6–8, pp. 825–838, 2008.

[32] L. A. Zadeh, "From circuit theory to system theory," *Proc. IRE*, vol. 50, no. 5, pp. 856–865, 1962.

[33] K. J. Åström and P. Eykhoff, "System identification—a survey," *Automatica*, vol. 7, no. 2, pp. 123–162, 1971.

[34] G. E. P. Box, G. M. Jenkins, and G. Reinsel, "Time series analysis: forecasting and control Holden-day San Francisco," *BoxTime Ser. Anal. Forecast. Control Holden Day1970*, 1970.

[35] K. J. Aström, "Introduction to Stochastic control theory, ser," *Math. Sci. Eng. New York Acad. Press*, vol. 70, 1970.

[36] P. Eykhoff, "System Identification-Parameter and State Estimation.[sl] John Wiley & Sons," *London I NewYork I Sydney I Toronto*, 1974.

[37] L. Ljung, "System Identification {Theory for the User. Prentice Hall Information and System Sciences Serie (T. Kailath, ed.)," *Englewood Cli s, NJ*, 1987.

[38] A. Juditsky *et al.*, "Nonlinear black-box models in system identification: Mathematical foundations," *Automatica*, vol. 31, no. 12, pp. 1725–1750, 1995.

[39] R. Pintelon and J. Schoukens, *System identification: a frequency domain approach*. John Wiley & Sons, 2012.

[40] G. Kerschen, K. Worden, A. F. Vakakis, and J.-C. Golinval, "Past, present and future of nonlinear system identification in structural dynamics," *Mech. Syst. Signal Process.*, vol. 20, no. 3, pp. 505–592, 2006.

[41] J. Sjöberg *et al.*, *Nonlinear black-box modeling in system identification: a unified overview*. Linköping University, 1995.

[42] L. Ljung, "System identification," *Wiley Encycl. Electr. Electron. Eng.*, pp. 1–19, 1999.

[43] K. G. Beauchamp, *Transforms for engineers: a guide to signal processing*. Clarendon Press, 1987.

[44] J. Schoukens, R. Pintelon, and Y. Rolain, *Mastering system identification in 100 exercises*. John Wiley & Sons, 2012.

[45] H. Keshvari-Khor, A. Karimpour, and N. Pariz, "Identification of continuous-time switched linear systems from low-rate sampled data," *IET Control Theory Appl.*, vol. 12, no. 14, pp. 1964–1973, 2018.

[46] C. Barbu and R. E. Trahan, "Frequency domain system identification: A full estimation approach," in *Proceedings of 2005 IEEE Conference on Control Applications, 2005. CCA 2005.*, 2005, pp. 1448–1454.

[47] I. Petras, L. Dorcak, and I. Kostial, "The modelling and analysis of fractional-order control systems in discrete domain," *arXiv Prepr. math/0006190*, 2000.

[48] H. Li, Y. Luo, and Y. Chen, "A fractional order proportional and derivative (FOPD) motion controller: tuning rule and experiments," *IEEE Trans. Control Syst. Technol.*, vol. 18, no. 2, pp. 516–520, 2009.

[49] O. Cois, A. Oustaloup, E. Battaglia, and J.-L. Battaglia, "Non integer model from modal decomposition for time domain system identification," *IFAC Proc. Vol.*, vol. 33, no. 15, pp. 989–994, 2000.

[50] C. Li and Y. Ma, "Fractional dynamical system and its linearization theorem," *Nonlinear Dyn.*, vol. 71, no. 4, pp. 621–633, 2013.

[51] A. Blaquiere, *Nonlinear system analysis*. Elsevier, 2012.

[52] G. W. Wester and R. D. Middlebrook, "Low-frequency characterization of switched dc-dc converters," in *1972 IEEE Power Processing and Electronics Specialists Conference*, 1972, pp. 9–20.

[53] N. M. Krylov and N. N. Bogoliubov, *Introduction to non-linear mechanics*, no. 11. Princeton University Press, 1949.

[54] I. Boiko, *Discontinuous control systems: frequency-domain analysis and design*. Springer Science & Business Media, 2008.

[55] D. P. Atherton, "Nonlinear control engineering," *Van Nostrand Rheinhold*, 1975.

[56] Y. Berkovich and A. Ioinovici, "Large-signal stability-oriented design of boost regulators based on a Lyapunov criterion with nonlinear integral," *IEEE Trans. Circuits Syst. I Fundam. Theory Appl.*, vol. 49, no. 11, pp. 1610–1619, 2002.

[57] R. D. Middlebrook, "Describing function properties of a magnetic pulse-width modulator," in *1972 IEEE Power Processing and Electronics Specialists Conference*, 1972, pp. 23–35.

[58] B.-Y. Moon, B.-S. Kang, and B.-S. Kim, “Dynamic analysis of harmonically excited non-linear structure system using harmonic balance method,” *KSME Int. J.*, vol. 15, no. 11, pp. 1507–1516, 2001.

[59] W. E. Vander Velde, *Multiple-input describing functions and nonlinear system design*. McGraw-Hill, New York, 1968.

[60] R. Pintelon and J. Schoukens, “Frequency domain system identification with missing data,” *IEEE Trans. Automat. Contr.*, vol. 45, no. 2, pp. 364–369, 2000.

[61] R. Pintelon, P. Guillaume, Y. Rolain, J. Schoukens, and H. Van Hamme, “Parametric identification of transfer functions in the frequency domain-a survey,” *IEEE Trans. Automat. Contr.*, vol. 39, no. 11, pp. 2245–2260, 1994.

[62] M. Eckert, M. Kupper, and S. Hohmann, “Functional fractional calculus for system identification of battery cells,” *at-Automatisierungstechnik*, vol. 62, no. 4, pp. 272–281, 2014.

[63] T. M. Apostol, *Introduction to analytic number theory*. Springer Science & Business Media, 2013.

[64] P. H. Zope, P. G. Bhangale, P. Sonare, and S. R. Suralkar, “Design and Implementation of carrier based Sinusoidal PWM Inverter,” *Int. J. Adv. Res. Electr. Electron. Instrum. Eng.*, vol. 1, no. 4, pp. 230–236, 2012.

[65] D. Czarkowski, D. V Chudnovsky, and I. W. Selesnick, “Solving the optimal PWM problem for single-phase inverters,” *IEEE Trans. Circuits Syst. I Fundam. Theory Appl.*, vol. 49, no. 4, pp. 465–475, 2002.

[66] S. S. Burrus, *Computer-based exercises for signal processing using MATLAB*. Prentice Hall PTR, 1993.

[67] C. K. Chui and G. Chen, *Signal processing and systems theory: selected topics*, vol. 26. Springer Science & Business Media, 2012.

[68] T. T. Hartley and C. F. Lorenzo, “Fractional-order system identification based on continuous order-distributions,” *Signal Processing*, vol. 83, no. 11, pp. 2287–2300, 2003.

[69] M. Nakagawa and K. Sorimachi, “Basic characteristics of a fractance device,” *IEICE Trans. Fundam. Electron. Commun. Comput. Sci.*, vol. 75, no. 12, pp. 1814–1819, 1992.

[70] T. McKelvey, “Frequency domain system identification with instrumental variable based subspace algorithm.” Linköping University Electronic Press, 1999.

[71] R. Pintelon, J. Schoukens, and G. Vandersteen, “Frequency domain system identification using arbitrary signals,” *IEEE Trans. Automat. Contr.*, vol. 42, no. 12, pp. 1717–1720, 1997.

[72] B. M. Vinagre, I. Podlubny, A. Hernandez, and V. Feliu, “Some approximations of fractional order operators used in control theory and applications,” *Fract. Calc. Appl. Anal.*, vol. 3, no. 3, pp. 231–248, 2000.

[73] A. Oustaloup, F. Levron, B. Mathieu, and F. M. Nanot, “Frequency-band complex noninteger differentiator: characterization and synthesis,” *IEEE Trans. Circuits Syst. I Fundam. Theory Appl.*, vol. 47, no. 1, pp. 25–39, 2000.

[74] R. Caponetto, *Fractional order systems: modeling and control applications*, vol. 72. World Scientific, 2010.

[75] D. Xue, Y. Chen, and D. P. Atherton, *Linear feedback control: analysis and design with MATLAB*. SIAM, 2007.

[76] E. C. Levy, “Complex-curve fitting,” *IRE Trans. Autom. Control*, no. 1, pp. 37–43, 1959.

[77] D. Valério and J. Costa, “Levy’s identification method extended to commensurate fractional order transfer functions,” in *Fifth EUROMECH Nonlinear Dynamics Conference*, 2005, pp. 1357–1366.

[78] H.-S. Ahn, Y. Chen, and I. Podlubny, “Robust stability test of a class of linear time-invariant interval fractional-order system using Lyapunov inequality,” *Appl. Math. Comput.*, vol. 187, no. 1, pp. 27–34, 2007.

[79] A. Benzaouia, H. M. Soliman, and A. Saleem, “Regional pole placement with saturated control for DC-DC buck converter through Hardware-in-the-Loop,” *Trans. Inst. Meas. Control*, vol. 38, no. 9, pp. 1041–1052, 2016.

[80] F. Merrikh-Bayat, “Optimal tuning rules of the fractional-order PID controllers with application to first-order plus time delay processes,” in *2011 International Symposium on Advanced Control of Industrial Processes (ADCONIP)*, 2011, pp. 403–408.

[81] C. Yeroglu and N. Tan, “Note on fractional-order proportional–integral–differential controller design,” *IET Control theory Appl.*, vol. 5, no. 17, pp. 1978–1989, 2011.

[82] C. I. Muresan, E. H. Dulf, and R. Both, “Vector-based tuning and experimental validation of fractional-order PI/PD controllers,” *Nonlinear Dyn.*, vol. 84, no. 1, pp. 179–188, 2016.

[83] A. Ahuja and S. K. Aggarwal, “Design of fractional order PID controller for DC motor using evolutionary optimization techniques,” *Wseas Trans. Syst. Control*, vol. 9, pp. 171–182, 2014.

[84] M. TAJJUDIN and R. ADNAN, “A Design on New Error Compensator for Fractional PI Controller and Its Application,” *WSEAS Trans. Syst. Control*, vol. 9, pp. 28–37, 2014.

[85] F. G. Prakash and V. Alamelumangai, “Design of predictive fractional order PI controller

for the quadruple tank process," *WSEAS, Trans. Syst. Control*, vol. 10, pp. 85–94, 2015.

[86] S. E. Hamamci, "An algorithm for stabilization of fractional-order time delay systems using fractional-order PID controllers," *IEEE Trans. Automat. Contr.*, vol. 52, no. 10, pp. 1964–1969, 2007.

[87] T. Amieur, M. Sedraoui, and O. Amieur, "Design of Robust Fractional-Order PID Controller for DC Motor Using the Adjustable Performance Weights in the Weighted-Mixed Sensitivity Problem," *IAES Int. J. Robot. Autom.*, vol. 7, no. 2, p. 108, 2018.

[88] F. Padula and A. Visioli, *Advances in robust fractional control*. Springer, 2015.

[89] M. Hossein Basiri and M. Saleh Tavazoei, "On robust control of fractional order plants: Invariant phase margin," *J. Comput. Nonlinear Dyn.*, vol. 10, no. 5, 2015.

[90] A. Visioli, *Practical PID control*. Springer Science & Business Media, 2006.

[91] A. O'Dwyer, *Handbook of PI and PID controller tuning rules*. Imperial college press, 2009.

[92] K. J. Åström, T. Hägglund, and K. J. Astrom, *Advanced PID control*, vol. 461. ISA-The Instrumentation, Systems, and Automation Society Research Triangle …, 2006.

[93] Y. Luo and Y. Chen, "Fractional order [proportional derivative] controller for a class of fractional order systems," *Automatica*, vol. 45, no. 10, pp. 2446–2450, 2009.

[94] B. D. O. Anderson, "JB Moore Optimal control, linear quadratic methods." Prentice-Hall International Editions, 1989.

[95] F. Lin, *Robust control design: an optimal control approach*, vol. 18. John Wiley & Sons, 2007.

[96] H. Tan, S. Shu, and F. Lin, "An optimal control approach to robust tracking of linear systems," *Int. J. Control*, vol. 82, no. 3, pp. 525–540, 2009.

[97] A. O'Dwyer, "An overview of tuning rules for the PI and PID continuous-time control of time-delayed single-input, single-output (SISO) processes," in *PID Control in the Third Millennium*, Springer, 2012, pp. 3–44.

[98] F. Padula, R. Vilanova, and A. Visioli, "H∞ model matching PID design for fractional FOPDT systems," in *2012 American Control Conference (ACC)*, 2012, pp. 5513–5518.

[99] F. Padula and A. Visioli, "Fractional-order proportional-integral-derivative controllers," in *Advances in Robust Fractional Control*, Springer, 2015, pp. 27–70.

[100] D. Xue and Y. Chen, "Sub-optimum H 2 rational approximations to fractional order linear systems," in *International Design Engineering Technical Conferences and Computers and*

Information in Engineering Conference, 2005, vol. 47438, pp. 1527–1536.

[101] J. R. Munkres, "Analysis On Manifolds. Adv. Books Classics Series." Westview Press, 1997.

[102] P. Ostalczyk, "Fractional-Order Backward Difference Equivalent Forms Part I–Horner's Form," in *Proc. 1-st IFAC Workshop Fractional Differentation and its Applications, FDA*, 2004, vol. 4, pp. 342–347.

[103] P. Ostalczyk, "Fractional-order backward difference equivalent forms Part II-Polynomial Form," in *Procc. of 1st IFAC Workshop on Fractional Differentiation and its Applications FDA*, 2004, vol. 4, pp. 348–353.

[104] K. H. Ang, G. Chong, and Y. Li, "PID control system analysis, design, and technology," *IEEE Trans. Control Syst. Technol.*, vol. 13, no. 4, pp. 559–576, 2005.

Appendix

Appendix A

Codes for Resamples input-output signal

```
function [yy,tt] = myresample(y,t,dtol,NN)

%function [yy,tt] = myresample(y,t,dtol,NN)
%
% Resamples y = y(t) on a uniform grid tt = min(t) : dt : max(t).
% y may have n columns but should have length(t) rows.
% This simply calls Matlab's interp1 (with 'linear' as METHOD), but preprocess
% t (and y) so that tt is monotone increasing.
%
% dtol is a threshold such that t(j+1)-t(j) < dtol, then t(j+1) (and y(j+1,:))
% is removed.
%
% NN is the number of new sample points (defaults to length(t)), giving dt above
% as   dt = (max(t) - min(t))/(NN-1)
%
if nargin < 4,
  NN = length(t);
  if nargin < 3,  dtol = 100*max(abs(t))*eps;  end
end
[yy,tt,p] = makestrict(y,t,dtol);
[m,n] = size(yy);  N = NN;

nt = tt(1):(tt(end)-tt(1))/(N-1):tt(end);  nt = nt(:);
yy = interp1(tt,yy,nt,'linear');  tt = nt;
```

Appendix *B*

Codes for Restore input-output signal

```
function [yy,tt,p] = makestrict(y,t,dtol);
%function [yy,tt,p] = makestrict(y,t,dtol);
% Sorts y and t for increasing t and removes duplicate entries in t
% (assuming y = y(t)).  Duplicates are defined by t(j+1)-t(j) < dtol.
% p is an permutation into 1:length(t), so that yy = y(p,:) and tt = t(p).
% If y is a (2d) matrix, then one of its dimensions must be length(t).
% If #rows(y) is ~= length(t), then it is transposed.  So on output
% #rows(yy) = length(tt), and tt is a column vector.
n = length(t);  t = t(:);
[ry,cy] = size(y);
if (ry ~= n & cy ~= n),
   error('myresample: t and y vectors must be same size');
end
if ry ~= n,  y = y';  end
dt = diff(t);  s = find(dt < 0);
if length(s),
   disp('myresample: must sort')
   [t,p] = sort(t);  y = y(p,:);
else,
   p = 1:n;  p = p(:);
end
dt = diff(t);  s = find(dt < dtol);  m = length(s);
if m,
   nots = find(dt >= dtol);
   yy = [y(nots,:);y(end,:)];  tt = [t(nots);t(end)];  p = [p(nots);p(end)];
   %[yy,tt] = makestrict(yy,tt,dtol);
else,
   yy = y;  tt = t;
end
```